universitätbonn igg

Institut für Geodäsie und Geoinformation

Schriftenreihe

26

Lihua Li

Separablity of deformations and measurements noises of GPS time series with modified Kalman filter for landslide monitoring in real-time

Lihua Li • **Separablity of deformations and measurement noises of GPS time series with modified Kalman filter for landslide monitoring in real-time**

universitätbonn igg

Institut für
Geodäsie und Geoinformation

Schriftenreihe **26**

Lihua Li

Separablity of deformations and measurements noises of GPS time series with modified Kalman filter for landslide monitoring in real-time

Diese Arbeit wurde am 26. Mai 2011 als Dissertation zur Erlangung
des Grades Doktor-Ingenieur (Dr.-Ing.) der Landwirtschaftlichen Fakultät
der Rheinischen Friedrich-Wilhelms-Universität Bonn vorgelegt.

Referent:	Prof. Dr.-Ing. Heiner Kuhlmann
Korreferent:	Prof. Dr. techn. Wolf-Dieter Schuh

Tag der mündlichen Prüfung: 14. Juli 2011

Diese Dissertation ist auf dem Hochschulschriftenserver der ULB Bonn
http://hss.ulb.uni-bonn.de/fakultaet/landw
elektronisch und mit allen farbigen Abbildungen publiziert.

Schriftenreihe des Instituts für Geodäsie und Geoinformation
der Rheinischen Friedrich-Wilhelms-Universität Bonn

Herausgeber:
Prof. Dr.-Ing. Wolfgang Förstner
Prof. Dr.-Ing. Theo Kötter
Prof. Dr.-Ing. Heiner Kuhlmann
Prof. Dr.-Ing. Jürgen Kusche
Prof. Dr. Lutz Plümer
Prof. Dr. techn. Wolf-Dieter Schuh

Die Aufnahme dieser Arbeit in die Schriftenreihe wurde von den Herausgebern
der Reihe einstimmig beschlossen.

Bonn 2012 ISSN 1864-1113

Institut für Geodäsie und Geoinformation
der Rheinische Friedrich-Wilhelms-Universität Bonn

Separablity of deformations and measurement noises of GPS time series with modified Kalman filter for landslide monitoring in real-time

Inaugural-Dissertation

zur

Erlangung des Grades

Doktor-Ingenieur

(Dr.-Ing.)

der

Landwirtschaftlichen Fakultät

der

Rheinischen Friedrich-Wilhelms-Universität

zu Bonn

vorgelegt am 26. May 2011

von Lihua Li

aus Hengshui, China

Referent: Prof. Dr.-Ing. Heiner Kuhlmann

Korreferent: Prof. Dr. techn. Wolf-Dieter Schuh

Tag der mündlichen Prüfung: 14.Juli 2011

Erscheinungsjahr: 2011

Abstract

The separation of the deformations and measurement noise of GPS coordinate time series and accuracy improvement of GPS real-time coordinates are major aspects of the thesis. In order to reduce the influence of the colored noise in the GPS position time series, three different methods have been compared: the Finite Impulse Response (FIR) filter, the Kalman filter model, and the sequential algorithm. Among these three methods, the Kalman filter is investigated in detail. The GPS real-time series contains the colored noise, yet the Kalman filter model requires white noise. The state vector can be augmented by appending to the state vector components of the shaping filter which can describe the long term movement of the colored noise. Thus the deformation analysis based on the Kalman filter model with a shaping filter technique, has been applied in the different movement trends of GPS real-time series. From the results, the Kalman filter model with a shaping filter can be widely used to process the GPS short baseline time series in real-time. The precise position coordinate can be obtained and the deformation epoch can be detected in time and with high reliability. It can be applied in the early warning system of the natural hazards.

The detection of a deformation with less time delay and the improvement of reliability of detecting deformation epoch is another key issue of the investigation. The proposed model makes use of the statistical criterion (MDL criterion) comparison instead of the hypothesis test. Considering the affection of colored noise in the GPS time series the multiple Kalman filters model was augmented by shaping filters which describe the long-term movement of the colored noise. By the GPS experiments, it has been verified that the proposed models have the ability to better capture the deformation epoch and to improve the reliability of detecting the deformation epoch. The proposed models can be used to detect stepwise changes of a variety of fields in real-time or near real-time.

Zusammenfassung

Schwerpunkte dieser Arbeit sind die Trennung von tatsächlicher Bewegung und Messrauschen in GPS-Koordinatenzeitreihen und die Genauigkeitssteigerung von Echtzeit-GPS-Koordinaten. Zur Verringerung des Einflusses von farbigem Rauschen bei Zeitreihen von GPS-Positionen wurden drei verschiedene Verfahren verglichen: FIR-Filter (Finite Impulse Response),Kalman-Filter-Modell und Sequentielle Ausgleichung. Von diesen drei Verfahren wird das Kalman-Filter genauer untersucht. In Echtzeit-GPS-Datenreihen ist farbiges Rauschen enthalten, das Kalman-Filter hingegen erfordert weißes Rauschen. Die Zustandsschätzung erfolgt durch die Erweiterung des Zustandsvektors um die shaping-Filter-Komponenten, die den langfristigen Einfluss des farbigen Rauschprozesses beschreiben. Dementsprechend wurde die Bewegungsanalyse durch ein Kalman-Filter-Modell mit shaping-Filter-Verfahren auf verschiedene Rauschprozesse von Echtzeit-GPS-Zeitreihen angewandt. Das Ergebnis ist, dass ein Kalman-Filter mit shaping-Filter kann häufig zur Echtzeitauswertung von Zeitreihen kurzer GPS-Basislinien genutzt werden. Die genauen Positionskoordinaten lassen sich bestimmen, und, eine Bewegungsepoche kann rechtzeitig und mit einer hohen Zuverlässigkeit bestimmt werden. Ein Einsatz in Frühwarnsystemen vor Naturgefahren ist möglich.

Die Erkennung von Bewegung mit geringer Zeitverzögerung und die Steigerung der Detektionszuverlässigkeit von Bewegungsepochen sind weitere Untersuchungsschwerpunkte. Der vorgeschlagene Ansatz nutzt statt eines Hypothesentests den Vergleich eines statistischen Kriteriums (Minimum Desciption Length). In Anbetracht des farbigen Rauschens, das in GPS-Zeitreihen enthalten ist, wurde das multiple Kalman-Filter um shaping-Filter erweitert, die den langfristigen Einfluss des farbigen Rauschens beschreiben. Durch GPS- Experiment konnte nachgewiesen werden, dass die vorgeschlagenen Modelle eine verbesserte Deformationserkennung und eine Steigerung der Zuverlässigkeit bezüglich der Deformationsepochendetektion ermöglichen. Diese erlauben die Erkennung stufenförmiger Änderungen bei vielfältigen Anwendungen und zur Vorhersage einiger Naturkatastrophenereignisse in Echtzeit beziehungsweise Nahezu-Echtzeit.

Table of Contents

1 Introduction

This chapter gives an introduction to the thesis. First, the motivation to the subject and the relevant research are given. Secondly the research objectives are stated and finally the thesis outline is given.

1.1 Background and relevant research

Landslide is one of the natural disasters, which causes the fatalities and severe economic loss. Therefore, early warning systems are the efficient tools to face landslide hazards and reduce the risk landslides, especially where no other mitigation strategies are suitable. The project of developing an integrated early warning system of landslides is funded by the Federal Ministry for Education and Research (BMBF). In the project terrestrial observations and measurement networks are coupled with different techniques. GPS is one of the important sensors to obtain the surface deformations of the landslide areas.

GPS is weather independent, capable of autonomous operation, and does not require a line-of-sight between target points. GPS is actively and broadly used for positioning in geodetic applications. A typical and highly challenging application – in terms of positioning accuracy –is deformation monitoring (Schüler 2007). Recent advances in GPS technology and data processing software have made GPS a much more convenient, accurate and cost-effective tool for deformation monitoring of natural hazards and man-made structures. To date, GPS is widely used to monitor volcano eruptions (Rizos et al. 2000; Roberts and Rizos 2001; Janssen 2002 & 2007), crustal movements (Qiao et al. 2002; Moghtased-Azar and Grafarend 2009), vertical land movements (Teferle et al. 2001), landslides (Brunner et al. 2000; Singer et al. 2009), the open-pit mine (Forward et al. 2001), dams (Hudnut and Behr 1998; Radhakrishnan 2006), buildings (Lovse et al. 1995; Guo and Ge 1997; Chen et al. 2001; Ogaja et al. 2002), and bridges (Roberts et al. 1999; Fujino et al. 2000; Wong et al. 2001; Roberts et al. 2004). A monitoring system for deformation of structures like bridges with real-time capabilities is described by Hein and Riedl (2003). The GPS-based monitoring system GOCA (GNSS based online Control and Alarm System) developed at the applied university of Karlsruhe can be applied to observe dams, landslides, etc (Jäger et al. 2006). Deformation experiments and GPS deformation monitoring applications have shown that GPS is capable to monitor deformations.

It's very important to monitor the deformation of the landslide area that threatens the lives or constructions. There are some successful applications in landslide deformation using GPS. For example, the GPS continuous deformation monitoring system, which employed the time stacking technique and the sigma models, was applied in Gradenbach landslide (Brunner et al. 2000). The authors present an application of GPS to monitor the La Valette landslide, located in the Ubaye Valley in the southern French Alps (Squarzoni et al. 2005); a low-cost GNSS system is devel-

oped to continuously record movements on the surface of the Hornbergl landslide (Glabsch et al. 2009).

The availability of precise and reliable deformation information in real-time is critical for generating warnings in time for the early warning systems. The Kalman filter model is one of the optimal methods to process the GPS position time series in real-time (Brown and Hwang 1992; Grewal and Andrews 2001; Yang et al. 2001). The Kalman filter model calculates the optimal value of the state vector in the recursive least square manner. The elements of the state vector in the Kalman filter are the unknowns of the kinematic/dynamic system. These are typically the position of the object, or also the variation of the position. This property of the Kalman filter is important for studying the behavior of deformations (Ince and Sahin 2000).

However, the Kalman filter model is used under the assumption that only white noise exists in this algorithm. But in the real-time application it requires high sampling rates of GPS receivers; in the case of the high sampling rate, time dependent systematic deviations arise in the observations between neighboring epochs in a similar way. Therefore, the correlated errors exist in the GPS measurement time series. The GPS measurement deviations can be divided into correlating errors and non-correlating errors. The colored noise influence the results of deformation analysis and the accuracy, sensitivity and separability criteria of GPS-control measurements (Schwieger 1999). The conventional Kalman filter cannot serve as the appropriate tool to process the GPS observations with colored noise.

Significant work has been done to reduce the colored noise using various methods which can be categorized as two main approaches: one approach uses measurement differencing to remove the colored noise (Minkler and Minkler 1993; Petovello et al. 2009), for example, Petovello et al. have presented a new Kalman filter formulation that considers time-correlated errors in the observations. The proposed method is also based on measurement differencing but does not have inherent time latency, nor are any redefinitions of the traditional Kalman filter parameters required (Petovello et al. 2009); the other approach augments the state vector with the correlated noise terms (Gelb 1974; Maybeck 1994; Grewal and Andrews 2001; Kuhlmann 2003). For example, Gelb presents that it can be useful to generate an autocorrelation function from real data and develop an appropriate noise model. The model can describe the movement of the colored noise, which is called a shaping filter. The state vector can be augmented by appending the shaping filter to the state vector components of the Kalman filter, with the resulting model having the form of a linear dynamic system driven by white noise. Additionally, Yang and Zhang proposed the Kalman filter model based on an adaptive fitting of systematic error and covariance matrices to control the influences of systematic error of the state equation in the Kalman filter model (Yang and Zhang 2005). Based on these approaches, the appropriate approach needs to be selected to reduce the colored noise in the GPS time series.

During the deformation analysis, deformation identification is of great importance and false warning should be given as few as possible. Therefore how to detect the deformation epoch and improve the reliability of detecting deformation epoch are other key issues. Previous work using statistical tests has been done to detect the changes in the time series. For example, the multiple hypothesis filter (Willsky 1976), the generalized likelihood ratio test by using the Kalman filter innovation (Willsky 1976; Teunissen 1990; Okatan et al. 2007), the cumulative sum test (Mertikas and Rizos 1997; Mertikas 2001). Since the detection of deformation epochs is important for the early warning system, more detailed research is needed to improve the accuracy and the reliability of the detected deformation epoch.

1.2 Research objectives

GPS can be used to monitor hazards, such as landslides and volcano eruptions. In order to reduce any human losses and economic damages, it is necessary to develop an early warning system for landslides. The real-time data processing with both high precision and high reliability is of great importance in the planed early warning system.

The main objective of the thesis is the development of the methodology which can separate GPS noise and deformation in the GPS coordinate time series, improve the accuracy of the GPS real-time series and improve the reliability of detecting deformation epochs.

The Kalman filter can be employed as the method to process the real time series. The deformation and outlier have some similarity but also some differences in the GPS observations so that they can be detected and distinguished simultaneously. It will be discussed in detail how to determine the state vector when an outlier and a deformation occur. Hence, monitoring and controlling the quality of the GPS observation series is one of the main objectives.

GPS observations obtained from GPS experiment at a high sampling rate needed to be studied. The noises in the GPS observations needed to be classified and separated. The autocorrelation function and the stochastic model are the main methods to analyze and determine the distribution of the GPS observations noise. The study on the effective method to separate the noise from the GPS observations is one of the research emphases in this thesis.

Many monitoring problems can be stated as the problem of detecting a change. It is very important to detect small changes in some applications, because some economic or catastrophic consequences that result from an accumulation of small changes can be avoided. False warnings should also be made to occur as little as possible. Therefore, the timely detection of any deformation with high reliability is very important. The model which can capture the deformation epochs and improve the reliability of detecting the deformation epoch should be proposed.

1.3 Dissertation outline

There are six chapters in this thesis. The general structure of the thesis is described as follows: The first chapter is a brief introduction of the research background and the objective of the research.

Chapter 2 provides the introduction of the project Integrative Landslides Early Warning Systems (ILEWS) and the subproject: Geodetic monitoring and modeling.

Chapter 3 describes the GNSS status and analyzes the noise of GPS real-time series.

Chapter 4 provides three different methods that will be used to reduce the colored noise in the GPS time series: the Finite Impulse Response (FIR) filter, the Kalman filter model with a shaping filter, and the sequential algorithm. The merits and the limitations of each method will be discussed in detail based on the GPS real-time series analysis. The Kalman filter model with a shaping filter is investigated in detail. It is not only applied to process the stepwise changes but also different forms of the deformation time series.

Chapter 5 is concerned with designing algorithms to detect the deformation epoch, in order to improve the quality of GPS measurements for the real-time deformation applications. In this regard, the multiple Kalman filters model based on the idea of model selection is proposed to improve the reliability of the detection of the deformation epoch. Because of the affection of the colored noise in the GPS time series, the proposed model can be augmented by shaping filters. The simulated data and the GPS time series are used to verify the effectiveness of the proposed models.

Chapter 6 is composed of the conclusions and the suggestions for the future work.

2 Integrative Landslides Early Warning Systems (ILEWS)

2.1 ILEWS introduction

Landslides cause economic damage and fatalities all over the world. In most of the cases, severe consequences could have been reduced if a reliable and understandable warning had been provided in time. Since both the possibilities to predict landslides as well as the early warning of landslides vary significantly, early warning of landslides is a challenging topic. New technologies are needed to set up reliably an early warning system. However, a well working technical early warning system might not be sufficient if the issued warning is not understood by the threatened people. Thus, the effective early warning system must integrate social science, humanities and decision making as well ensure that the early warning system meets the needs of the involved players and the threatened people (Glade et al. 2007).

The main aim of the project ILEWS is to design and implement an integrative early warning system for known and new landslides and debris flows, which provides information on future events with regard to local and regional requirements. One study area is in the community of Lichtenstein-Unterhausen in Germany. In this area regularly occurring house damages and inclinometer measurements show a recent but very slow sliding activity of the slope. Therefore the slope represents ideal conditions to test modern measurement technology. The other is South Tyrol in Italy. The early warning systems are to be implemented in these two european test areas(Glade et al. 2007).

The subprojects are composed of

- Monitoring of landslide movement and early warning modeling
- Coordination, integration and optimization of a multi-sensor system for monitoring of landslides
- Cooperative risk communication
- Historical comparative regional analysis of frequency and magnitude of landslides
- Integration of early warning into an integrated risk management
- Central spatial data infrastructure, open web services and web processing services and web processing services for the development of an information management in early warning systems for landslides
- Development of an adequate data model schema for an information and decision support system for risk management in landslides early warning systems
- Geodetic monitoring and modeling
- Spatial monitoring of soil parameters with geophysical survey methods

- Standardized, wireless sensor networks for the efficient acquisition, transmission, storage and visualization of geodata (Glade et al. 2007).

2.2 Subproject: geodetic monitoring and modeling

The main task of geodetic monitoring measurements is to "get a confirmation of predictable changes (e.g. subsidence behavior of structures) or the proof for a non-expected or non-predictable change of an object (e.g. landslide). Information is generally being supplied through selected measuring points. The behavior of the object can be quantified by analyzing the movements over time. Closely related with the determination of movements is also the question of reasons in order to derive a causal connection" (Glade et al. 2007).

A specially created geodetic point network spreads over stable as well as critical slope areas. Those areas should be identified whose movement intervals differ significantly from other areas due to certain other effects (e.g. change of pore water pressure, increase of humidity, etc.). Via measuring methods such as GPS and electronic precision tacheometry, absolute movements of ground points in slope areas are being recorded and compared to reference points. Besides those geodetic network points, further measuring stations are being created which are equipped with sensors for relative measurements. The relative measurements can be linked with the movement of the geodetic measuring points in order to get best redundant but assignable measuring information on movements (Glade et al. 2007).

Both geodetic measuring methods can be applied one after another. It is supposed that the movement intervals are about 0.3mm/month, the measuring resolution of the precision tacheometer of about 0.2-0.3mm will be sufficient if episodic measurements are carried out and measurements are repeated about every 2-3 months. Both the monitoring of the geodetic point network and the respective integration of all measuring stations for relative measurements are covered. The redundant information is delivered on areas close to each other. The automatic relative measurements can serve as indicators for beginning movements in order to possibly initiate monitoring measurements outside the scheduled measuring epochs (Glade et al. 2007).

Although it is not the focus of this thesis, it should be mentioned here. A regular examination of the measuring instrument will be necessary in order to get a relative precision of tacheometric measurement clearly less than 1 ppm. It is also not sufficient to introduce the gained meteorological parameters of the end point as representative factors for the entire measuring distance. The determination of the refractive index is the precision limiting factor for the distance measuring especially in mountained areas. Hence it is important to determine the refractive index (Glade et al. 2007).

In the 1990s the high-precision distance measuring was taken successfully. Based upon the light dispersion in a turbulent medium, the fluctuations due to atmospheric exchange processes are

described in a model by means of statistic factors. Suitable commercial systems, which can measure these atmospheric fluctuations, have been developed by Scintec/Tübingen in the form of the scintillometer measuring systems. Regarding the chosen study areas a scintillometer will be used, which can do measurements up to 4-5 km. A significant improvement in the application of the modeling of the refractive index has been achieved. Its application therefore covers huge parts of the refractive components which have previously been difficult to determine (Müller 2010).

In the chosen study areas, changes are being expected that have an explicit time connection. The movements collected can be modeled together as a function of pore water pressure, rainfall, ground parameters and slope inclination, etc. This will then be the basis for an early warning system via which an according measure and emergency concept should be initiated in order to best handle the current situation (Glade et al. 2007; Thiebes et al. 2010).

2.3 Main work: GPS real-time series processing and analysis

GPS has been used to monitor landslide over last couple of years. The landslide monitoring demands the observations in real-time and with high accuracy. The demand for increasing accuracy in this application has required a deeper understanding of GPS positioning errors and methods to reduce or eliminate them.

GPS measurements can be carried out with the same measuring epoch. They have advantages with continuous monitoring methods over several weeks, if they are being carried out as static measurements. The data collected in the local network come together in a central control and evaluation unit, in that it is possible to calculate the baselines between the network points automatically and continuously in order to obtain station movements (Glade et al. 2007).

The GPS observation deviations demonstrate a certain auto-correlation in the range of a few minutes up to a few hours. The auto-correlation of GPS measurement observations are caused by the multipath, propagation effects of the electromagnetic waves and so on. The dimension of the deviations lies above the point movement to be expected. The GPS observation deviations can be reduced during long observation periods and an analysis using post processing method. Because of the planned early warning system a real time process is required here which analyze that a separation of measurement deviations and point movements will be done in a filter approach (Glade et al. 2007).

Although GPS cannot be used in the Schwabian Alb area, the related research works need to be done. The main works should be done as described in the following:

- Analysis of GPS noise
- Separation of colored noise from GPS real-time series
- Accuracy improvement of the GPS real-time series
- Reliability improvement of detecting deformation epochs.

3 GNSS Overview and Noise Analysis

3.1 GNSS introduction

Global Navigation Satellite Systems (GNSS) are designed to provide position, velocity, and timing capabilities to users all over the world. The GNSS combine GPS, GLONASS, GALILEO, COMPASS, etc.

It is originally designed that GPS consists of 24 satellites orbiting the earth at an altitude of about 20200 km. The satellites are distributed in six equally spaced orbit planes of inclination of 55 degrees with respect to the equator. Every satellite circulates the earth in a period of 12 hours sidereal time. The satellite sends timed signals at two L-band frequencies, 1.57 and 1.22 GHz, namely L1 and L2. The signals contain codes which can identify every satellite, satellite clock corrections of the satellite, time of the emitted signal, position, and other data related to ionosphere and satellite. The L1 signals are modulated by a Coarse/Acquisition (C/A) code, which is available for civilian use, and a more precise P(Y) code, which is available only for authorized users. The C/A code, which is for the civilian use, has a unique sequence of 1023 chips with a width of 300m and repeats every 1ms. The P code, which is for the military use, is extremely long ($\sim 10^{14}$ chips) but with a smaller chip width, 30m, and repeats itself every one week. Several techniques such as squaring and cross correlation were taken by high quality receivers in order to acquire the P code on L1 and L2 but with noise characteristics compared with the original codes (Hoffmann-Wellenhof 2001).

One of the most important issues in GPS positioning is to observe the time difference between the satellites and users; therefore, GPS satellites use high quality redundant atomic clocks. The structure of GPS system is composed of three main segments which are customary for navigation satellites: space segment, control segment and user segment. The space segment consists of different generations of active satellites. The constellation was changed to a non-uniform arrangement with the increased number of satellites. The reliability and availability of the system have been improved in such an arrangement. The responsibility of control segment is to maintain the satellites in orbits, adjust satellite clocks, and upload navigation data. The control segment is composed of the master operational control center, six monitoring stations, four ground antenna upload stations and an alternate master control station. The user segment is to receive the GPS signals by different satellite receivers.

GPS has been used for the solution of geodetic problems since about 1983 (Seeber). GPS is weather independence, capable of autonomous operation, and does not require a line-of-sight between target points. Because of the mentioned advantages, GPS can be used to continuously monitor deformations even during unfavorable weather conditions such as rain, snow and fog. The developments of GPS receivers, antennas, and data processing software have made GPS as a

very effective tool for deformation monitoring with sub-centimeter accuracy. GPS receivers measure the satellite signals at a high sampling rate. GPS technique is widely used to monitor the deformations of all kinds of buildings and constructions.

As any other developing technology, GPS technology has its own disadvantages when it is applied in the precise engineering applications. A major barrier is the achievable accuracy of GPS positioning solution, which is affected by many factors and restraints. In particular, multipath is one of the major limitations. Usually the systematic effects in the position results are amplified by weak satellite constellations. An effective solution is still elusive, although many efforts have been made in multipath mitigation (Meng 2002). Multipath and significant signal diffraction effects are often unavoidable in complicated GPS environments. Therefore, noise reduction of GPS observations, improvement of the accuracy of the GPS time series and detection of deformation epochs are the key issues of deformation analysis.

Currently GNSS are modernized. Until now (May. 2011) GLONASS has 23 operational satellites. Three other satellites are in maintenance and one satellite is in commissioning phase. Galileo positioning system is scheduled to be operational in 2014 (Öhler et al. 2009). China has indicated it will expand its regional Beidou navigation system into the global Compass navigation system by 2020 (Cao 2009).

The combined use of navigation systems will increase the overall performance, robustness, and the inherent safety of the services achieved from GNSS. It will allow for worldwide acceptability of the exploitation and use of satellite navigation for the benefit of all potential users. All these changes and improvements of the navigation systems will undoubtedly have a positive effect on Geodetic GNSS positioning.

3.2 GPS observation errors

A lot of error sources affect the accuracies of GPS measurements. The error sources can be grouped into three categories, the satellite related errors, the atmosphere related errors, and the receiver related errors. The satellite related errors include satellite clock error, satellite orbit error, and satellite inter-frequency bias. Atmosphere related errors consist of ionospheric delay error and tropospheric delay error. Receiver related errors are comprised of antenna phase center variations, receiver clock error, multipath, receiver inter-frequency bias, and receiver noise.

Generally, if the appropriate procedures or models are adopted, the error sources can be mitigated or corrected. Most of them can also be mathematically modeled and alleviated to a minimum degree. For instance, the tropospheric delay error can also be effectively corrected using certain models (Hopfield 1969; Saastamoinen 1973; Black and Eisner 1984). The multipath error can be reduced by the careful selection of GPS site, GPS receiver and antenna (e.g. choke ring) (Langley 1998). Most of the error sources variate only very slowly in real-time and may be can-

celled by differential observation techniques, for example, the ionospheric error and the tropospheric error. The following subsections describe the characteristic of each type of error sources.

Ephemeris errors

When the GPS message does not transmit the correct satellite location it will result in ephemeris errors (Parkinson 1996). The navigation messages, which are generated at control segment and uploaded by the four ground antennas of the control segment's monitor stations, are prediction results based on the past tracking information. Therefore, based on the navigation messages, the calculated GPS satellite positions are different from their true positions. Now the accuracy of broadcast orbit provided by International GNSS Service (IGS) is about 1 m (IGS).

If the satellite ephemeris data contain the errors, then the validity of the corrections will decrease as the distance between the user and the reference station increases (Parkinson and Enge 1996). The ephemeris errors are nearly the same for neighboring stations as long as they are sufficiently close. This is a negligible source of error for DGPS, provided the user is within 500 km of the reference station.

Satellite clock errors

Even though all the GPS satellites are equipped with atomic clocks for the generation of GPS signals, the atomic clock performance still results in an error to the GPS frequency standard because of its instability. A quadratic function of time is used to model the deviation of a particular clock from GPS system time. The parameters of the model are estimated, uploaded to the satellite, and are broadcast within the navigation message. The satellite clocks can be kept synchronized within 5 to 10 ns according to the parameters in the broadcast message (Misra and Enge 2001).

The actual behavior of each clock slightly differs from this model, because there are some unpredictable, correlated frequency errors. These errors are small and change slowly. The clock corrections are valid with time and not with the distance between the reference station and the user. The satellite clock errors can be cancelled by differencing the GPS observations between two satellites.

Ionosphere errors

The ionosphere layer is the higher stratum of the atmosphere with an extension from about 40 to 1000 km, which contains ionized particles created by sun's ultraviolet. When GPS signals transit this region, they don't travel at the vacuum speed of light because of free electrons in the ionosphere. The modulation on the signal is proportional to the inverse of the carrier frequency squared and is also delayed in proportion to the number of free electrons encountered.

The propagation delay in the ionosphere depends on the electron content along the signal path and also depends on the frequency selected. The influencing parameters are mainly solar activity

and the frequency used. Therefore, ionospheric refraction varies with geographic location, time, and frequency. For the GPS frequencies, the resulting error can vary from less than 1 m to more than 100 m (Wells 1986; Klobuchar 1996).

With differential corrections, the separation of the user and the reference station and the elevation angles of the satellites will affect the size of residual pseudorange error for the ionosphere. The ionosphere is not a significant problem for kinematic DGPS system under 50-km separation of reference station and the user. Usually, the effects of the ionosphere on differential GPS users are small, at least when the relative geographic area of the differential region used is small (Parkinson and Enge 1996).

Troposphere errors

Troposphere is the lower layer of atmosphere, extending from the sea level up to about 40 km (Hofmann-Wellenhof 2001). The troposphere causes another deviation from the vacuum speed of light. The variations in the speed of light of radio waves are caused by variations in temperature, pressure, and humidity. Usually, the influence of the neutral atmosphere on range measurements to satellites in the radio frequency domain can be divided into two integral terms: the dry component and the wet component. The wet component is caused by the lower portion of troposphere, 11 km from sea level, and it contains most of the water vapor. The modeling of the wet component is difficult, because of the variation of water vapor density with position and time. The wet component represents 10% of the total troposphere delay (Misra and Enge 2001).

The dry component represents the remaining 90% of the troposphere and can be easily modeled. Unlike the wet component, the dry component is caused by the higher portion of atmosphere lying directly above the wet components, and it contains mainly gases. The average total troposphere delay at zenith is about 2.5 m. It changes but does not suffer much from rapid change or large variation.

The tropospheric propagation delay is critical for the determination of precise position and baseline, in particular in the height component, because the tropospheric parameters are only poorly correlated over larger distances. Furthermore, it is difficult to separate error components stemming from the radial orbital errors, signal propagation errors, clock errors, antenna phase center variation, and errors in the station height.

This model typically removes 90% of the delay, but the unmodeled error can reach 2-3 m about 5 deg elevation without differential corrections. The residual error is almost always very small with differential corrections (Parkinson and Enge 1996). If the stations are close together, the tropospheric residual error almost completely disappears by differencing in the relative observation mode. The troposheric errors are highly correlated over short distances, thus, most of their delays are common to both stations. An exception to this rule might apply to nearby stations that are located at significantly different elevations in terms of the tropospheric effect.

The error could be troublesome for demanding applications if the signal ray paths to the user and reference station traverse volumes with significantly different meteorological parameters. In these cases, a differential tropospheric model that accounts for the altitude difference can be selected by the DGPS user (Parkinson and Enge 1996).

Multipath errors

Multipath propagation means that one or more reflected signals reach the antenna, in addition to the direct signal. It is possible that the antenna only receives the reflected signal under particular circumstances. There can be reflection off horizontal, vertical and inclined surfaces, which can be streets, buildings, waterways, and vehicles. When choosing observation sites, in particular for permanent reference stations, it must be considered. Multipath propagation affects both code and carrier measurements (Seeber 2003).

Multipath is the error caused by reflected signals entering the front end of the receiving antenna and masking the real correlation peak. In a static receiving antenna near large reflecting surfaces these effects tend to be more pronounced. 15 m or more in ranging error can be found in extreme cases (Parkinson 1996).

A variety of techniques, most notably narrow correlator spacing, have been developed to mitigate multipath errors. The receiving antenna itself can recognize the wayward signal and discard it for long delay multipath. Regarding shorter delay multipath from the signal reflecting off the ground, specialized antennas (e.g., a choke ring antenna) could be used to reduce the signal power as received by the antenna. Because short delay reflections interfere with the true signal, causing effects almost indistinguishable from routine fluctuations in atmospheric delay, it is harder to filter them out.

Multipath is a function of the specific receiver-satellite-reflector geometry and it doesn't cancel in the double-difference observable. It is the major error source for DGPS.

Receiver errors

The main error sources in the receiving system are antenna phase center variations, receiver noise, interchannel bias and oscillator instability.

The phase center positions of all antennas are very important for the determination of the height component. The phase center variations can reach millimeters to a few centimeters. Different antenna calibration procedures have been developed and a laboratory procedure was developed at the University of Bonn and a new anechoic chamber is operable since February 2009 (Zeimetz and Kuhlmann 2010).

The measurements of GPS receivers refer to the electronic center of the antenna. A receiver's antenna phase center is not a physical mark that GPS users can refer to. Additionally, according to the elevation of the incoming GPS signals, the receiver's antenna phase center changes, and

this variation is a function of the antenna fabrication. As a result, every GPS antenna will have an offset in addition to a variable element because of the elevation angle of the satellite.

The remaining phase center offsets and variations are eliminated in the differencing process, if antennas of the same type are used within one observation session over short baselines. If different antenna types are selected within the same project, the observations have to be corrected for the phase center variations.

GPS phase and code observables cannot be measured perfectly but are subject to random influences. For instance, the observations are influenced by unwanted disturbances in the antenna, amplifiers, cables, and the receiver itself. The double difference observations make the cancellation of the large receiver clock errors. The receiver clock errors cancel completely as long as observations to satellites are taken at the same time.

Different signal propagation delays for each hardware channel can be exhibited by multichannel receivers. The instrument makers try to calibrate and to compensate these interchannel biases. It is suggested that the parameter estimation models include the parameters for satellite and receiver hardware delays (Seeber 2003). Oscillator instabilities play only a minor role in carefully designed.

In case of landslide monitoring by GPS, the baselines are usually short baselines and the differential GPS measurements are computed in real-time. Most of the errors can be cancelled by differencing GPS observations, but the remaining system errors are correlated when the GPS observations are collected with a high sampling rate. Multipath effect is one of the reasons for interepochal correlations. Therefore the autocorrelation of GPS time series should be investigated in the following section.

3.3 Autocorrelation analysis of the GPS time series

With the electronic technology development, the GPS receivers can provide three-dimensional positions with high sampling rates. Because of the high sampling rate, time dependent systematic deviations arise in neighboring epochs in a similar way, resulting in autocorrelation (Schwieger 1999). Therefore, GPS measurements contain colored noise which negatively affects the deformation analysis. The assumption of white noise is not justified. The noise property must be taken into account in the high-precision GPS real-time positioning applications.

The distribution of the GPS colored noise has been analyzed by the autocorrelation function. Firstly the autocorrelation function (Strang and Borre 1997) is introduced as follows.

3.3.1 Introduction of the autocorrelation function

In statistics, the autocorrelation of a random process describes the correlation between values of the process at different points in time as a function of the two times or of the time difference.

The observation time series is described as (l_1, l_2, l_3, …, l_k,…, l_N), which are made at equidistant time intervals Δt. N is the total number of the observations. Firstly, we compute the mean value M of all observations; secondly, we compute the autocovariance coefficient $\hat{C}(i)$ of the observation series according to the definition below.

$$\hat{C}(0) = \sum_{k=1}^{N} (l_k - M)(l_k - M) / (N-1) \tag{3.1}$$

$$\hat{C}(1) = \sum_{k=2}^{N} (l_k - M)(l_{k-1} - M) / (N-2) \tag{3.2}$$

…

$$\hat{C}(i) = \sum_{k=i+1}^{N} (l_k - M)(l_{k-i} - M) / (N-i-1) \tag{3.3}$$

The normalized autocorrelation coefficient R_i is defined by the following formula,

$$R_i = \frac{\hat{C}(i)}{\hat{C}(0)} \tag{3.4}$$

Where i is the normalized autocorrelation coefficient's index, the time lag between l_k and l_{k-i} is $i \cdot \Delta t$. The autocorrelation coefficients for varying i of the GPS static observations are obtained by the Equations 3.1-3.4. The plot of R_i for varying i is called the correlogram for the random process l_k. One simple use of the correlogram is to check whether there is evidence of any serial dependence in an observed time series.

3.3.2 GPS experiment and results analysis

In order to analyze the GPS observation noise, a GPS experiment is needed. The sites were selected on the roofs of the Institute of Geodesy and Geoinformation (IGG) and the Max-Planck Institute (MPI) in Bonn, Germany. The baseline was about 1.2 km. The GPS equipment (Fig. 3.1) consisted of Trimble 5700 receivers and Zephyr antennas. A cut-off angle of 10° was chosen and the sampling rate Δt was 1 second. The kinematic observations of 9 hours with both fixed antennas (Fig. 3.2, Fig. 3.3 and Fig. 3.4) have been used for the noise analysis of GPS time series.

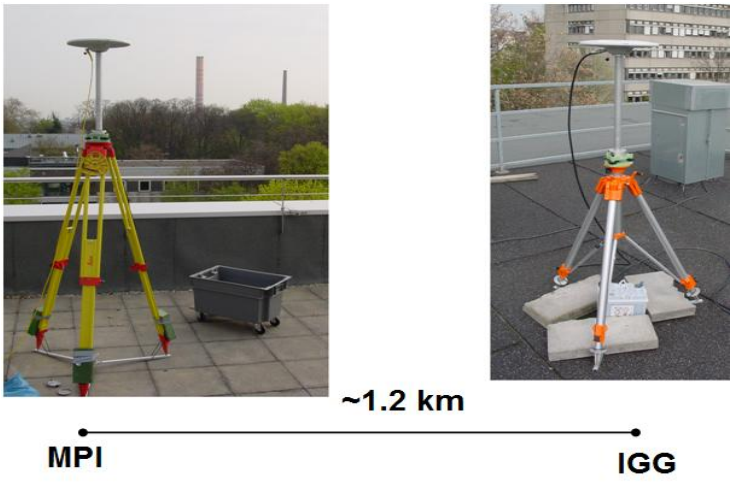

Fig. 3.1 GPS experiment

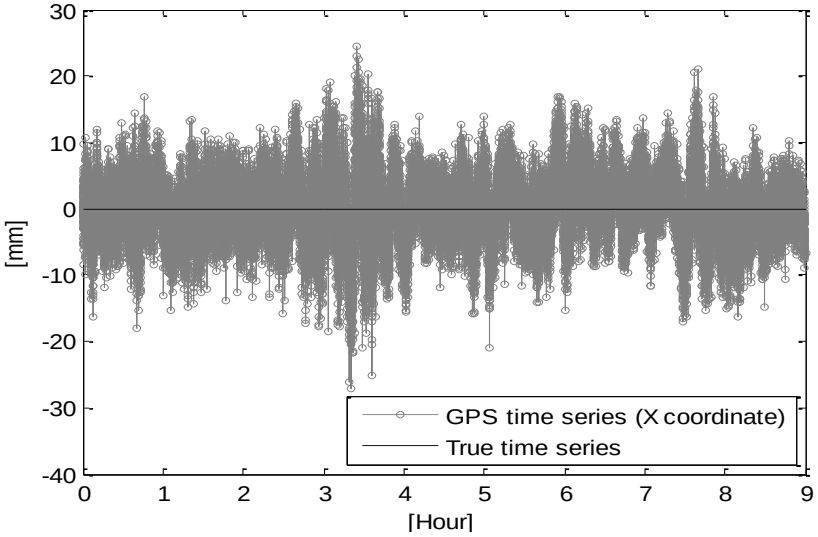

Fig. 3.2 GPS static X-coordinate time series

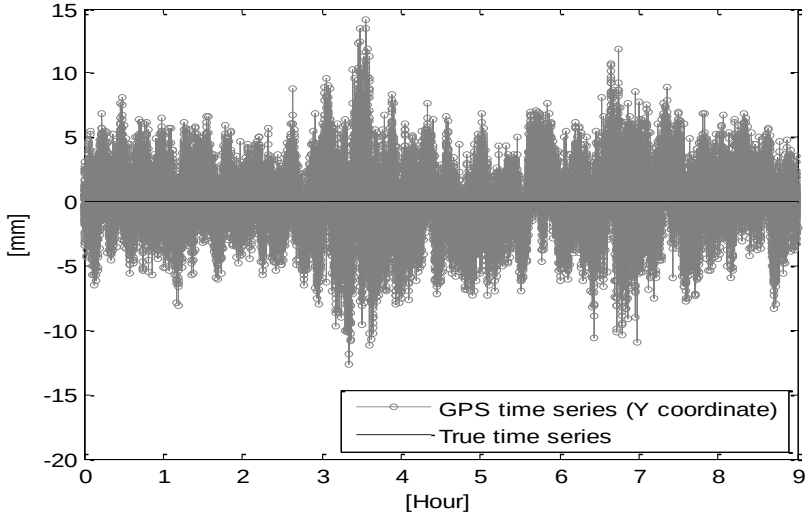

Fig. 3.3 GPS static Y-coordinates time series

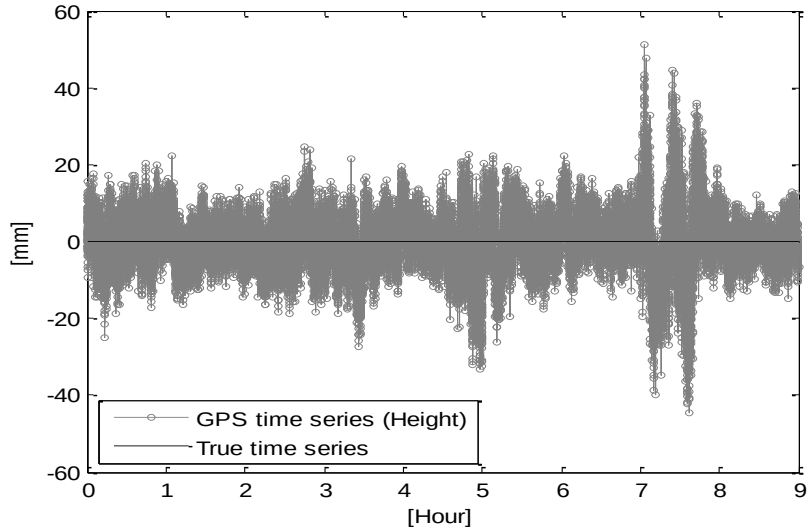

Fig. 3.4 GPS static Height time series

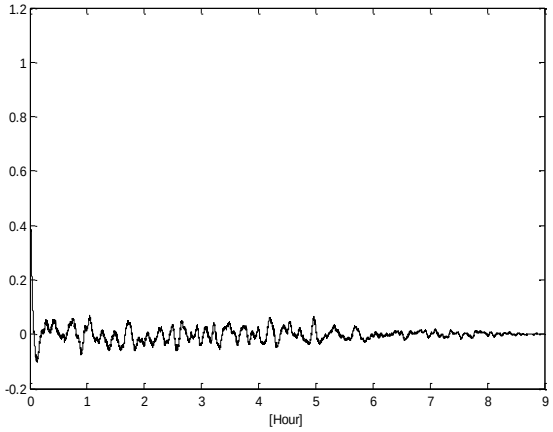

Fig. 3.5a Correlogram of X-coordinate

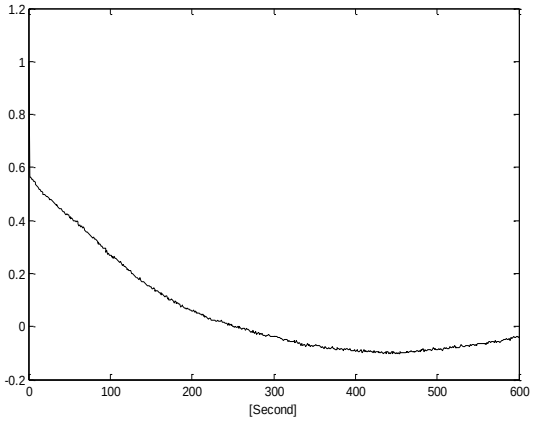

Fig. 3.5b Correlogram of X-coordinate (time lag: 0 to 600 second)

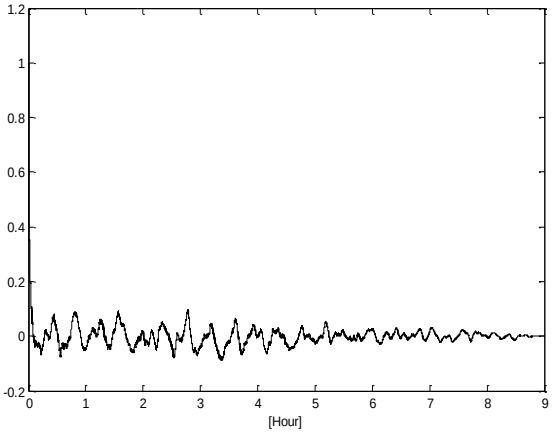

Fig. 3.6a Correlogram of Y-coordinate

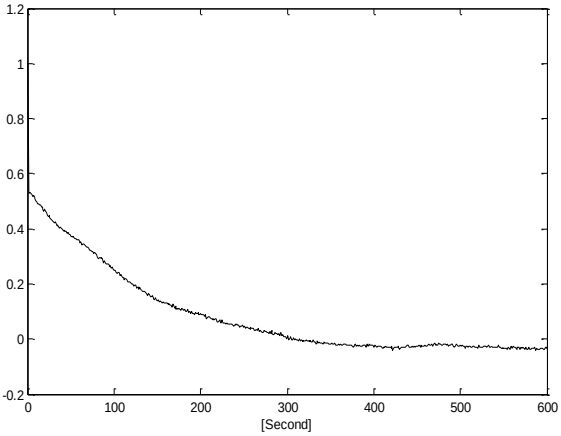

Fig. 3.6b Correlogram of Y-coordinate (time lag: 0 to 600 second)

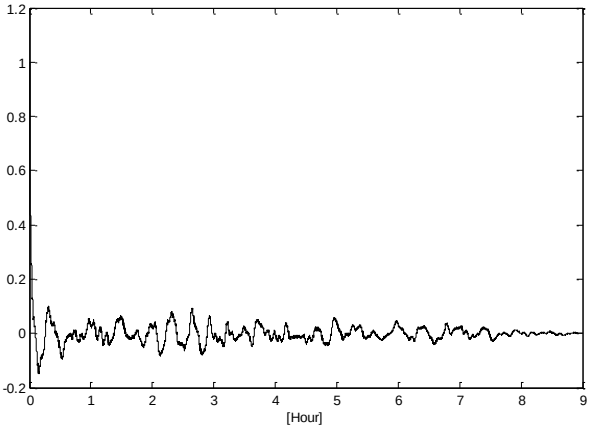

Fig. 3.7a Correlogram of Height

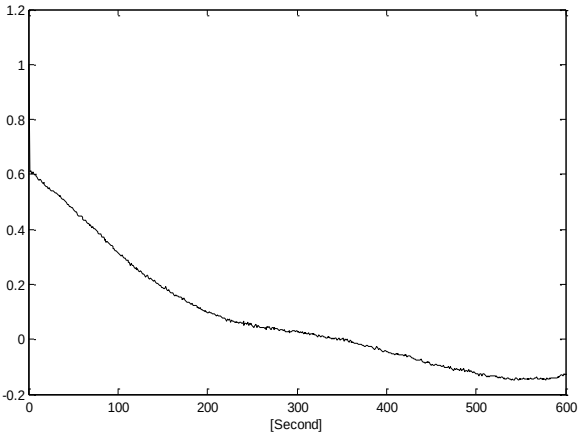

Fig. 3.7b Correlogram of Height (time lag: 0 to 600 second)

The autocorrelation functions of the GPS static coordinate time series (X, Y, H) (Fig. 3.2, Fig. 3.3 and Fig. 3.4) have been separately shown in Fig. 3.5, Fig. 3.6 and Fig. 3.7. In order to get a better understanding of the autocorrelation function, the autocorrelation coefficients of all the GPS static observations (X, Y, H) were zoomed to the first 600 autocorrelation coefficients where the time lag is from 0 to 600 second (Fig. 3.5b, Fig. 3.6b and Fig. 3.7b).

It is known that the autocorrelation of a continuous-time white noise signal will have a strong peak at $i \cdot \Delta t = 0$ and will be absolutely 0 for all other $i \cdot \Delta t$. The results in Fig. 3.5b, Fig. 3.6b and Fig. 3.7b demonstrate that, the autocorrelation functions take the maximum values $R_0 = 1$ at zero shift. But at all other time lag $i \cdot \Delta t$ in Fig. 3.5b, Fig. 3.6b and Fig. 3.7b, these values decrease exponentially. These are colored noise in the GPS observations.

In Fig. 3.5b, Fig. 3.6b and Fig. 3.7b, it is obtained that the GPS measurement deviations are composed of white noises and colored noises. The colored noises follow the exponential distribution, resulting in a correlated coefficient of about 0.6 at $i \cdot \Delta t = 1$. When the time lag $i \cdot \Delta t$ is larger, for example 400 seconds, the autocorrelation of the observations is not so obvious. But when the time lag is smaller, for example 1 second, the autocorrelation coefficient between these two observations becomes larger ($R_1 = 0.6$). Therefore if the GPS receiver collects the observations at a high sampling rate (such as the sampling rate $i \cdot \Delta t = 1$second), the auto-correlated error should be taken into account when processing the GPS coordinate time series. The white noise can be described by the difference of the value 1 at $i \cdot \Delta t = 0$ and 0.6 at $i \cdot \Delta t = 1$. As analyzed above, GPS measurements contain white noise and colored noise which decreases exponentially when the time lag is larger.

3.4 Stochastic model determination of GPS time series

The GPS measurement deviations can be divided into correlating errors and non-correlating errors (Schwieger 1999). The magnitude of the non-correlating and correlating errors can be described by the standard deviations σ_δ and σ_Δ.

As shown in Fig. 3.5b, Fig. 3.6b and Fig. 3.7b, the correlating deviations follow a Gauß-Markov-process with exponentially decreasing autocorrelation function

$$C_l(i) = e^{-\alpha \cdot i \cdot \Delta t} \quad . \tag{3.5}$$

The stochastic model of the measurement deviation is given by (Schwieger 1999; Kuhlmann 2003)

$$\left(\sum_{ll} \right)_{n \times n} = \begin{bmatrix} \sigma_\delta^2 + \sigma_\Delta^2 e^{-\alpha \cdot 0 \cdot \Delta t} & \sigma_\Delta^2 e^{-\alpha \cdot 1 \cdot \Delta t} & \cdots & \sigma_\Delta^2 e^{-\alpha \cdot (n-1) \cdot \Delta t} \\ \sigma_\Delta^2 e^{-\alpha \cdot 1 \cdot \Delta t} & \sigma_\delta^2 + \sigma_\Delta^2 e^{-\alpha \cdot 0 \cdot \Delta t} & \ddots & \vdots \\ \vdots & \ddots & \ddots & \sigma_\Delta^2 e^{-\alpha \cdot 1 \cdot \Delta t} \\ \sigma_\Delta^2 e^{-\alpha \cdot (n-1) \cdot \Delta t} & \cdots & \sigma_\Delta^2 e^{-\alpha \cdot 1 \cdot \Delta t} & \sigma_\delta^2 + \sigma_\Delta^2 e^{-\alpha \cdot 0 \cdot \Delta t} \end{bmatrix} \tag{3.6}$$

3.4.1 Parameter estimation of the stochastic model

In order to calculate three parameters σ_δ, σ_Δ and α in Equation 3.6, the basic idea of the parameter estimation of the stochastic model (Kuhlmann 2003) should be first briefly introduced.

The mean value of *n* observations is given by

$$M = \frac{1}{n} U^T l = Fl \quad \text{with } \left(U^T\right)_{1\times n} = [1 \quad 1 \quad \cdots \quad 1];\ l = [l_1, l_2, \ldots, l_n]^T;\ F = \frac{1}{n} U^T \tag{3.7}$$

According to the variance propagation law,

$$\sigma_M{}^2 = F \sum_{ll} F^T \tag{3.8}$$

the corresponding variance is derived as

$$\sigma_M{}^2 = F \sum_{ll} F^T = \frac{1}{n^2} U^T \sum_{ll} U \tag{3.9}$$

The numerator $U^T \sum_{ll} U$ in Equation 3.9 is the sum of elements of $\sum_{ll}$.

Supposing a Gaussian white noise process with variance σ^2, the covariance matrix of observations is $\sum_{ll} = \sigma^2 I$, thus

$$\sigma_M{}^2 = \frac{1}{n^2} U^T \sum_{ll} U = = \frac{n\sigma^2}{n^2} = \frac{\sigma^2}{n}$$

In case of colored measurement noise in Equation 3.6 this leads to (Meier and Keller 1990)

$$\sigma_M^2 = \frac{1}{n^2} U^T \sum_{ll} U = \frac{1}{n^2}\{n\sigma_\delta{}^2 + n\sigma_\Delta{}^2 + 2[(n-k)\sigma_\Delta{}^2 e^{-\alpha\cdot 1\cdot\Delta t} + (n-k)\sigma_\Delta{}^2 e^{-\alpha\cdot 2\cdot\Delta t} + (n-k)\sigma_\Delta{}^2 e^{-\alpha\cdot 1\cdot\Delta t}$$
$$+ \cdots + (n-k)\sigma_\Delta{}^2 e^{-\alpha\cdot(n-1)\cdot\Delta t} + \cdots + (n-k)\sigma_\Delta{}^2 e^{-\alpha\cdot 2\cdot\Delta t} + (n-k)\sigma_\Delta{}^2 e^{-\alpha\cdot 1\cdot\Delta t}]\}$$

$$\sigma_M^2 = \frac{1}{n}\sigma_\delta{}^2 + \frac{1}{n}\sigma_\Delta{}^2 + \frac{2}{n^2}\sum_{k=1}^{n-1}(n-k)\sigma_\Delta{}^2 e^{-\alpha\cdot k\cdot\Delta t} \tag{3.10}$$

As shown in Equation 3.10, the theoretical standard deviation σ_M is the function of the elements of $\sigma_\delta, \sigma_\Delta, \alpha$ which are unknowns for observations l. s_M can be calculated empirically from different new generating samples of observations. Taking the app. 32400 observations of time series separately in Fig. 3.2, Fig. 3.3 and Fig. 3.4, new samples can be generated by calculating mean values of each group composed of *m* observations. For *m*=10 this leads to a new sample with 3240 mean values. Out of this new sample of mean values, an empirical standard deviation s_M can be calculated. If different numbers *m* have been chosen, all the corresponding empirical standard deviations of the new generating samples can be calculated. Therefore, these three unknown parameters can be estimated by least square adjustment by observed empirical variances s_M^2.

3.4.2 Experiment and result analysis

The GPS observations selected from the GPS static experiment shown in Fig. 3.2, Fig. 3.3 and Fig. 3.4, can be used to estimate of the parameters of the stochastic model for GPS time series. The stochastic model illustrates the noise property of the chosen GPS time series.

3.4.2.1 Calculation of the statistical parameters

The unknown parameters in the statistical model (Equation 3.10) are described as the standard deviation of the uncorrelating errors σ_δ, the standard deviation of the correlating errors σ_Δ and α .

The known parameters s_M^2 can be computed from the selected samples from the GPS experiment given the different numbers *m*. The process to compute the empirical standard deviation s_M is described as follows: first 9 hours observations have been chosen to compute these unknown parameters. As we know, in this GPS static experiment, the sampling rate is 1 second, therefore, 32400 observations are used in total. Given the different numbers *m*, the different new samples can be generated. In each new generating sample, the degree of freedom and the variance can be computed.

Degree of freedom of the new samples

According to the different chosen number of *m*, the degree of freedom ν of each sample can be obtained as

$$\nu = \frac{N}{m} - 1$$

Table 3.1 Degrees of freedom

ID Nr.	1	2	3	4	5	6	7	8	9	10
Number(*m*)	1	2	3	4	5	6	8	9	10	12
Freedom degree	32399	16199	10799	8099	6479	5399	4049	3599	3239	2699
ID Nr.	11	12	13	14	15	16	17	18	19	20
Number(*m*)	15	16	18	20	24	25	27	30	36	40
Freedom degree	2159	2024	1799	619	1349	1295	1199	1079	899	809
ID Nr.	21	22	23	24	25	26	27	28	29	30
Number(*m*)	45	50	54	60	72	75	80	81	90	100
Freedom degree	719	647	599	539	449	431	404	399	359	323
ID Nr.	31	32	33	34	35	36	37	38	39	40
Number(*m*)	108	135	162	200	225	270	300	400	450	600
Freedom degree	299	239	199	161	143	119	107	80	71	53

Variance of the new samples

According to different number *m*, the variance of each new generating sample is shown in Table 3.2, Table 3.3 and Table 3.4.

The equation of the variance is given as

$$s^2 = \frac{1}{n-1}\sum_{i=1}^{n}(x_i - M)^2$$

where x_i denotes the mean value of every group of m observations and n is the number of elements in each new sample, $n = N/m$

Table 3.2 Empirical variances of the new samples (X-coordinate)

	1	2	3	4	5	6	7	8	9	10
Number(m)	1	2	3	4	5	6	8	9	10	12
Empirical Variance (mm^2)	25.03	19.60	17.80	16.81	16.23	15.89	15.34	15.10	15.01	14.77
	11	12	13	14	15	16	17	18	19	20
Number(m)	15	16	18	20	24	25	27	30	36	40
Empirical Variance (mm^2)	14.45	14.39	14.22	14.15	13.93	13.84	13.72	13.69	13.40	13.20
	21	22	23	24	25	26	27	28	29	30
Number(m)	45	50	54	60	72	75	80	81	90	100
Variance (mm^2)	13.14	12.91	12.83	12.78	12.32	12.43	12.06	12.11	11.82	11.60
	31	32	33	34	35	36	37	38	39	40
Number(m)	108	135	162	200	225	270	300	400	450	600
Empirical Variance (mm^2)	11.52	10.69	10.21	9.67	8.58	7.94	7.34	5.26	5.02	3.91

Table 3.3 Empirical variances of the new samples (Y-coordinate)

	1	2	3	4	5	6	7	8	9	10
Number(m)	1	2	3	4	5	6	8	9	10	12
Empirical Variance (mm^2)	6.65	5.10	4.59	4.31	4.16	4.04	3.89	3.86	3.81	3.74
	11	12	13	14	15	16	17	18	19	20
Number(m)	15	16	18	20	24	25	27	30	36	40
Empirical Variance (mm^2)	3.66	3.64	3.59	3.56	3.51	3.50	3.47	3.43	3.37	3.33
	21	22	23	24	25	26	27	28	29	30
Number(m)	45	50	54	60	72	75	80	81	90	100
Empirical Variance (mm^2)	3.28	3.24	3.21	3.15	3.06	3.05	2.98	2.99	2.91	2.85
	31	32	33	34	35	36	37	38	39	40
Number(m)	108	135	162	200	225	270	300	400	450	600
Empirical Variance (mm^2)	2.84	2.64	2.48	2.20	2.19	1.94	1.85	1.48	1.45	0.96

Table 3.4 Empirical variances of the new samples (Height-coordinate)

	1	2	3	4	5	6	7	8	9	10
Number(*m*)	1	2	3	4	5	6	8	9	10	12
Empirical Variance (mm^2)	55.14	44.44	40.91	38.90	37.98	37.23	36.25	35.86	35.62	35.14
	11	12	13	14	15	16	17	18	19	20
Number(*m*)	15	16	18	20	24	25	27	30	36	40
Empirical Variance (mm^2)	34.58	34.45	34.29	34.04	33.54	33.47	33.38	33.06	32.58	32.37
	21	22	23	24	25	26	27	28	29	30
Number(*m*)	45	50	54	60	72	75	80	81	90	100
Empirical Variance (mm^2)	32.17	31.74	31.69	31.20	30.47	30.22	29.87	29.60	29.65	29.04
	31	32	33	34	35	36	37	38	39	40
Number	108	135	162	200	225	270	300	400	450	600
Empirical variance(mm^2)	28.11	26.81	25.28	24.25	21.15	20.97	19.29	16.47	15.47	13.65

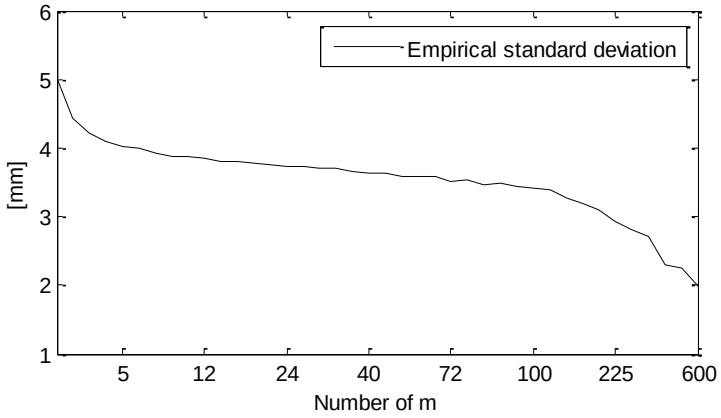

Fig. 3.8 Empirical standard deviations of X-coordinate

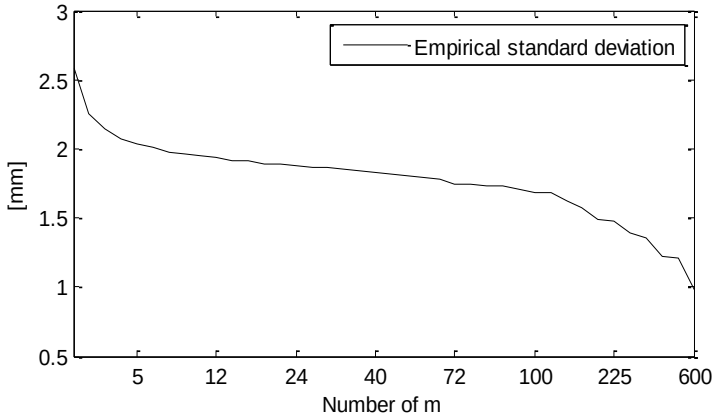

Fig. 3.9 Empirical standard deviations of Y-coordinate

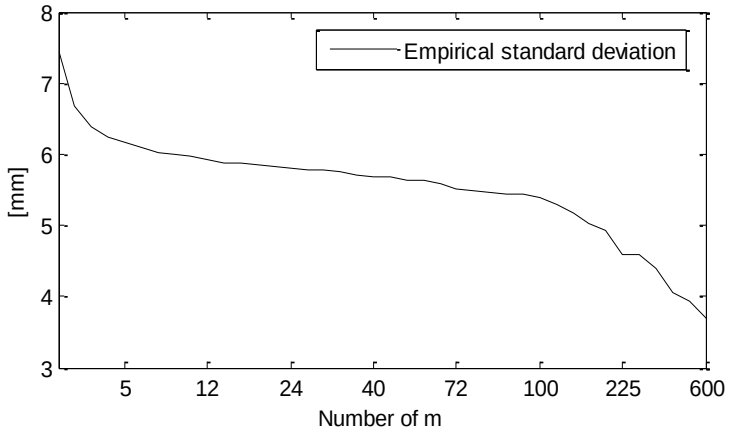

Fig. 3.10 Empirical standard deviations of Height-coordinate

Results of the three parameters in the stochastic model

The results of the parameters of stochastic model for the coordinates (X, Y, H) are calculated based on least square adjustment, neglecting that variances σ_M^2 follow a χ^2 distribution. For $\nu > 10$, χ^2 distribution is asymptotically equal to normal distribution (Mikhail 1976).These results are shown as follows:

Table 3.5 Parameters results (X coordinate)

Unkown parameters	Results	Standard deviations (mm)
α	0.0090	0.00066 1/s
σ_δ	3.21	0.18
σ_Δ	3.68	0.098

Table 3.6 Parameters results (Y coordinate)

Unkown parameters	Results	Standard deviations (mm)
α	0.0089	0.00066 1/s
σ_δ	1.71	0.085
σ_Δ	1.86	0.045

Table 3.7 Parameters results (Height)

Unkown parameters	Results	Standard deviations (mm)
α	0.0062	0.0004 1/s
σ_δ	4.53	0.18
σ_Δ	5.75	0.12

To show the quality of the adjustment, the adjusted standard deviations are shown in Table 3.8, Table 3.9 and Table 3.10.

Table 3.8 Empirical and adjusted variances under different numbers *m* (X-coordinate time series)

Number	1	2	3	4	5	6	8	9	10	12
Empirical Variances(mm^2)	25.03	19.60	17.80	16.81	16.23	15.89	15.34	15.10	15.01	14.77
Adjusted Variances(mm^2)	23.83	18.63	16.87	15.97	15.41	15.03	14.52	14.34	14.18	13.94
Number	15	16	18	20	24	25	27	30	36	40
Empirical Variances(mm^2)	14.45	14.39	14.22	14.15	13.93	13.84	13.72	13.69	13.40	13.20
Adjusted Variances(mm^2)	13.65	13.57	13.42	13.29	13.06	13.00	12.90	12.76	12.49	12.32
Number	45	50	54	60	72	75	80	81	90	100
Empirical Variances(mm^2)	13.14	12.91	12.83	12.78	12.32	12.43	12.06	12.11	11.82	11.60
Adjusted Variances(mm^2)	12.13	11.94	11.79	11.58	11.19	11.10	10.94	10.91	10.65	10.37
Number	108	135	162	200	225	270	300	400	450	600
Empirical Variances(mm^2)	11.52	10.69	10.21	9.67	8.58	7.94	7.34	5.26	5.02	3.91
Adjusted Variances(mm^2)	10.15	9.48	8.88	8.14	7.70	7.02	6.62	5.53	5.10	4.12

Table 3.9 Empirical and adjusted variances under different numbers *m* (Y-coordinate time series)

Number	1	2	3	4	5	6	8	9	10	12
Empirical Variances(mm^2)	6.65	5.10	4.59	4.31	4.16	4.04	3.89	3.86	3.81	3.74
Adjusted Variances(mm^2)	6.38	4.90	4.40	4.15	3.99	3.89	3.74	3.69	3.65	3.58
Number	15	16	18	20	24	25	27	30	36	40
Empirical Variances(mm^2)	3.66	3.64	3.59	3.56	3.51	3.50	3.47	3.43	3.37	3.33
Adjusted Variances(mm^2)	3.50	3.48	3.44	3.41	3.35	3.33	3.30	3.27	3.20	3.15
Number	45	50	54	60	72	75	80	81	90	100
Empirical Variances(mm^2)	3.28	3.24	3.21	3.15	3.06	3.05	2.98	2.99	2.91	2.85
Adjusted Variances(mm^2)	3.10	3.05	3.02	2.96	2.86	2.84	2.80	2.79	2.72	2.65
Number	108	135	162	200	225	270	300	400	450	600
Empirical Variances(mm^2)	2.84	2.64	2.48	2.20	2.19	1.94	1.85	1.48	1.45	0.96
Adjusted Variances(mm^2)	2.60	2.42	2.27	2.08	1.97	1.80	1.69	1.42	1.31	1.06

Table 3.10 Empirical and adjusted variances under different numbers *m* (Height-coordinate time series)

Number	1	2	3	4	5	6	8	9	10	12
Empirical Variances(mm^2)	55.14	44.44	40.91	38.90	37.98	37.23	36.25	35.86	35.62	35.14
Adjusted Variances(mm^2)	53.57	43.22	39.72	37.94	36.84	36.09	35.10	34.74	34.45	33.97
Number	15	16	18	20	24	25	27	30	36	40
Empirical Variances(mm^2)	34.58	34.45	34.29	34.04	33.54	33.47	33.38	33.06	32.58	32.37
Adjusted Variances(mm^2)	33.43	33.28	33.01	32.77	32.34	32.24	32.05	31.79	31.30	31.00
Number	45	50	54	60	72	75	80	81	90	100
Empirical Variances(mm^2)	32.17	31.74	31.69	31.20	30.47	30.22	29.87	29.60	29.65	29.04
Adjusted Variances(mm^2)	30.64	30.30	30.04	29.65	28.92	28.75	28.46	28.40	27.90	27.36
Number	108	135	162	200	225	270	300	400	450	600
Empirical Variances(mm^2)	28.11	26.81	25.28	24.25	21.15	20.97	19.29	16.47	15.47	13.65
Adjusted Variances(mm^2)	26.95	25.62	24.41	22.85	21.92	20.38	19.46	16.84	15.75	13.13

3.4.2.2 Results analysis

Fig. 3.8, Fig. 3.9, and Fig. 3.10 illustrate that the decrease of empirical standard deviation is less than it should be for white noise. It also demonstrates that the colored noise exists in GPS observations. The similar conclusion can be obtained from the results in Table 3.8, Table 3.9 and Table 3.10. In order to have an in-depth understanding of the colored noise, the correlation coefficients of the colored noise of GPS observations at different time intervals are shown in Table 3.11. Table 3.11 demonstrates that there is high auto-correlation of the colored noise. However when the time interval is more than 5 min, the correlation coefficient of the colored noise is nearly zero; the white noise assumption is fulfilled in practice. In our case the sampling rate $\Delta t = 1$ second belongs to the high sampling rate, the colored noise of the measurement deviations should be taken into account.

Table 3.11 Autocorrelation coefficients of the coloured noise of GPS observations at different time intervals

Δt	α	1 s	5 s	10 s	30 s	1min	5min	10min
ρ_x	0.0089	0.99	0.96	0.91	0.76	0.58	0.06	0.004
ρ_y	0.0090	0.99	0.96	0.91	0.76	0.59	0.07	0.005
ρ_h	0.0062	0.99	0.97	0.94	0.83	0.69	0.16	0.02

According to the results above, the autocorrelation coefficients of the colored noise in X-coordinate observations are similar to that of Y-coordinate observations. The coloured noise of height observation time series has a higher autocorrelation than that of the coordinate components X and Y time series. That is because the height is more easily affected by the systematic error sources, for example, troposphere propagation errors and multipath errors. The autocorrelation of height observations is stronger than the autocorrelation of X or Y observations.

Summary

The GPS coordinate real-time series are analyzed by the autocorrelation function. The GPS real-time measurement deviations are correlated. Therefore in the deformation data analysis it is not proper to just take the measurement deviations as the white noise. The property of the noise has been explored in detail, especially the determination of the correlated error property of the GPS coordinate time series. The methods of determining the stochastic model of GPS coordinate (X, Y, H) measurement deviations are discussed in detail. The results show that the GPS real–time measurement deviations have a high autocorrelation, which should be considered in the GPS high-precision positioning.

4 Models to Process GPS Real-time Series

Real-time GPS technology is an important tool to monitor continuous deformation of natural disasters and structures. In these applications, it requires GPS position coordinates with high accuracy. However, as analyzed in the last chapter, the error sources that restrain the accuracy of the GPS positioning solutions are the multipath effect, the atmosphere propagation error, inaccurate orbits information, etc. Because of the high sampling rate, time dependent systematic deviations arise in neighbouring epochs in a similar way, which results into autocorrelation. Thus GPS observations contain colored random noise which negatively affects the deformation analysis. Three different methods will be used to reduce the colored noise in the GPS time series: the Kalman filter model with a shaping filter, the Sequential algorithm and the Finite impulse response (FIR) filter. The merits and the limitations of each method will be discussed in detail based on the GPS coordinates time series analysis.

4.1 Kalman filter model with a shaping filter

The Kalman filter is an important tool for deformation analysis combining information on object behavior and measurement quantities. System and measurement equation are combined in a well-known algorithm for estimating an optimal state vector X, containing parameters describing deformation behavior (Welsch et. al. 2000). Due to the recursive algorithm -working from epoch t_{k-1} to t_k - the Kalman filter is applicable in real time.

However, the Kalman filter requires white noise. As mentioned in Chapter 3, it is proved that the GPS observations with high sampling rates are correlated. If there are non-white noises in the system model or measurement model, the state vector can be augmented by appending the shaping filter to the state vector components of Kalman filter (Grewal 2001; Kuhlmann 2003). In this way a shaping filter can describe long movement of the colored noise. Therefore, Kalman filter model with a shaping filter can be applied to process the GPS observations with high sampling rates. The principle of Kalman filter model with a shaping filter is introduced.

4.1.1 Principle of Kalman filter model with a shaping filter

In order to have a better understanding of the principle of Kalman filter model with a shaping filter, the principles of Kalman filter and Shaping filter should be explained in detail separately, and then comes to the introduction of the modified Kalman filter model.

4.1.1.1 Principle of Kalman filter

The Kalman filter, first derived by Kalman (1960) for use in electrical control systems, is a widely used method to process the real-time series nowadays. The Kalman filter is an optimal recur-

sive data processing algorithm. The user does not need to save previous observations; instead, all previous information is carried forward in the filter.

Let us start with a continuous process described by the linear, time varying mathematical model

$$\dot{X}(t) = F(t)X(t) + G(t)U(t) + C(t)\Omega(t) \tag{4.1}$$

where *F(t)* denotes the coefficient matrix of state vector; *U(t)* is input forces of the system equation; *G(t)* is the coefficient matrix of the input forces; *Ω(t)* is the system noise and *C(t)* denotes its coefficient matrix *Ω*.

The solution of the general mathematical model is composed by the solution of the homogeneous part $\dot{X}(t) = F(t)X(t)$ and the particular solution of Equation 4.1. First if an matrix-valued function $\Phi(t)$ satisfies the conditions $\dot{\Phi}(t) = F(t)\Phi(t)$ and $\Phi(0) = I_n$, the $n \times n$ identity matrix, then $\Phi(t)$ is a fundamental solution of the homogeneous part $\dot{X}(t) = F(t)X(t)$ on the interval $t \in [0, T]$. Additionally, for any possible initial vector $X(0)$, the vector $X(t) = \Phi(t)X(0)$ satisfies the equation $\dot{X}(t) = F(t)X(t)$. That is, $X(t) = \Phi(t)X(0)$ is the solution of the homogeneous equation $\dot{X}(t) = F(t)X(t)$ with initial value $X(0)$. $\Phi(t)$ transforms any initial state $X(0)$ of the dynamic system to the corresponding state $X(t)$ at time t. If $\Phi(t)$ is nonsingular, then the products $\Phi^{-1}(t)X(t) = X(0)$ and $\Phi(\tau)\Phi^{-1}(t)X(t) = X(\tau)$. That is, the matrix product $\Phi(\tau, t) = \Phi(\tau)\Phi^{-1}(t)$ transforms a solution from time *t* to the corresponding solution at time *τ*. The matrix $\Phi(\tau, t)$ is called the state transition matrix. The state transition matrix demonstrates the transition to the state at time *τ* from the state at time t (Grewal and Andrews 2001).

The solution of Equation 4.1 is given

$$\begin{aligned} X(t) &= \Phi(t_0, t)X(t_0) + \int_{t_0}^{t} \Phi(t, \tau)\left[G(\tau)U(\tau) + C(\tau)\Omega(\tau)\right]d\tau \\ &= \Phi(t)\Phi^{-1}(t_0)X(t_0) + \Phi(t)\int_{t_0}^{t} \Phi^{-1}(\tau)\left[G(\tau)U(\tau) + C(\tau)\Omega(\tau)\right]d\tau \end{aligned} \tag{4.2}$$

If there are no input forces then the solution of this linear differential equation can be written as

$$X(t) = \Phi(t_0, t)X(t) + \int_{t_0}^{t} \Phi(t, \tau)C(\tau)\Omega(\tau)d\tau \tag{4.3}$$

Discrete-time processes may arise in either of two following ways. First, a sequence of events takes place naturally in discrete steps. A sequence of chance experiments, such as the discrete random-walk problems of statistics, might occur in discrete steps. Discrete-time processes may also arise from sampling a continuous process at discrete times. One possibility is that the sampling is intentional and is under the control of the designer, as is the case when analog data are converted to digital form. Or another possibility is that the sampling is unintentional and forced on us by a measurement constraint that allows observation of the process only at discrete points in time (Brown and Hwang 1997).

If one is only interested in the system state at discrete time epochs $t_0, t_1, \ldots, t_k \ldots$, then one can use the formula

$$X(t_k) = \Phi(t_{k-1}, t_k) X(t) + \int_{t_{k-1}}^{t_k} \Phi(t,\tau) C(\tau) \Omega(\tau) d\tau \tag{4.4}$$

Let $\omega(t_k) = \int_{t_{k-1}}^{t_k} \Phi(t,\tau) C(\tau) \Omega(\tau) d\tau$,

where $\omega(t_k)$ is a white sequence in the discrete model.

Shorthand notation for discrete time system

It is more efficient to shorten $X(t_k)$ to X_k, so long as it is understood that it stand for $X(t_k)$, and not the *k*th component of X. If one must refer to a particular component at a particular time, one can resort to writing $X_i(k)$ to remove any ambiguity. It is better to drop *t* as a symbol when we are talking about discrete-time systems.

The system equation is described by (Welch and Bishop 2006)

$$X_k = \Phi_{k-1,k} X_{k-1} + \omega_k \tag{4.5}$$

where X_k, X_{k-1} are the state vectors at different epochs t_k and t_{k-1} which represent all the main characteristics of the dynamic system. The measurement of the process is assumed to occur at discrete points in time in accordance with the linear relationship

$$L_k = H_k X_k + \varepsilon_k \tag{4.6}$$

where L_k is the measurement vector at epoch t_k; H_k is the observation transition matrix; ε_k is the measurement noise.

The covariance matrices for the ω_k and ε_k are given by

$$E\left[\omega_k \omega_i^T\right] = \begin{cases} Q_k, & i = k \\ 0, & i \neq k \end{cases} \tag{4.7}$$

$$E\left[\varepsilon_k \varepsilon_i^T\right] = \begin{cases} R_k, & i = k \\ 0, & i \neq k \end{cases} \tag{4.8}$$

$$E\left[\omega_k \varepsilon_i^T\right] = 0 \qquad \text{for all } k \text{ and } i \tag{4.9}$$

The Kalman filter recursively evaluates an optimal estimate of the state of a linear system (Kalman 1960; Gelb 1974; Strang and Borre 1997; Welch and Bishop 2006). The Kalman filter process consists of two sub-processes: i.e. the time update process and the measurement update process (Welch and Bishop 2006). The time update equations are

$$\bar{X}_k = \Phi_{k-1,k} \hat{X}_{k-1} \tag{4.10}$$

$$P_{\bar{X}_k} = \Phi_{k-1,k} P_{\hat{X}_{k-1}} \Phi_{k-1,k}^T + Q_k \tag{4.11}$$

where $\bar{X}_k$ is the predicted value of the state vector, and $\hat{X}_{k-1}$ is the optimal estimator of the state vector at the previous epoch t_{k-1}; $P_{\bar{X}_k}$ is the covariance matrix of $\bar{X}_k$, and $P_{\hat{X}_{k-1}}$ is the covariance matrix of $\hat{X}_{k-1}$; The measurement update equations are:

$$G_k = P_{\bar{X}_k} H_k^T (H_k P_{\bar{X}_k} H_k^T + R)^{-1} \quad (4.12)$$

$$V_k = L_k - H_k \bar{X}_k \quad (4.13)$$

$$Q_{V_k} = H_k P_{\bar{X}_k} H_k^T + R \quad (4.14)$$

$$\hat{X}_k = \bar{X}_{k-1} + G_k V_k \quad (4.15)$$

$$P_{\hat{X}_k} = (I - G_k H_k) P_{\bar{X}_k} \quad (4.16)$$

where G_k is the Kalman gain matrix; V_k is the prediction error between the measurement vector and the predicted measurement which is called the innovation and Q_{V_k} is the covariance matrix of V_k.

In the measurement update process, the newest updated state estimate $\hat{X}_k$ is computed by using the predicted value of the state vector $\bar{X}_k$ and the newest observations. The minimum mean-square error is used as the performance criterion. The generalized likelihood ratio test using the Kalman filter innovation V_k is one of the approaches to detect the changes in the time series (Willsky 1976; Teussian 1990; Okatan et al. 2007).

Because of the presence of the system's noise, the predicted state is usually less precise than the previous filtered results. Due to the additional measurements, however, the filtered results are usually of a better precision than its predicted counterpart.

The Kalman filter satisfies the three general optimality conditions as given in the Equations 4.17-4.19 (Mikhail 1976)

Consistence

$$\lim_{n\to\infty} P(\left|\hat{X}_k - X\right| < \xi) = 1 \quad (4.17)$$

Unbiased

$$E(\hat{X}_k) = X \quad (4.18)$$

Minimum mean square error

$$E\left\{(\hat{X} - E(\hat{X}_k))^T (\hat{X} - E(\hat{X}_k))\right\} = \min \quad (4.19)$$

where n denotes the sample size; ξ denotes a very small value; P is the statistical probability and E is the statistical expectation.

4.1.1.2 Shaping filter

The demand for increasing accuracy has required a deeper understanding of GPS position errors and methods to reduce or eliminate them. It is known that for the standard Kalman filter model, the noises in the system model and measurement model are white Gaussian noises which are not correlated with any other random variables. But in many real cases, it may not be justified to assume that all noises are white Gaussian noise processes. It is useful to generate an autocorrelation function from real-time series and then develop an appropriate noise model using differential or difference equations. These models are called shaping filters. If there are non-white noises

in the system model or measurement model, the state vector can be augmented by appending the shaping filter to the state vector components of the Kalman filter (Grewal 2001).

In case the GPS receiver provides the real-time measurements with the sampling rate, the time-correlated measurement noise exists in the measurement equation. The measurement equation includes not only the white noise but also the colored noise. The state vector is augmented by another variable x_{sf} that is used to describe the long term movement of correlating measurement deviations.

The new augmented state vector is defined as

$$X_k = \begin{bmatrix} x_1(k) \\ x_{sf}(k) \end{bmatrix} \tag{4.20}$$

where $x_1(k)$ denotes the state vector of GPS coordinates or other vectors (velocities, accelerations).

The measurement equation can be augmented as

$$L_k = H_k x_1(k) + x_{sf}(k) + \varepsilon_k \tag{4.21}$$

Let the colored noise of the measurements be modeled by the difference equations

$$x_{sf}(k) = \Phi_{sf}(k-1,k)x_{sf}(k-1) + B_{sf}(k)\omega_2(k) \tag{4.22}$$

where $\Phi_{sf}(k-1,k)$ and $B_{sf}(k)$ are the coefficient matrices, $\omega_2(k)$ denotes the zero-mean white noise.

The system equation can be augmented by the shaping filter

$$\begin{bmatrix} x_1(k) \\ x_{sf}(k) \end{bmatrix} = \begin{bmatrix} \Phi_{k,k-1} & 0 \\ 0 & \Phi_{sf}(k,k-1) \end{bmatrix} \begin{bmatrix} x_1(k-1) \\ x_{sf}(k-1) \end{bmatrix} + \begin{bmatrix} 1 & 0 \\ 0 & B_{sf}(k) \end{bmatrix} \begin{bmatrix} \omega_1(k) \\ \omega_2(k) \end{bmatrix} \tag{4.23}$$

4.1.1.3 Different Kalman filter models with shaping filters

The motivation for this investigation is a landslide problem. GPS can be used to monitor the movement of a landslide. With the development of the electronic technologies, GPS receivers can provide positions with high sampling rates. Due to the high sampling rates used today, time dependent systematic deviations arise in neighboring epochs in a similar way resulting into auto-correlation. Because of the correlated noise in GPS real-time measurements, the shaping filter x_{sf} is used to describe the long-term movement of correlated measurement deviations.

In our case, short measurement periods deviations are following a Gauss-Markov-process with correlation function

$$C(\tau) = e^{-\alpha|\tau|}$$

For a Gauss-Markov-Process with auto-correlation function, the following differential equation representing a linear dynamic system is suitable (Schrick 1977)

$$\dot{x}_{sf}(t) = -\alpha x_{sf}(t) + \omega_2(t) \tag{4.24}$$

The piecewise solution leads to the following equation as second part of the system equation

$$x_{sf}(k+1) = e^{-\alpha\Delta t} x_{sf}(k) + e^{-\alpha\Delta t}\omega_2(k) \tag{4.25}$$

where the state variable x_{sf} describes the long term movement of correlating measurement deviations. The system noise ω_2 is a white noise process. Equation 4.25 can be considered as the second part of the system equation.

The deformation models can be classified into the identity model, the static deformation model, the kinematic deformation model and the dynamic deformation model. In the dynamic deformation model, the deformations as the output signal are a function of time and (varying) loads; in the static systems the deformations are a function of (varying) loads only; in the kinematic deformation model the deformation can be described as a function of time; in the identity deformation model the motion is random, a function of time cannot be established (Kuhlmann and Pelzer 1997). The landslide in Schwabian Alb area moves very slow, e.g. the velocity is 12 cm/year. When the GPS is used to observe the movement of the surface, there are no acting forces available, the deformation can be considered as a random-walk-process (Identity model) or a kinematic model.

The identity model with a shaping filter can be described as follows:

$$\begin{bmatrix} x_1(k) \\ x_{sf}(k) \end{bmatrix} = \begin{bmatrix} I & 0 \\ 0 & e^{-\alpha\Delta t} I \end{bmatrix} \begin{bmatrix} x_1(k-1) \\ x_{sf}(k-1) \end{bmatrix} + \begin{bmatrix} \Delta t I & 0 \\ 0 & e^{-\alpha\Delta t} I \end{bmatrix} \begin{bmatrix} \omega_1(k) \\ \omega_2(k) \end{bmatrix} \tag{4.26}$$

$$l(k) = \begin{bmatrix} I & I \end{bmatrix} \begin{bmatrix} x_1(k) \\ x_{sf}(k) \end{bmatrix} + \varepsilon(k) \tag{4.27}$$

If state vector includes the position coordinates and their velocities or if the state vector contains the position coordinates, velocities and accelerations, then the kinematic model can be chosen. For example, the kinematic model with a shaping filter whose state vector contains positions and velocities is shown as follows

$$\begin{bmatrix} x_1(k) \\ \dot{x}_1(k) \\ x_{sf}(k) \end{bmatrix} = \begin{bmatrix} I & \Delta t I & 0 \\ 0 & I & 0 \\ 0 & 0 & e^{-\alpha\Delta t} I \end{bmatrix} \begin{bmatrix} x_1(k-1) \\ \dot{x}_1(k-1) \\ x_{sf}(k-1) \end{bmatrix} + \begin{bmatrix} 0.5\Delta t^2 I & 0 \\ \Delta t I & 0 \\ 0 & e^{-\alpha\Delta t} I \end{bmatrix} \begin{bmatrix} \omega_1(k) \\ \omega_2(k) \end{bmatrix} \tag{4.28}$$

$$l(k) = \begin{bmatrix} I & 0 & I \end{bmatrix} \begin{bmatrix} x_1(k) \\ \dot{x}_1(k) \\ x_{sf}(k) \end{bmatrix} + \varepsilon(k) \tag{4.29}$$

Note that the size of I is same to the dimension of state vector $x_1(k)$. In the following application $x_1(k)$ is selected as the height component of GPS coordinates.

4.1.2 Application in the stepwise deformation time series

The deformation time series includes different types of movements. The stepwise change is one type of the landslide deformation (e.g. Fig. 4.2). When GPS measurements are taken, an observation may be for any reason grossly falsified. Such an observation is said to contain an outlier. In

case of high sampling rates, the GPS time series could be composed of white noise, colored noise, outliers and deformations. The main tasks of this subsection are how to reduce the affections of the white noise, colored noise and outliers of the GPS time series and how to detect the smaller deformation with less time delay.

Kalman filter with a shaping filter is used to reduce the white noise and the colored noise in the GPS time series. If there are outliers in the time series, the outliers must be detected and the affections must be reduced. In case of the stepwise deformations, there are some similarities and differences between the stepwise deformations and outliers in the GPS time series, so the Kalman filter model with a shaping filter can be modified to detect deformations and outliers simultaneously. The simulated time series and the GPS time series have been used to test the modified algorithm and the results demonstrate that the robustness of the proposed algorithm has been improved and the deformation epochs have been detected with short time delay. The modification of the Kalman filter with a shaping filter and the result analysis of the experiment will be given in the following parts.

4.1.2.1 Modification of the Kalman filter model with a shaping filter

In order to monitor and control the quality of the GPS stepwise time series, the modified algorithm aims at detecting the deformation and the outlier with short time delay. It is described in detail in the following.

Algorithm of detecting deformations and outliers

It aims at developing algorithms which can detect the deformation and the outlier with short time delay when processing the stepwise deformation time series. In this case the residuals $(x_1(k)-u)$ are defined as the differences between the filtered results and the true values and are assumed to follow the normal distribution, neglecting the processed results of the correlation between different epochs . If there are no changes in the time series, for example no deformation or no outlier in the GPS time series, the residual $(x_1(k)-u)$ between the filtered results $x_1(k)$ and the estimated true value u, from a statistical point of view, should follow the normal distribution with a zero mean μ and a variance σ^2. If the GPS time series contains stepwise deformations or outliers, the residual $(x_1(k)-u)$ does not follow the normal distribution at the epoch k when a stepwise deformation or an outlier occurs.

When the hypothesis test is applied to test the changes in the GPS time series, firstly, the statistical properties of the residual time series should be computed based on large data samples. For example, n static GPS observations have been chosen and processed by the Kalman filter model with a shaping filter. The empirical variance s^2 of the residual time series is obtained by the Equation 4.30

$$s^2 = \frac{1}{n-1}\sum_{k=1}^{n}(x_1(k) - u - \mu)^2 \tag{4.30}$$

where $x_1(k)$ denotes the filtered result of the selected GPS time series; u is the mean value of the filtered results in the GPS static time series $u = \frac{1}{n}\sum_{k=1}^{n} x_1(k)$. In case of the GPS time series the mean value of the residual result $\mu = 0$.

Because of the large data set collected during the static GPS experiment in Chap.3.3.2, the empirical determined covariance factor is determined as a priori known quality.

The test factor

$$T_{est} = \frac{|x_1(k) - u_0|}{s} \tag{4.31}$$

is used to detect these changes. Here u_0 is the initial value of the state vector x_1 which can be computed as the mean value of the former epoch's filtered results.

By the hypothesis testing, the null hypothesis H_0 $x_1(k) = u_0$ seeks to test that the distribution of the residual time series is equal to some a priori known distribution. In this case it follows a normal distribution. The alternative hypothesis H_a $x_1(k) \neq u_0$ means that T_{est} doesn't follow the normal distribution at the epochs when a deformation or an outlier occurs. With a given significance level α, we can get the boundary z_α of T_{est} from the normal distribution table.

When the null hypothesis is rejected, this means that it is possible to detect the residual time series which does not follow the normal distribution. The change may be caused by a deformation or an outlier. This test can detect the change but it cannot distinguish if it is caused by an outlier or a deformation.

The difference between the deformation and the outlier is that the outlier occurs isolated, that means that the test should be accepted at the next following epochs. The test factor T_{est} will change suddenly and then still follow the normal distribution for the next following epochs. The situation is different when a deformation occurs. If there is a deformation, the observations at this epoch and the next following epochs are all changed and as a consequence the test factor T_{est} will not follow the normal distribution any more at the following epochs.

To make use of the described behavior another factor *j* is used. *J* is the number of continuous rejected tests. If *j* is smaller than a chosen boundary *J*, it means that an outlier occurs. If *j* is larger than the boundary *J*, a deformation is found.

Thus, the test factors T_{est} and *J* are two factors to distinguish outliers and deformations. The test factors T_{est} and *J* should detect the deformation epochs with short time delay and generate less false alarms (when a deformation is detected, the system will generate an alarm). Hence, a suitable decision for the factors is important. Of course according to different significance levels and

different sampling rates, J is selected as different numbers. The selection of J requires considerable experience and the knowledge of the GPS time series.

The above hypothesis test are carried out with defined some a priori known distribution. Although it is possible to develop other statistic test factor, we will restrict ourselves to the defined distribution in the thesis.

Modification of the filtered results when an outlier is detected

Generally, there are two different concepts for dealing with the outliers in the observations. One basic attempt is to try to identify and eliminate outliers and blunders within the input observations. The alternative way is to use robust methods, which are less sensitive to outliers. Such robust methods have been extensively studied during the last two or three decades and were successfully applied in various geodetic fields.

In this case the robust method is selected to modify the Kalman filter with a shaping filter and reduce the outlier's influence on the estimation of the state vector after the detection of the outlier. The gain matrix must be modified, because the outlier affects the filtered results by the gain matrix. The method accepted here is based on the idea of the equivalent weights function (Yang 2002). If an outlier occurs, the modified Kalman gain matrix G_k is constructed as follows:

$$\gamma_k = \begin{cases} 1 & |C_k| < c_0 \\ \dfrac{c_0}{|C_k|}\left(\dfrac{c_1 - |C_k|}{c_1 - c_0}\right) & c_0 < |C_k| < c_1 \\ 0 & |C_k| > c_1 \end{cases} \qquad (4.32)$$

$$G_k = G_k \cdot \gamma_k$$

where c_0 and c_1 are two constants, usually chosen as 2.0-3.0 and 4.5-8.5 respectively; $V_i(k) = L_i(k) - H_i(k)\bar{X}_k$ and $C_k = |V_i(k)|\, Q_{V_i,V_i}(k)^{-1/2}$; $H_i(k)$ is the i_{th} row vector of the observation transition matrix; $V_i(k)$ and $L_i(k)$ are i_{th} element of V and L at epoch k.

Determination of the new initial value at the epoch when a deformation is detected

As we know, if a deformation is detected, the initial state value μ_0 is changed to a new value which should be equal to the new deformation result $x_{1new}(k)$. Another stepwise change can be found afterwards. Three different methods are discussed to determine the new deformation value as the new initial mean value (Li and Kuhlmann 2008a).

a) 1st Method

According to the idea of the equivalent weight function, the weight of the observations can be changed. When a deformation occurs, the observations play a main role. Hence, the weight of the observations should be increased. Because the gain matrix can be considered as the weight of the observations, the gain matrix of $x_1(k)$ is modified as follows:

$$G_1(k) = \frac{|\hat{x}_1(k) - u_0|}{\sigma} \cdot G_1(k) \tag{4.33}$$

where u_0 is the initial value of $x_1(k)$.

The new state vector $X_{new}(k)$ can be obtained as

$$X_{new}(k) = \begin{bmatrix} x_{1new}(k) \\ x_{2new}(k) \end{bmatrix} = \begin{bmatrix} \overline{x}_1(k) + \frac{|\hat{x}_1(k) - u_0|}{\sigma} \cdot G_1(k) \cdot V_1(k) \\ \mathrm{e}^{-\alpha\Delta t}\, x_2(k-1) \end{bmatrix} \tag{4.34}$$

b) 2nd Method

If a deformation occurs at epoch t_k, the system equation does not describe the transformation between two neighboring state vectors correctly. But the state vector's value at epoch t_k can be obtained from the measurement equation. As we know, the colored noise is correlated and follows the exponential function; we can get the predicted colored noise's value at epoch t_k $x_2(k)$. That is $x_2(k) = \mathrm{e}^{-\alpha\Delta t}\, x_2(k-1)$.

From the measurement equation,

$$l(k) = \begin{bmatrix} 1 & 1 \end{bmatrix} \begin{bmatrix} x_1(k) \\ x_2(k) \end{bmatrix} + \varepsilon(k) = x_1(k) + x_2(k) + \varepsilon(k)$$

the state vector's approximate value at epoch t_k can be obtained

$$x_{2new}(k) = \mathrm{e}^{-\alpha\Delta t}\, \hat{x}_2(k-1) \tag{4.35}$$

$$x_{1new}(k) = l(k) - x_{2new}(k) \tag{4.36}$$

The new state vector $x_{new}(k)$ can be obtained as

$$x_{new}(k) = \begin{bmatrix} x_{1new}(k) \\ x_{2new}(k) \end{bmatrix} = \begin{bmatrix} l(k) - \mathrm{e}^{-\alpha\Delta t}\, \hat{x}_2(k-1) \\ \mathrm{e}^{-\alpha\Delta t}\, \hat{x}_2(k-1) \end{bmatrix}. \tag{4.37}$$

c) 3rd Method

Because the shaping filter $x_2(k)$ follows the exponential distribution, $x_2(k)$ can be obtained $x_2(k) = \mathrm{e}^{-\alpha\Delta t}\, \hat{x}_2(k-1)$. Furthermore, the new state vector $x_{1new}(k)$ can be obtained by

$$x_{1new}(k) = \hat{x}_1(k-1) + velocity \tag{4.38}$$

The velocity was determined by the observation equations,

$$\begin{aligned} velocity &= x_1(k) - x_1(k-1) \\ \vdots \quad &= l(k) - x_2(k) - \varepsilon(k) - l(k-1) - x_2(k-1) - \varepsilon(k-1) \\ \vdots \quad &= l(k) - \mathrm{e}^{-\alpha\Delta t}\, \hat{x}_2(k-1) - \varepsilon(k) - l(k-1) - \hat{x}_2(k-1) - \varepsilon(k-1) \end{aligned} \tag{4.39}$$

The new state vector $x_{new}(k)$ at this epoch t_k can be described as follows,

$$x_{new}(k) = \begin{bmatrix} x_{1new}(k) \\ x_{2new}(k) \end{bmatrix} = \begin{bmatrix} \hat{x}_1(k-1) + velocity \\ \mathrm{e}^{-\alpha\Delta t}\, \hat{x}_2(k-1) \end{bmatrix}. \tag{4.40}$$

Final results computation

Three different filtered results including the state vector and the covariance of the state vector are obtained. Considering the weight affection of filtered results of different methods, the final result at epoch t_k is computed by the weighted average method which is described by the following equation

$$X_k = \frac{\sum_{j=1}^{n} \hat{x}_k(j) / p_{\hat{x}_k}(j)}{\sum_{j=1}^{n} 1/p_{\hat{x}_k}(j)} \tag{4.41}$$

where n means the amount of different models. In this case n (the maximum j) equals to 3.

4.1.2.2 Flowchart of the modified Kalman filter model with a shaping filter

The flowchart of this algorithm is described in Fig. 4.1.

4.1.2.3 Experiment and results analysis

Simulation Test

The time series (Figs 4.2, 4.3 and 4.4) were simulated from the simple to the complicated cases. Different simulated time series were used to verify the abilities of deformation detection, outlier detection and the noise reduction of the proposed model.

a) Simulated deformation time series with white noise

The white noise was simulated by the Matlab function which can generate the normally distributed random numbers with the specific mean and variance. The simulated deformation time series was composed of 3600 observations. The identity Kalman filter model has been modified to process the simulated observation time series.

Fig. 4.2 shows that the time series was simulated by the white noise and 3600 observations. In this time series the first half (from epoch 1 to epoch 1800) was set as 0 mm and the other half (from epoch 1801 to epoch 3600) was set as 10 mm. The deformation 10 mm occurred at epoch 1801. No outliers were added into the time series. The variance of the simulated normally distributed random noise was 1 mm^2.

The standard deviation is calculated based on the equation

$$s = \sqrt{\frac{1}{n-1}\sum_{i=1}^{n}(x_{filter}(i) - x(i))^2}$$

where: x_{filter} denotes the processed time series by the modified Kalman filter, x is the simulated true deformation time series, n is the size of the simulated time series.

The standard deviation of the processed time series is 0.48 mm. The deformation epoch 1801 has been detected by the modified Kalman filter model.

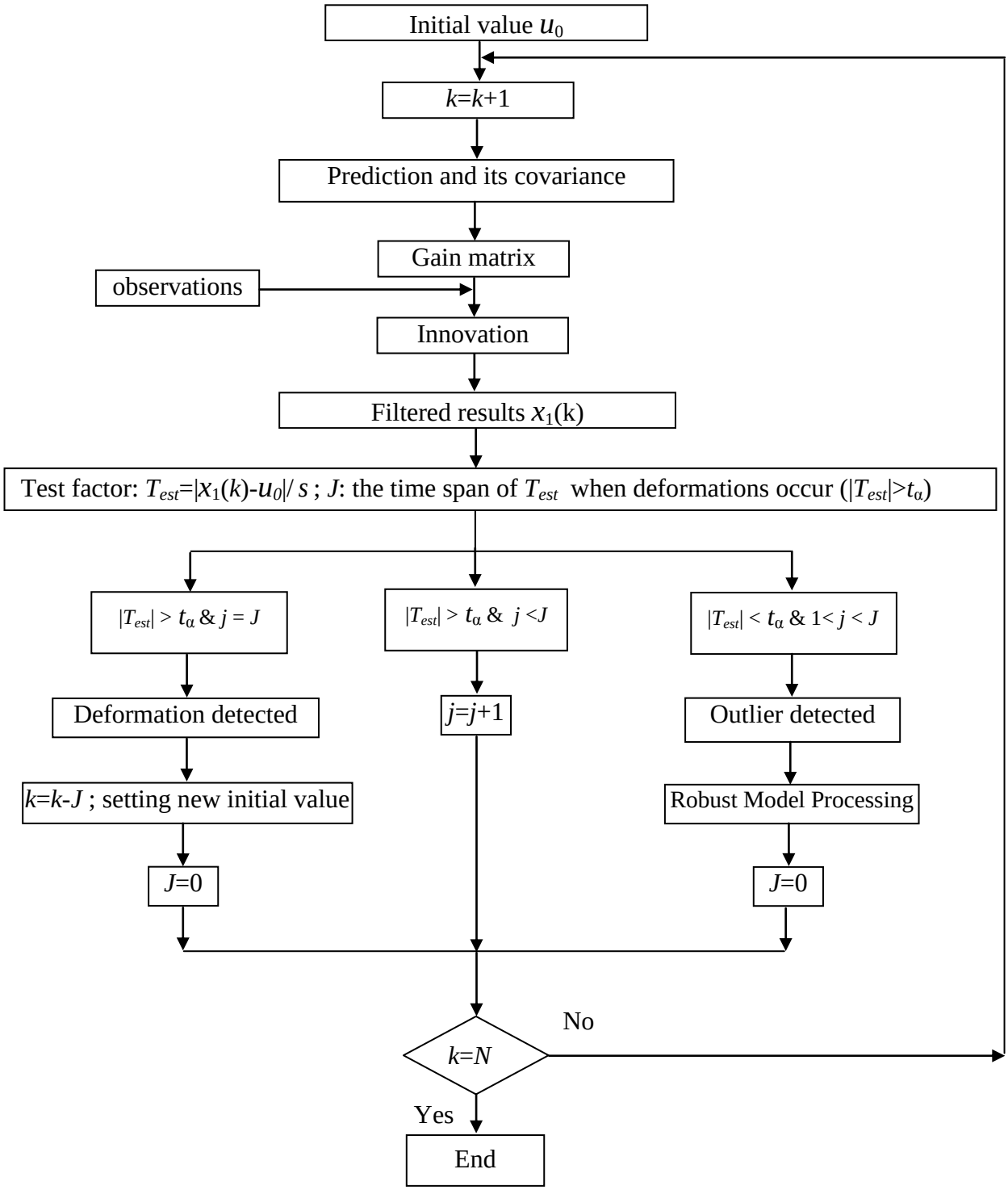

Fig. 4.1 Flowchart of the test procedure for the modified Kalman filter

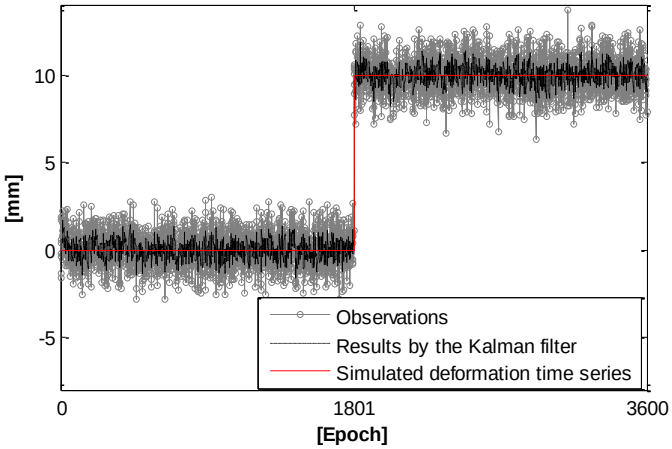

Fig. 4.2 Simulated time series and processed results

The time series shown in Fig. 4.3 was simulated by the white noise and added outliers. No step-wise deformation occurred in this time series. The outliers were added into the time series at epochs 500, 1000, 2500 and 3000. In this case if an outlier occurs, its affection can be reduced by the modified Kalman gain matrix G_k. The modified Kalman gain matrix G_k is constructed as follows:

$$\gamma_k = \begin{cases} 1 & |C_k| < c_0 \\ \dfrac{c_0}{|C_k|}\left(\dfrac{c_1 - |C_k|}{c_1 - c_0}\right) & c_0 < |C_k| < c_1 \\ 0 & |C_k| > c_1 \end{cases}$$

$$G_k = G_k \cdot \gamma_k$$

where c_0 and c_1 are chosen as 2.0 and 5.0 respectively; $V_1(k) = L_1(k) - H_1(k)\bar{X}_k$, $C_k = |V_1(k)|\, Q_{V_1,V_1}(k)^{-1/2}$.

The processed results are shown in Fig. 4.3. The standard deviation of the processed time series is 0.48 mm. All the added outlier epochs have been detected and reduced by the modified Kalman filter.

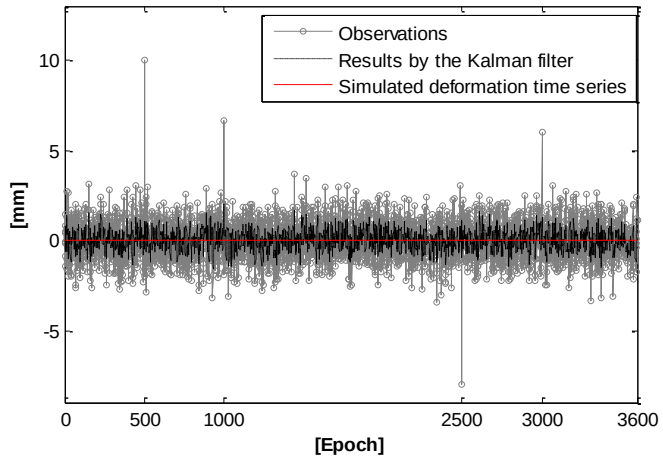

Fig. 4.3 Simulated time series and processed results

The time series composed of the white noise, outliers and the step deformation was shown in Fig. 4.4. The outliers were added into the time series at epochs 500, 1000, 2500 and the deformation epoch was added at the epoch 1801. The processed results were demonstrated in Fig. 4.4. In Fig. 4.4 the deformation epoch has been detected and the outliers have been detected and the affections have been reduced.

In Fig.4.2, Fig. 4.3 and Fig. 4.4, all the added outlier epochs and the deformation epochs have been detected by the proposed Kalman filter model. The standard deviations of the processed time series are 0.48 mm.

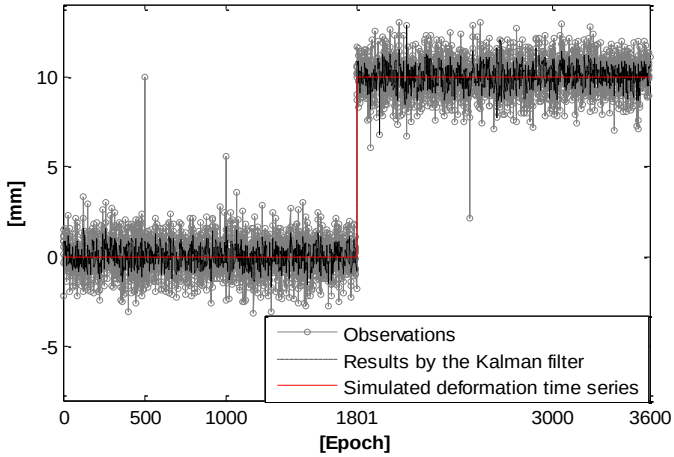

Fig. 4.4 Simulated time series and processed results

b) Simulated deformation time series with colored noise

The colored noise and the white noise were added into the deformation time series. This simulated time series was processed by the Kalman filter model with a shaping filter. The white noises followed the normally distributed random numbers with the variance 1 mm^2. The colored noise followed the exponential distribution: $e^{-0.008 \cdot \Delta t}$. The standard deviation of the colored noise was 1 mm. The simulated deformation time series were composed of 3600 observations. The three parameters of the time series σ_δ σ_Δ and α were given as 1 mm, 1 mm and 0.008. The identity Kalman filter model (Equations 4.26-4.27) has been used to process the followed simulated observation time series (Fig.4.5-4.7).

The simulated time series (Fig. 4.5) was composed of the white noise, the colored noise and the outliers. In Fig. 4.5 the deformation were set as 0 mm and no deformation epoch was added into the simulated time series.

Based on parameter estimation of the stochastic model in Chapter 3, the standard deviations of the colored noise and the white noise of the processed static time series by Kalman filter with a shaping filter can be computed. The standard deviation of the white noise and the colored noise in the processed static time series are 0.3 mm and 0.6 mm. α is 0.0018. Fig. 4.5 and Table 4.1 show the processed results by the Kalman filter model with a shaping filter.

Table 4.1 Stochastic model paramenters of the original and processed simulated time series

Time series	σ_δ (mm)	σ_Δ (mm)	α (1/second)
Simulated time series	1.0	1.0	0.008
Fig. 4.5	0.3	0.6	0.0018

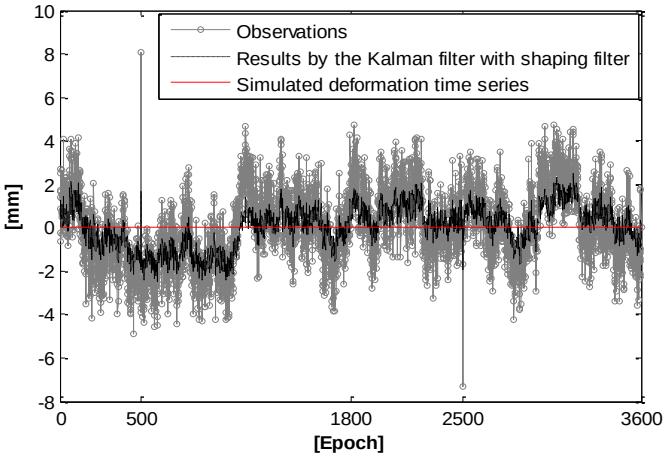

Fig. 4.5 Simulated time series and processed results

Fig. 4.6 shows that the observations are composed of the white noise, the colored noise and 3600 deformation values. In this time series the first half (from epoch 1 to epoch 1800) was set as 0 mm and the other half (from epoch 1801 to epoch 3600) was set as 10 mm. The deformation 10 mm occurred at epoch 1801. No outliers were added into the time series.

The processed time series by the Kalman filter model with a shaping filter is shown in Fig. 4.6. The deformation epoch 1801 has been detected. Based on the differences between the processed time series and the true observations, the standard deviation of the processed time series is 0.67 mm.

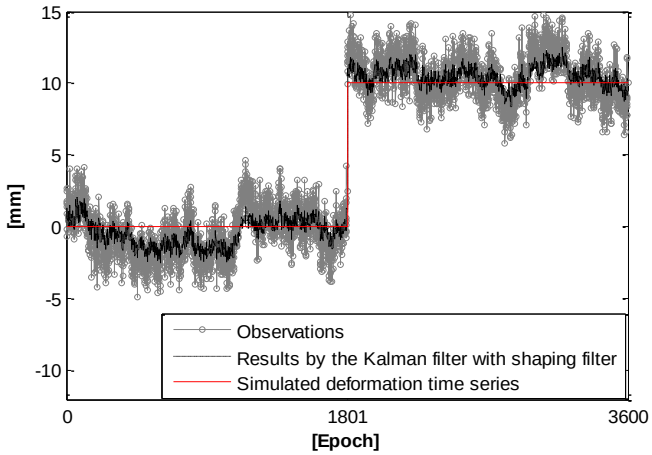

Fig. 4.6 Simulated time series and processed results

In Fig. 4.7 the simulated time series was composed of the white noise, the colored noise, the added outlier epochs and the added deformation epoch. This time series was used to check the efficiency of the modified Kalman filter model with a shaping filter.

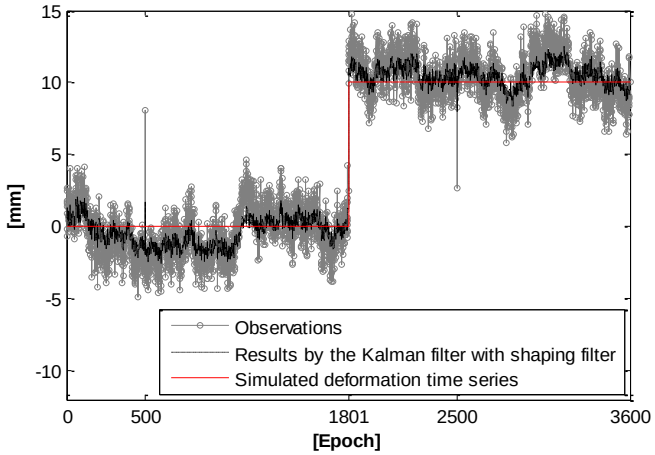

Fig. 4.7 Simulated time series and processed results

All the outlier epochs and the stepwise deformation epochs added in all the simulated time series have been detected. The colored noise can be reduced by a shaping filter which can describe long movement of the colored noise. Compared to the true observations, the standard deviation of the processed time series is 0.67 mm.

Fig. 4.5, Fig. 4.6 and Fig. 4.7 demonstrate that the noises of the simulated time series have been reduced by the Kalman filter model with a shaping filter and the accuracy has been improved. All the processed results of the simulated observations demonstrate the validity of the proposed Kalman filter model with a shaping filter.

The GPS experiment and result analysis

The GPS experiment was carried out on the roofs of the Institute of Geodesy and Geoinformation and the Max-Planck Institute in Bonn, Germany. The baseline was about 1.2 km. The GPS equipment consisted of Trimble 5700 receivers and Zephyr antennas. A cut-off angle of 10° was chosen and the sampling rate Δt was 1 second. During the GPS kinematic measurements, the height of the rover station which was on the roof of the Institute of Geodesy and Geoinformation was changed with a crank every 30 minutes in steps of 12.5 mm. The kinematic measurement lasted for 6 hours (Fig. 4.8). The static observations which are illustrated in Chapter 3 are used for the estimation of the parameters of the stochastic model. The static observations time series and the kinematic observations time series can be used to verify the feasibility of the proposed approach.

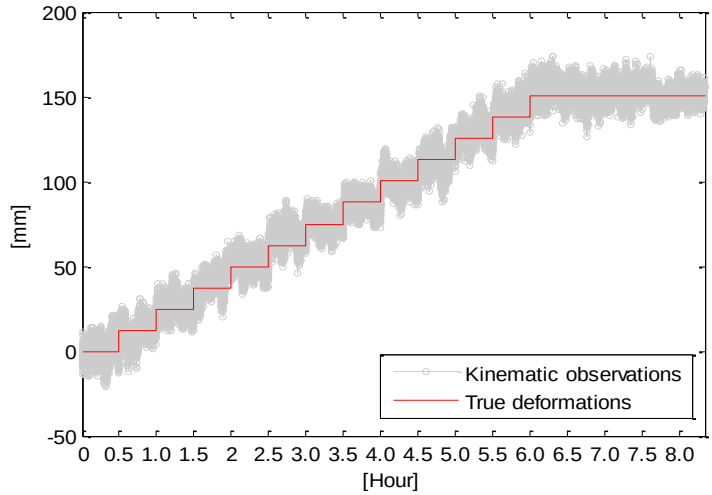

Fig. 4.8 GPS kinematic height observation time series

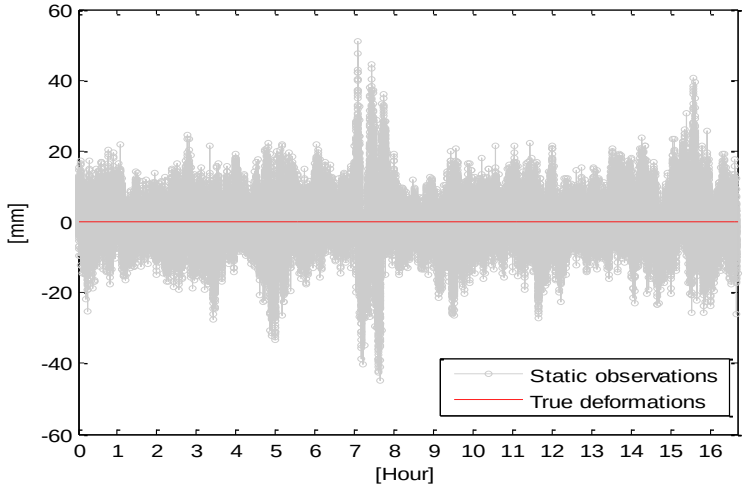

Fig. 4.9 GPS static height observation time series

a) Results analysis of the static time series

As shown in Table 3.7 in Chapter 3, the colored noises in the GPS height observations time series follow the exponential distribution. The standard deviation of colored noise is 5.75 mm and α is 0.0062 and the standard deviation of white noise is 4.53 mm. The shaping filter is used to describe the long term movement of the colored noise.

The identity Kalman filter model with a shaping filter (Equation 4.26) has been used to process the GPS observation time series. It is specified as

$$\begin{bmatrix} x_1(k) \\ x_{sf}(k) \end{bmatrix} = \begin{bmatrix} 1 & 0 \\ 0 & e^{-0.0062\Delta t} \end{bmatrix} \begin{bmatrix} x_1(k-1) \\ x_{sf}(k-1) \end{bmatrix} + \begin{bmatrix} \Delta t & 0 \\ 0 & e^{-0.0062\Delta t} \end{bmatrix} \begin{bmatrix} \omega_1(k) \\ \omega_2(k) \end{bmatrix}$$

According to Equation 4.29

$$s^2 = \frac{1}{n-1}\sum_{k=1}^{n}(x_1(k)-u)^2$$

where $x_1(k)$ is the processed results and u is the true deformation time series, the standard deviation s of the static time series processed by the Kalman filter model with a shaping filter is obtained as 2.5 mm.

The method to detect the deformation epoch described above is applied to the static time series and the kinematic time series in order to check whether it works. In this example, the significance level is selected as 5%, J is selected as 3 epochs, s is 2.5 mm obtained from the static height time series processed by the Kalman filter model with a shaping filter.

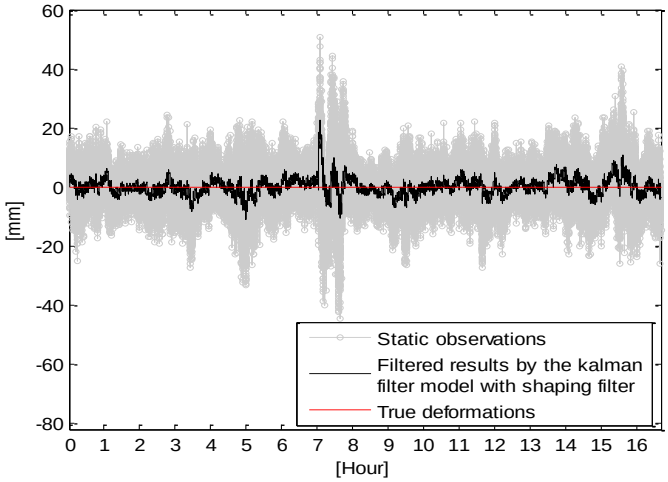

Fig. 4.10 Processed GPS Static time series

As mentioned above, there are three different methods to process the time series, so three different results are obtained. According to Equation 4.41, the final results are shown in Fig.4.10.

Table 4.2 Static data processing results from three different methods

	Detected Epochs (height changed)		Standard Deviations (mm)
True epoch	No deformation epoch		
1st method	25339	25413	2.67
2nd method	25339		2.68
3rd method	25339		2.72

As we know, the time series processed is static time series; there should be no deformation epochs detected. But from the Table 4.2, epoch 25339 was detected in the results of every method. Therefore, more attention should be paid to this epoch. It was discovered that at epoch 25339 the satellite geometry became poor. Geometric Dilution of Precision (GDOP) was about 20. That is why the result at this epoch is not accurate and this epoch is taken as the deformation epoch. Fig. 4.10 shows that the noise has been reduced a lot and the accuracy has been improved. The standard deviation of GPS static time series is 7.3 mm. The standard deviation of the processed time series by the modified Kalman filter with a shaping filter has been improved to 2.7 mm.

b) Results analysis of Kinematic time series

For the kinematic time series, the height was changed by the crank every 30 minutes. The deformation epochs are known. J=3 is the best chosen number compared to the other numbers and s is computed as 2.5 mm.

For the kinematic time series, it is more important to determine the new deformation value. Because the new deformation value will be set as the new initial value in order to detect the next deformation epoch. We can compare the results from three different methods in order to obtain more accurate deformation epochs with short time delay. Table 4.3 shows the epochs detected by three different methods.

In this experiment, the height was changed every half an hour. The epoch should be detected at epochs1800, 3600, 5400,…, 21600, which are described in the first column of the Table 4.3. In fact, the epochs are detected with different time delay by different methods. The principle to get more accurate epochs is to choose the earliest epoch among three different detected results. For example, at the epoch 3600, the height was changed, but from the results, the detected results with different time delay were 3633, 3601, 3604. We chose the earliest epoch 3601 with the least time delay as the best result. The last column of the Table 4.3 shows the results with the least time delay when the height was changed every time. From the last column of the Table 4.3, we can see that the fastest detection is with 1 second time delay, the slowest detection is with 433 seconds time delay.

The processed filtered results (Fig 4.11) can describe the deformation tendency more precisely than the observations because the noise in the time series is reduced from the observation time series.

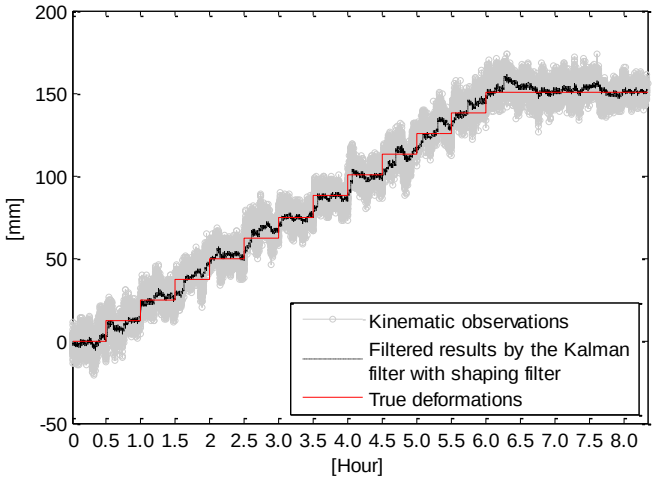

Fig. 4.11 Kinematic data processing results

Table 4.3 Kinematic data processing results from three different methods

Epochs when height was changed				Earliest detection	Earliest time delay
True Epochs	detected epoch results from 3 methods				
	1st method	2nd method	3rd method		
1800	1847	1847	1847	1847	47
3600	3633	3601	3604	3601	1
5400	6015	5833	5833	5833	433
7200	7243	7476	7525	7243	43
9000	9314	9379	9367	9314	314
10800	Not detected	11026	10932	10932	132
12600	12776	13465	12811	12776	176
14400	14540	14512	14612	14512	112
16200	16477	16377	16893	16377	172
18000	18128	18327	18297	18128	128
19800	20011	19899	20675	19899	99
21600	21650	22098	22530	21650	50
Max time delay	615s	865s	930 s		433s

4.1.3 Application in the continuous deformation time series

In the last section deformation appears suddenly and stepwise. In reality deformations often appear more slowly. The deformation time series includes different types of movements (Fig. 4.12-Fig. 4.15). A series of simulated observations were processed by the Kalman filter model with a shaping filter in order to illustrate the algorithm's efficiency. The true deformation time series were simulated by matlab functions. The simulated GPS observation time series consist of the simulated true deformation time series and the GPS noise obtained from the GPS static observations.

Four different deformation trends were simulated. They are shown in Fig. 4.12-Fig. 4.15. The identity model with a shaping filter (Equations 4.26-4.27) and the kinematic model with a shaping filter (Equations 4.28-4.29) were selected to process the different simulated continuous deformations. The kinematic model describes the deformation as a function of time and in the identity model the motion is random, a function of time cannot be established. The observations and the processed time series are shown in Fig. 4.12a-Fig. 4.15a and Fig. 4.12b- Fig. 4.15b. The standard deviations of the processed time series by these two algorithms have been shown in Table 4.4 and Table 4.5. In order to compare the effectiveness of the shaping filter, the observations also have been processed with the standard Kalman filter models without shaping filters (the identity model and the kinematic model). Fig. 4.12c-Fig. 4.15c and Fig. 4.12d-Fig. 4.15d demonstrate the processed results by the standard Kalman filter models.

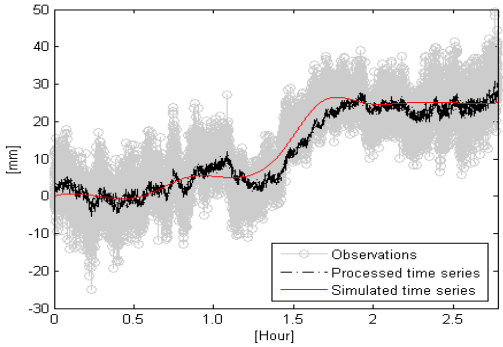

Fig. 4.12a Processed results by the identity model with a shaping filter

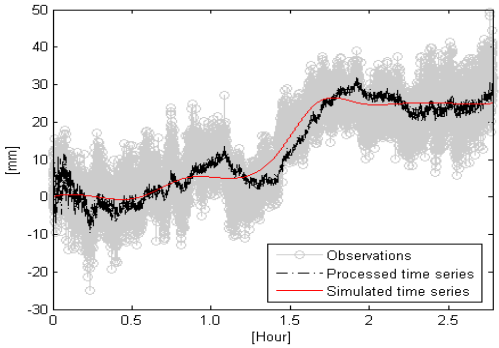

Fig. 4.12b Processed results by the kinematic model with a shaping filter

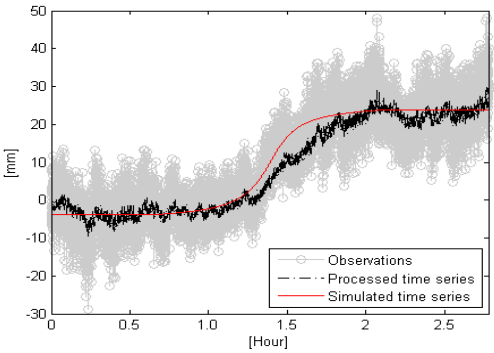

Fig. 4.13a Processed results by the identity model with a shaping filter

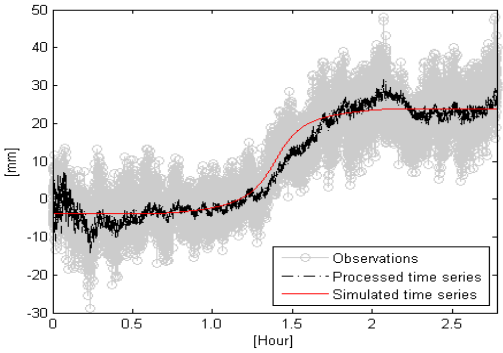

Fig. 4.13b Processed results by the kinematic model with a shaping filter

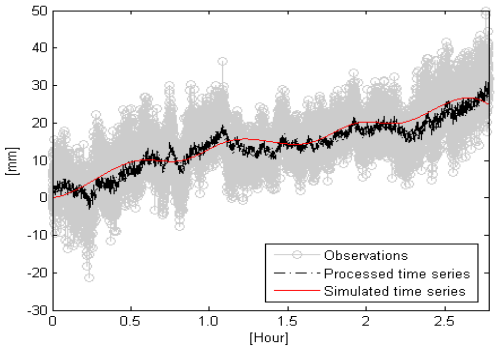

Fig. 4.14a Processed results by the identity model with a shaping filter

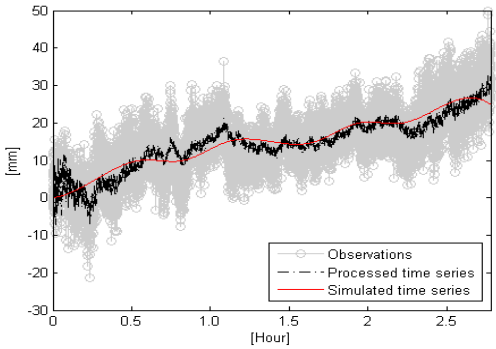

Fig. 4.14b Processed results by the kinematic model with a shaping filter

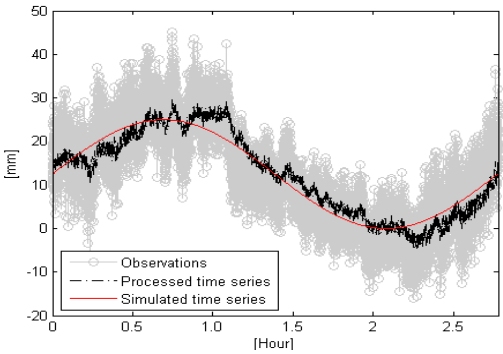

Fig. 4.15a Processed results by the identity model with a shaping filter

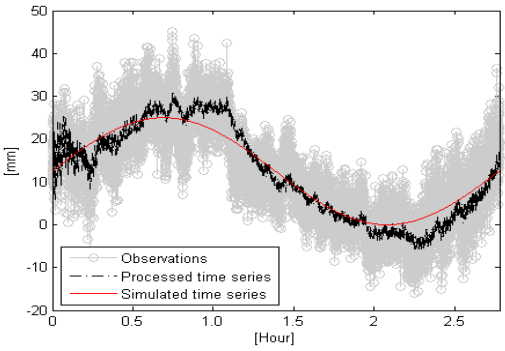

Fig. 4.15b Processed results by the kinematic model with a shaping filter

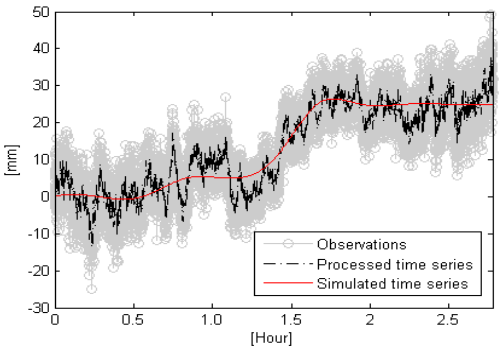

Fig. 4.12c Processed results by the identity model

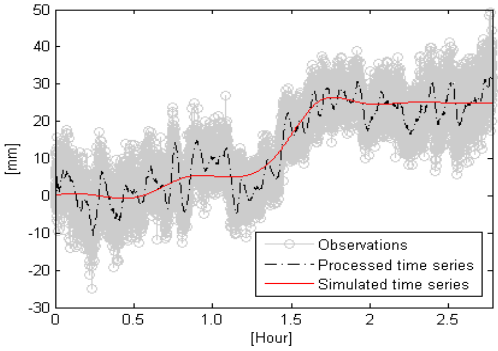

Fig. 4.12d Processed results by the kinematic model

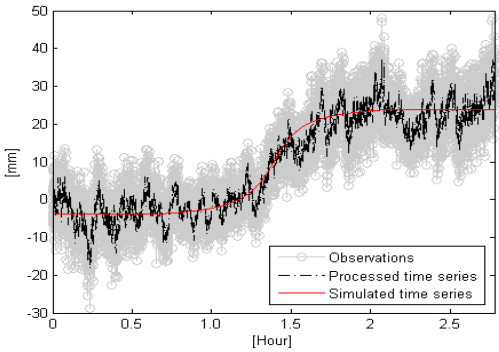

Fig. 4.13c Processed results by the identity model

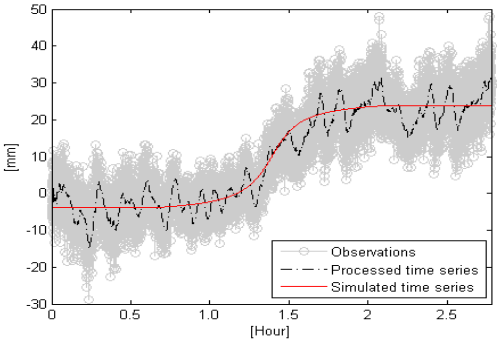

Fig. 4.13d Processed results by the kinematic model

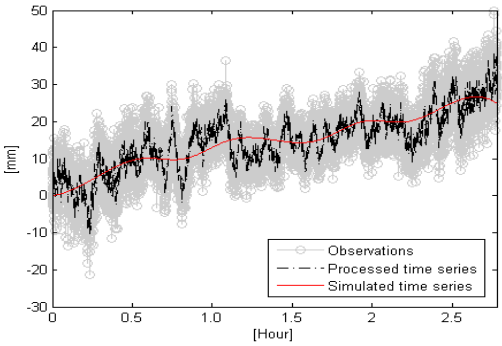

Fig. 4.14c Processed results by the identity model

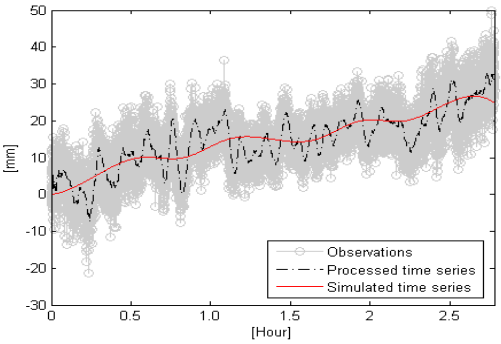

Fig.4.14d Processed results by the kinematic model

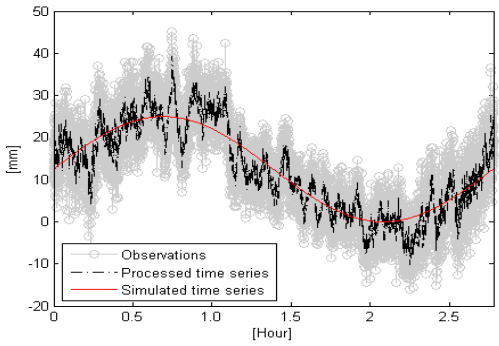

Fig. 4.15c Processed results by the identity model

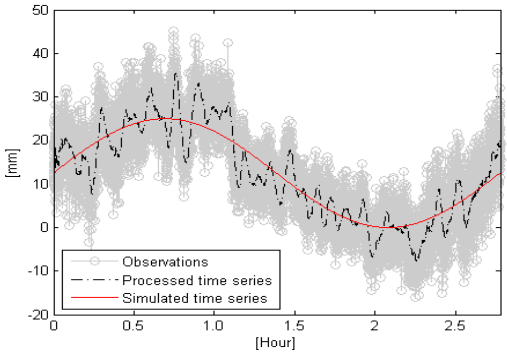

Fig. 4.15d Processed results by the kinematic model

Fig. 4.12a-Fig. 4.15a and Fig. 4.12b-Fig. 4.15b demonstrate clearly that the differences between the processed time series and the simulated series are significantly smaller than the differences between the observations and the simulated series. The influence of the GPS colored noise is reduced significantly by the shaping filter in the identity model and the kinematic model.

In Fig. 4.12c-Fig. 4.15c and Fig. 4.12d-Fig. 4.15d, the identity model without shaping filter and the kinematic model without shaping filter cannot reduce the colored noise. The results of the identity model with a shaping filter and kinematic model with a shaping filter are superior to those of the standard Kalman filter models (the identity and the kinematic models without shaping filter). Obviously, the shaping filter does reduce the GPS colored noise. Without the shaping filter the colored noise remains in the processed time series.

Based on the difference between the processed time series and the simulated true time series, the standard deviation of the processed time series is calculated. The standard deviations of the time series processed with the identity model with a shaping filter and the kinematic model with a shaping filter are shown in Table 4.4 and Table 4.5 separately.

Table 4.4 Results of four simulation time series processed with the identity model with a shaping filter

Time series	Std of observations (mm)	Std of processed time series(mm)	Improved percentage(%)
Fig. 4.12	5.72	2.72	52.4
Fig. 4.13	5.72	2.95	48.4
Fig. 4.14	5.72	2.34	59.1
Fig. 4.15	5.72	2.59	54.7

Std: standard deviation

Table 4.5 Results of four simulation time series processed with the kinematic model with a shaping filter

Time series	Std of observations (mm)	Std of processed time series(mm)	Improved percentage(%)
Fig. 4.12	5.72	2.98	47.9
Fig. 4.13	5.72	2.67	53.3
Fig. 4.14	5.72	2.49	56.5
Fig. 4.15	5.72	3.01	47.4

Std: standard deviation

Table 4.6 Results of four simulation time series processed by different models without shaping filter

Models	Std of observation (mm)	Std of processed time series(mm)	Improved percentage(%)
Identity model	5.72	4.14	27.6
Kinematic model	5.72	4.24	25.9

Std: standard deviation

Relative to the simulated time series (the true value), the standard deviations of the processed time series are from 2.34 mm to 2.95 mm in Table 4.4, and, thus are smaller than the standard deviations of the observations (5.72 mm which is roughly estimated). It is obvious that the noise of the observations can be significantly reduced in different continuous time series by using the identity model with a shaping filter. As a consequence the accuracy of the deformation time series greatly improves.

As shown in Tables 4.4 and 4.5, the identity model with a shaping filter and the kinematic model with a shaping filter can reduce the colored noise in the GPS observations and improve the accuracy of the position coordinates. Table 4.6 illustrates that the identity and the kinematic models without shaping filter can reduce the noise to some extent. But when comparing the standard deviations of the processed time series in Table 4.4 and Table 4.5 to those in Table 4.6, the identity and the kinematic models with a shaping filter are found to be better in reducing the GPS colored noise than the models without shaping filters.

Table 4.7 Deformation epoch detection of different time series processed by the identity model without a shaping filter

Time series	Standard deviation of the processed time series (mm)	Detected deformation epoch (the true time series) (s)	Detected deformation epoch (the processed time series) (s)	Time delay (s)
Fig. 4.12a	2.72	3160	3160	0
Fig. 4.13a	2.95	4493	4495	2
Fig. 4.14a	2.34	938	1004	66
Fig. 4.15a	2.59	665	938	273

Table 4.8 Deformation epoch detection of different time series processed by the kinematic model without a shaping filter

Time series	Standard deviation of the processed time series (mm)	Detected deformation epoch (the true time series) (s)	Detected deformation epoch (the processed time series) (s)	Time delay (s)
Fig. 4.12b	2.98	4496	4822	326
Fig. 4.13b	2.67	4434	4436	2
Fig. 4.14b	2.49	983	1021	38
Fig. 4.15b	3.01	782	995	213

Table 4.9 Deformation epoch detection of different time series processed by the identity model with a shaping filter

Time series	Standard deviation of the processed time series (mm)	Detected deformation epoch (the true time series) (s)	Detected deformation epoch (the processed time series) (s)	Time delay (s)
Fig. 4.12c	4.14	4830	4830	0
Fig. 4.13c	4.14	4642	4709	67
Fig. 4.14c	4.14	1489	1507	18
Fig. 4.15c	4.14	1123	1123	0

Table 4.10 Deformation epoch detection of different time series processed by the kinematic model with a shaping filter

Time series	Standard deviation of the processed time series (mm)	Detected deformation epoch (the true time series) (s)	Detected deformation epoch (the processed time series) (s)	Time delay (s)
Fig. 4.12d	4.24	4851	4851	0
Fig. 4.13d	4.24	4624	4805	181
Fig. 4.14d	4.24	1525	1544	19
Fig. 4.15d	4.24	1156	1156	0

Detected deformation epoch in the column of Tables 4.7-4.10 is defined as the first detected deformation epoch in the time series. The movement should be paid more attention after this epoch. Time delay is the difference between the detected epoch of the true time series and the detected epoch of the processed time series.

The detection of a deformation epoch is based on the hypothesis testing with a given significance level α. Given a significance level $\alpha = 0.05$, the difference between the magnitude of the deformations at the current epoch and the first epoch, is larger than z_α times the measuring precision, it is defined that a deformation epoch is detected. The epoch indicates that a significant deformation occurs. The deformation at a magnitude of 4.5 mm-8.3 mm in Tables 4.7-4.10 can be detected by the statistical method.

The accuracies of the processed time series are different when different models process the same time series. By the hypothesis testing, the significance deformations of the true time series are detected at different epochs by different models. For the same time series, when the accuracy of the processed time series is higher, smaller deformations can be detected and the epoch of the deformation event can be detected earlier.

For example, four different models are used to process the time series shown in Fig. 4.14. The processed results by the identity model with a shaping filter are with highest accuracy. Given a significance level $\alpha = 0.05$, of the hypothesis testing, the detected epoch of the deformation with the identity model with a shaping filter is epoch 1004, which is earlier than the epoch 1021 detected with the kinematic model with a shaping filter, the epoch 1507 obtained with the identity model without shaping filter and the Epoch 1544 obtained with the kinematic model without shaping filter. Given a significance level $\alpha = 0.05$, by the hypothesis testing, the identity model with a shaping filter can detect the smallest deformation (4.6 mm), which is smaller than the magnitude of the deformation (4.9 mm) by the kinematic model with a shaping filter and the magnitude of the deformation (8.1 mm) by the identity model and the magnitude of the deformation (8.3 mm) by the kinematic model.

As shown in Tables 4.7-4.10, the Kalman filters with shaping filters (the identity model with a shaping filter and the kinematic model with a shaping filter) can detect the smaller deformations earlier. The Kalman filters with shaping filters perform better than the standard Kalman filters when they are used to process the real-time deformation series.

4.1.4 Summary

From the experiment computation and comparison, the following conclusions can be drawn.

The standard Kalman filter can reduce the white noise and improve the precision of GPS observations, but the coloured noise remains in the processed time series. A deformation analysis based on Kalman filters with shaping filters, which uses the identity model and the kinematic model, was applied to GPS time series with different movement trends. Not only stepwise deformations but also the continuous deformations can be processed by Kalman filters with shaping filters. The results show that the Kalman filters with shaping filters can reduce the coloured noise, improve the accuracy of the coordinates and estimate the movement closer to the true trajectory. The Kalman filters with shaping filters can detect smaller deformations earlier and perform better than the standard Kalman filters without shaping filters when used to process deformation time series.

The Kalman filter with shaping filter can be used to process GPS short baseline time series in real-time to obtain precise positions and detect deformation events in time and with a high reliability. Its use is recommended for the following applications: dam deformation monitoring, bridge deformation monitoring, landslide deformation monitoring, etc.

4.2 Sequential algorithm

When an older adjustment has been performed and new observations become available, it is rather uneconomical that if we combine the new information with all the old information and

perform a complete readjustment, especially, if the new information is relatively limited compared to the old information. Instead of performing a complete readjustment, it would be better to perform a sort of an 'add-on' adjustment because of the computational saving (Mikhail 1976). Therefore, we can use the sequential algorithm to process the data.

4.2.1 Principle of sequential algorithm

Firstly, all the preceding derivations were completed using some matrix relationships.
a) Give the matrix expression

$$X_{n,n} = Y_{n,n} \pm U_{n,p} Z_{p,p} V_{p,n} \tag{4.42}$$

then

$$X^{-1} = Y^{-1} \mp Y^{-1} U (Z^{-1} \pm V Y^{-1} U)^{-1} V Y^{-1} \tag{4.43}$$

provided that all inverses of matrixes *X*, *Y*, *U*, *Z* and *V* in Equation 4.43 do exist.

b)

$$\begin{aligned} (A+B)^{-1} &= A^{-1}(A^{-1}+B^{-1})^{-1}B^{-1} \\ &= B^{-1}(A^{-1}+B^{-1})^{-1}A^{-1} \end{aligned} \tag{4.44}$$

provided that all inverses of matrixes *A* and *B* exists (Mikhail 1976).

The derivation of the Sequential algorithm is described as,
At the epoch t_k, the conditional equations are given

$$\begin{aligned} &\varepsilon_1 = H_1 X - l_1 \qquad W_{l_1} \\ &\varepsilon_2 = H_2 X - l_2 \qquad W_{l_2} \\ &\cdots \quad \cdots \\ &\varepsilon_k = H_k X - l_k \qquad W_{l_k} \end{aligned} \tag{4.45}$$

where l_k is the observations, W_{l_k} is the weight matrix of the observations l_k, H_k is the measurement transition matrix. X is the unknown parameters, its expectation and the variance of the parameters X are given as $E(X) = \hat{X}_0, \mathrm{var}(X) = P_X$. ε_k is the residual, its expectation value and the variance are $E(\varepsilon) = 0, \mathrm{var}(\varepsilon) = R$. The covariance of ε_i and ε_j is $\mathrm{cov}(\varepsilon_i, \varepsilon_j) = 0 \quad (i \neq j)$.

The least square solution of the given observation equations is given as,

$$N = \sum_{i=1}^{k} H_i^T W H_i \tag{4.46}$$

$$S = \sum_{i=1}^{k} H_i^T W l_i \tag{4.47}$$

$$X = N^{-1} S \tag{4.48}$$

Stopping the summation at an intermediate step and denoting the partially formed (or incomplete) normal equations by

$$N_{k-1} = \sum_{i=1}^{k-1} H_i^T W H_i \tag{4.49}$$

$$S_{k-1} = \sum_{i=1}^{k-1} H_i^T W l_i \tag{4.50}$$

It then follows from Equations 4.46 and 4.47 that the succeeding step would be

$$N_k = N_{k-1} + H_k{}^T W H_k \tag{4.51}$$

$$S_k = S_{k-1} + H_k^T W l_k \tag{4.52}$$

A possibility now arises if a solution is supposed possible from both pairs of Equations 4.49-4.50 and Equations 4.51-4.52, respectively, that is

$$X_{k-1} = N_{k-1}^{-1} S_{k-1} \tag{4.53}$$

$$X_k = N_k^{-1} S_k \tag{4.54}$$

Supposing that both inverses N_{k-1}^{-1} and N_k^{-1} exist. The possibility is to find the value of X_k from a previous solution vector X_{k-1} , not from N_k^{-1} and S_k .

The case of getting N_k^{-1} from N_{k-1}^{-1} for the addition of conditions is shown.
First the matrix inversion Equations 4.42 and 4.43 are applied to the Equation 4.51, then,

$$N_k^{-1} = N_{k-1}^{-1}\left[I \mp H_k^T (R \pm H_k N_{k-1}^{-1} H_k^T)^{-1} H_k N_{k-1}^{-1} \right] \tag{4.55}$$

The updated constant term vector can be written as

$$S_k = S_{k-1} + H_k^T W l_k \tag{4.56}$$

Using Equations 4.55 and 4.56 into Equation 4.54 results in

$$X_k = \left[N_{k-1}^{-1} - N_{k-1}^{-1} H_k^T (R \pm H_k N_{k-1}^{-1} H_k^T)^{-1} H_k N_{k-1}^{-1} \right] \times (S_{k-1} + H_k^T W l_k) \tag{4.57}$$

X_k can be obtained as,

$$\begin{aligned} X_k = {} & N_{k-1}^{-1} S_{k-1} \\ & - N_{k-1}^{-1} H_k^T (R \pm B_k N_{k-1}^{-1} B_k^T)^{-1} H_k N_{k-1}^{-1} S_{k-1} \\ & + N_{k-1}^{-1} H_k^T W l_k \\ & - N_{k-1}^{-1} H_k^T (R \pm B_k N_{k-1}^{-1} B_k^T)^{-1} H_k N_{k-1}^{-1} H_k^T W l_k \end{aligned} \tag{4.58}$$

The last term in Equation 4.58 is defined as

$$G_k = -N_{k-1}^{-1} H_k^T (R \pm B_k N_{k-1}^{-1} B_k^T)^{-1} B_k N_{k-1}^{-1} B_k^T W l_k$$

which when using Equation 4.44 leads to

$$G_k = -N_{k-1}^{-1} H_k^T W (W \pm (B_k N_{k-1}^{-1} B_k^T)^{-1})^{-1} W l_k$$

and applying Equation 4.43, realizing that $U = V = I$ in the present case, gives

$$\begin{aligned} G_k &= -N_{k-1}^{-1} H_k^T W (R \pm R(B_k N_{k-1}^{-1} B_k^T + R)^{-1} R)^{-1} W l_k \\ &= -N_{k-1}^{-1} H_k^T W l_k \pm N_{k-1}^{-1} H_k^T (R + B_k N_{k-1}^{-1} B_k^T)^{-1} l_k \end{aligned}$$

which when used in Equation 4.59 leads to

$$X_k = X_{k-1} - N_{k-1}^{-1} H_k^t (R + B_k N_{k-1}^{-1} B_k^T)^{-1} H_k X_{k-1} + N_{k-1}^{-1} H_k^t (R + B_k N_{k-1}^{-1} B_k^T)^{-1} l_k$$

Finally

$$X_k = X_{k-1} + N_{k-1}^{-1} H_k^T (R + H_k N_{k-1}^{-1} H_k^T)^{-1} (l_k - H_k X_{k-1}) \tag{4.59}$$

Including the case of condition deletion yields

$$X_k = X_{k-1} + N_{k-1}^{-1} H_k^T (R \pm H_k N_{k-1}^{-1} H_k^T)^{-1} (l_k - H_k X_{k-1}) \tag{4.60}$$

thus with X_{k-1}, N_{k-1}^{-1} known, the new matrices X_k and N_k^{-1} can be computed from the recursive formulas.

The sequential equations can be described as

$$\left.\begin{aligned} X_{k+1} &= X_k + G_{k+1}(l_{k+1} - H_{k+1}^T X_k) \\ G_{k+1} &= P_k H_{k+1}^T (R \pm H_{k+1}^T P_k H_{k+1})^{-1} \\ P_{k+1} &= P_k - G_{k+1} H_{k+1}^T P_k \end{aligned}\right\} \tag{4.61}$$

where $X_k = P_k H_{k+1}^T W_{l_k l_k} l_k$, $P_k = (H_k^T W_{l_k l_k} H_k)^{-1}$, G_{k+1} is the gain matrix of the Sequential algorithm, X_{k+1}, X_k are optimal values at epoch t_k and t_{k+1}, P_{k+1} , P_k are the covariance matrixes of X_{k+1}, X_k, R is the covariance of the residual.

4.2.2 Analysis of sequential algorithm

The sequential algorithm would be capable of real-time or near real-time computations. The sequential algorithm has the capabilities of handling both problems of adding information as well as deleting information. The algorithm can be used with only minor sign changes to remove the effect of any designated condition equations from the adjustment. The ability of eliminating the effect of undesirable information, or to reinstating the effect of that which has proven to be useful, sequentially and at the same time of the adjustment, can lead to computational savings (Mikhail 1976).

The recursive formulas that have been derived from the above exhibit an apparent advantage in avoiding the inversion of the normal equation coefficient matrix. When the system equation of the Kalman filter model is to be the equation $x_k = x_{k+1}$ without system noise, the Equations 4.12-4.16 are the same as the Equation 4.61. Therefore, the sequential algorithm is the special case of the Kalman filter model.

4.2.3 Modification of sequential algorithm

Considering the detection of deformations and outliers by sequential algorithm, it is similar to the part of Kalman filter with a shaping filter in previous section 4.1.2. So the main idea is described in the following.

As analyzed in chapter 3, colored noises exist in the GPS time series. Because of colored noise in the GPS time series, the state vector is augmented by a shaping filter (Equation 4.25) describing the long term movement of correlated measurement deviations, which is similar to the process of the Kalman filter model with a shaping filter.

Since the sequential algorithm is the special case of the Kalman filter, its state equation can be described as,

$$x_k = x_{k+1} \tag{4.62}$$

The augmented state equation can be described as

$$\begin{bmatrix} x_{k+1} \\ x_{sf}(k+1) \end{bmatrix} = \begin{bmatrix} 1 & 0 \\ 0 & e^{-\alpha\Delta t} \end{bmatrix} \begin{bmatrix} x_k \\ x_{sf}(k) \end{bmatrix} + \begin{bmatrix} 0 \\ e^{-\alpha\Delta t} \end{bmatrix} \omega_k \tag{4.63}$$

and the observation equation is

$$l(k) = \begin{bmatrix} 1 & 1 \end{bmatrix} \begin{bmatrix} x_1(k) \\ x_{sf}(k) \end{bmatrix} + \varepsilon(k) \tag{4.64}$$

Algorithm of detecting deformations and outliers

The basic idea of this algorithm of detecting deformations and outliers is same to the algorithm described in section 4.1.2.1. The statistical test can be used to detect the deformations and outliers in the time series. When the statistical test is selected to test the distribution of the residuals $(x_1(k)-u)$, firstly, the statistical properties of the GPS time series should be computed based on samples.

For example, *n* static GPS observations have been chosen and processed by the sequential algorithm with a shaping filter. The mean value of *n* residuals in the static time series is 0. The variance s^2 is obtained from the GPS static observations time series by the equation

$$s^2 = \frac{1}{n-1} \sum_{k=1}^{n} (x_1(k)-u)^2 \tag{4.65}$$

where $x_1(k)$ denotes the processed coordinate result of the selected GPS time series; *u* is the mean value of the processed results in the GPS static time series.

The test factor

$$T_{est} = \frac{|x_1(k)-u_0|}{s} \tag{4.66}$$

is used to detect these changes. Here u_0 is the initial value of the state vector x_1 which can be computed as the mean value of the former epoch's processed results.

According to the similarity and difference between deformations and outliers, in the following GPS experiment *J* is selected as 3 during the computation by sequential algorithm with a shaping filter.

The test factors T_{est} and *J* are two factors to distinguish outliers and deformations. The test factors T_{est} and *J* should detect the deformation epochs with short time delay and generate less false alarms.

Modification of the results when an outlier is detected

The results sometimes are deteriorated by an outlier. Therefore, after the detection of the outlier we should eliminate the outlier's influence on the estimation of the state vector. The gain matrix must be modified, because the outlier affects the results by the gain matrix. The method

accepted here is also based on the idea of the equivalent weights function (Yang 2002), which is same as last section 4.1. If an outlier occurs, the Equations 4.32 and 4.33 are used here:

$$\gamma_k = \begin{cases} 1 & |C_k| < c_0 \\ \dfrac{c_0}{|C_k|}\left(\dfrac{c_1 - |C_k|}{c_1 - c_0}\right) & c_0 < |C_k| < c_1 \\ 0 & |C_k| > c_1 \end{cases}$$

$$G_k = G_k \cdot \gamma_k$$

In the following experiment c_0 and c_1 are 2 and 5 during the computation by sequential algorithm with a shaping filter.

Determination of the new initial value at the epoch when a deformation is detected

If a deformation is detected, the initial state value μ_0 is changed to a new value which should be equal to the new deformation result $x_{1new}(k)$. Another stepwise change can be found afterwards. The third method in last section 4.1 is used to determine the new deformation value as the new initial mean value.

The shaping filter $x_2(k)$ follows the exponential distribution, $x_2(k)$ can be obtained $x_2(k) = \mathrm{e}^{-\alpha \Delta t}\, \hat{x}_2(k-1)$. Furthermore, the new state vector $x_{1new}(k)$ can be obtained by

$$x_{1new}(k) = \hat{x}_1(k-1) + velocity$$

The velocity is determined by the observation Equation 4.39 and the new state vector $x_{new}(k)$ at this epoch t_k can be determined by Equation 4.40.

4.2.4 Experiment and results analysis

Data sources: the GPS static height observations from the GPS experiment described in Chapter 4 (Fig. 4.9).

The processed time series is shown in Fig. 4.16.

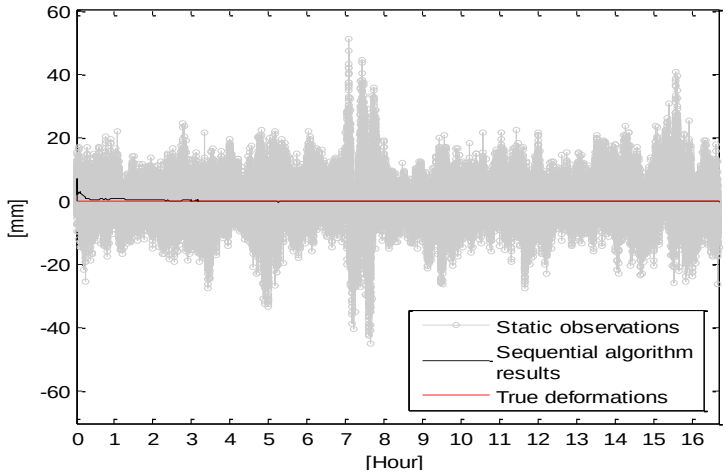

Fig. 4.16 Results of static time series processed by sequential algorithm

The estimation principle of the statistical model of GPS time series (Equation 3.6) has already been introduced in Chapter 3. The unknown parameters in this statistical model (Equation 3.10) are described as the standard deviation of the uncorrelating errors σ_δ, the standard deviation of the correlating errors σ_Δ and α . By the estimation of the stochastic model, the three parameters of the stochastic model of the processed time series are obtained as $\sigma_\delta = 0.008$ mm, $\sigma_\Delta = 0.35$ mm, $\alpha = 0.00005$ 1/Second. The differences of the stochastic model between the processed time series and the GPS observation time series show the performance of the sequential algorithm with a shaping filter.

Table 4.11 Stochastic model parameters of the original and processed GPS time series

Static Time series / Methods	σ_δ (mm)	σ_Δ (mm)	α (1/second)	$\sigma = \sqrt{\sigma_\Delta^2 + \sigma_\delta^2}$ (mm)
Original	4.6	5.7	0.0063	7.3
Sequential Algorithm	0.008	0.35	0.00005	0.35

The standard deviation of the colored noise has been reduced from 4.6 mm to 0.008 mm. The standard deviation of the non-correlated noise has been reduced from 5.7 mm to 0.35 mm. Table 4.11 illustrates that the colored noise of the GPS time series and the white noise have been reduced significantly by the Sequential algorithm with a shaping filter. The stepwise deformation detection by the sequential algorithm is shown in following subsection 4.4.

Summary

The principle of the sequential algorithm has been introduced and its modification has been given when it was used to process the GPS static time series and the GPS stepwise deformation time series. The GPS experiment has been used to test its efficiency.

4.3 FIR filter model

When the contaminated GPS time series are obtained, an optimal algorithm should be found to extract the noise from the time series. This process can be considered as one simple signal processing system.

From a system-engineering point of view, there are three basic components, an input sequence $l(k)$, an operator $D(\cdot)$, and an output sequence $x(k)$. Their general relationship can be described as follows (Dodson et al. 2001; Kuo and Lee 2001; Meng 2002):

$$x(k) = D\big(l(k)\big) \tag{4.67}$$

During the signal processing, there are two kinds of impulse response filters: the Finite Impulse Response (FIR) filter, and the Infinite Impulse Response (IIR) filter. The principle of impulse response filter is described in the following parts.

4.3.1 FIR filter introduction

In general, a causal IIR filter is represented as

$$x_k = \sum_{p=0}^{P-1} a_p x_{k-p} + \sum_{q=0}^{Q-1} b_q l_{k-q} \tag{4.68}$$

where coefficients a_p and b_q are used to define the linear operators $D(\cdot)$; the indexes p and q start from 0; P and Q are the filter lengths of digital filters. The output at a given epoch is given as a linear combination of the input signals and the output signals from previous epochs. The IIR filter is demonstrated by and a set of feedforward coefficients $\{b_q;\ q = 0,1,\ldots,P-1\}$ a set of feedback coefficients $\{a_p;\ p = 0,1,\ldots,Q-1\}$. Equation 4.68 is also called Auto-Regressive Moving Average (ARMA) model (Meng 2002).

An FIR digital filter is considered as a system with input sequence $l(k)$ and output sequence $x(k)$. The output $x(k)$ at any discrete epoch t_k depends on the present and past values of $l(k)$. An FIR filter can be represented in the following well-known convolution sum equation form, where b_q is the filter coefficients, usually we start indexing q at zero; Q is the filter length (Its order is $Q-1$) and the number of the coefficients.

$$x_k = \sum_{q=0}^{Q-1} b_q l_{k-q} \tag{4.69}$$

The previously determined output signal has no impact on the estimates of the following output signal. The output sequence can be expressed as a convolution of filter coefficients and the input sequence. The output sequence is a weighted average of the input values. The Equation 4.69 is also called the Moving Average filter.

Note that when all the a_p are zero, Equation 4.68 is identical to Equation 4.69. Therefore an FIR filter is a special case of an IIR filter without feedback coefficients. Thus, this type of system is known as a non-recursive system.

In the frequency domain, the description of the FIR filter (Oppenheim and Schafer 1989) is given as follows:
If the input to a causal linear stationary system l_k is a complex exponential with frequency ω,

$$l_k = e^{j\omega k} \tag{4.70}$$

$$x_k = \sum_{q=0}^{Q-1} b_q l_{k-q} = \sum_{q=0}^{Q-1} b_q e^{j\omega(k-q)} = e^{j\omega k}\left[\sum_{q=0}^{Q-1} b_q e^{-j\omega q}\right] \tag{4.71}$$

Let $b(\omega) = \sum_{q=0}^{Q-1} b_q e^{-j\omega q}$, then $x_k = b(\omega) l_k$ where $b(\omega)$ represents the frequency response.

Generally, b_q can be represented as the product of the desired impulse response $b_d(q)$ and a finite-duration window w_q; i.e.,

$$b_q = b_d(q) w_q \tag{4.72}$$

For the lowpass FIR filter, its cut off frequency is ω_c ,then

$$b_d(q) = \frac{1}{2\pi}\int_{-\omega_c}^{\omega_c} b_d(\omega) e^{j\omega q} d\omega \tag{4.73}$$

Hamming window is defined by the following equation

$$w_q = \begin{cases} 0.54 - 0.46\cos(2\pi q / Q) & 0 \le q \le Q \\ 0 \end{cases} \tag{4.74}$$

The window has the desirable property that their Fourier transforms are concentrated around $\omega = 0$. They have a simple functional form that allows them to be computed easily. Finally, the impulse response coefficients are described as $b_q = b_d(q) w_q$.

4.3.2 Analysis of the FIR filter

The choice of an FIR filter is determined by practical considerations. Some advantages and disadvantages of an FIR filter can be summarized as follows (Kuo and Lee 2001; Elali 2003): An FIR filter is always stable, because there is no feedback of past outputs as defined in Equation 4.64. That is, a bounded input results in a bounded output; An FIR filter has finite memory because all inputs before the (*Q*-1) th previous one are not considered; The finite-precision errors of an FIR filter are less severe than those in an IIR filter; An FIR filter can be easily implemented.

Compared with an IIR filter, a relatively higher order FIR filter is required to achieve a given level of performance. Therefore, more computations are required, and/or longer time delay maybe arise in the case of an FIR filter (Rabiner 1975).

4.3.3 Experiment and result analysis

The three parameters σ_δ, σ_Δ, α in the stochastic model of the processed time series represent the performance of FIR filters. Different FIR filters with different orders have been compared when processing the GPS time series. The main task is to determine the coefficients of FIR filters when FIR filters are used to process the GPS time series and to compare the accuracies of the processed GPS time series by FIR filters.

4.3.3.1 Results analysis of the processed GPS static time series

If there is no deformation in the GPS time series, it is that the antennas at the rover station and reference station are fixed during the GPS measurement. The time series described in Fig. 3.4 has been chosen. The purpose is to explore the relationship between the order of an FIR filter and the accuracy of the processed time series by an FIR filter.

Visualising the power spectrum of the static time series (Fig. 3.4), it is necessary to plot the figure of the frequency *f* and the amplitude spectrum *y(f)* (Fig. 4.17).

If the noises in the time series are white noise, the spectrum should be very flat. However, in Fig. 4.17 and Fig. 4.18, it demonstrates that besides the white noise, there also exist colored

noise. In Fig 4.18, it shows that the frequency of the colored noise is mainly below 0.01Hz. The high pass filter can be primarily used to reduce the colored noise.

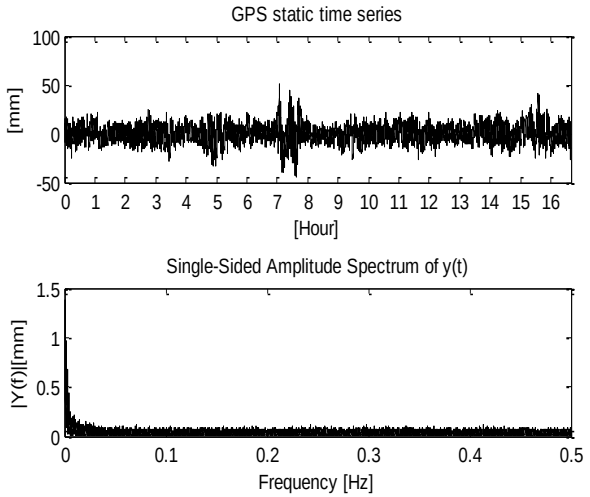

Fig. 4.17 The static time series and its amplitude spectrum

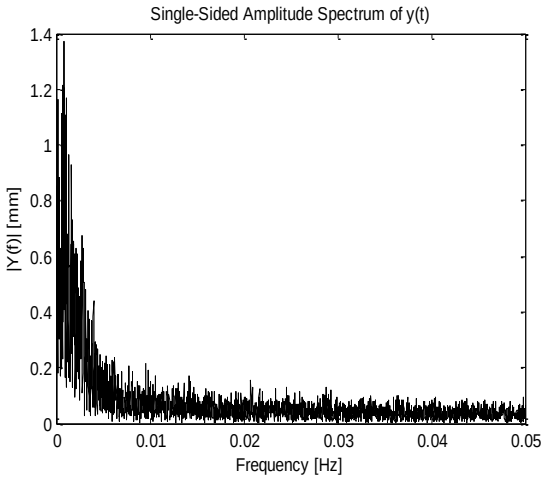

Fig. 4.18 The amplitude spectrum (zommed to 0.05 Hz)

The spectrum of the white noise is constant. In Fig. 4.17, the white noise of the time series is in the higher frequency. So the random noise is eliminated from the coordinates time series using the low-pass FIR filter based on Hamming window. The design of the FIR filter employed a cut-off frequency of 0.1Hz. Different FIR filters with different orders have been used to process the static time series. In Chapter 3, the stochastic model of the time series is described as the function of the three parameters: the standard deviation of the uncorrelating errors σ_δ, the standard deviation of the correlating errors σ_Δ and α . By the estimation of the stochastic model, the three parameters of the stochastic model of the processed time series can be calculated. The stochastic models of time series processed by different FIR filters show the performance of different FIR filters. The results of the parameter estimation of the stochastic model of the corresponding processed static time series have been shown in Table 4.12.

Compared with the three parameters from the original time series $\sigma_\delta = 4.6\,\text{mm}$, $\sigma_\Delta = 5.7\,\text{mm}$, $\alpha = 0.0063$ 1/Second, in Table 4.12 it can be seen that the white noise has been reduced a lot. Regarding the colored noise, it has been reduced more when the time series is processed by the higher order FIR filter. However, the colored noise is not reduced significantly when the order of the FIR filter is higher. But the higher order FIR filter causes larger time delay.

For the GPS static time series, there are no deformations in the time series. The affection of the time delay of deformation epochs is not considered in this case. When the order of the FIR filter increases, the accuracy of the processed static time series is improved (Fig. 4.19).

Table 4.12 Stochastic model of the processed static time series by FIR filters with different orders

Static time series / FIR Order	σ_δ (mm)	σ_Δ (mm)	α (1/second)	$\sigma = \sqrt{\sigma_\Delta^2 + \sigma_\delta^2}$ (mm)
1	4.60	5.70	0.0063	7.30
10	1.08	5.57	0.0076	5.67
20	0.04	5.28	0.0076	5.28
30	0.27	4.97	0.0076	4.98
40	0.27	4.67	0.0078	4.68
50	0.65	4.37	0.0080	4.40
60	0.85	4.09	0.0082	4.18
70	1.03	3.80	0.0082	3.93
80	1.13	3.53	0.0085	3.70
90	1.19	3.26	0.0090	3.47
100	1.26	3.01	0.0096	3.26

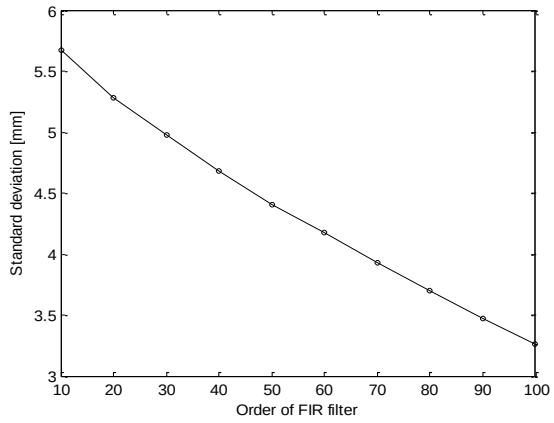

Fig. 4.19 Standard deviations of the processed GPS static time series by different orders FIR filters

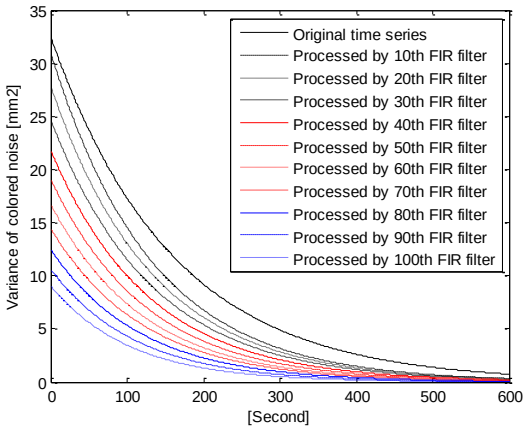

Fig. 4.20 Distributions of the variances of colored noise in the processed GPS static timeseries by different orders FIR filters

4.3.3.2 Stepwise deformation detection using different orders' FIR filters

When there is a deformation in the time series, it is necessary to find out the relationship between the time delay of the detected deformation epoch and the accuracies of the processed time series.

Data sources: The first hour's kinematic observations have been selected from the GPS experiment described in Chapter 4.

The standard deviations of the processed time series by different order FIR filter are computed based on the differences between the processed time series and the true deformations time series.

Table 4.13 Detected deformation epochs and the accuracies of the processed kinematic time series

Kinematic time series / FIR Order	Detected epochs	Time delay (Second)	Standard deviation (mm)
10	1817	17	5.39
20	1828	28	5.19
30	1838	38	5.15
40	1847	47	5.20
50	1857	57	5.28
60	1866	66	5.41
70	1876	76	5.58
80	1886	86	5.75
90	1896	96	5.95
100	1905	105	6.15

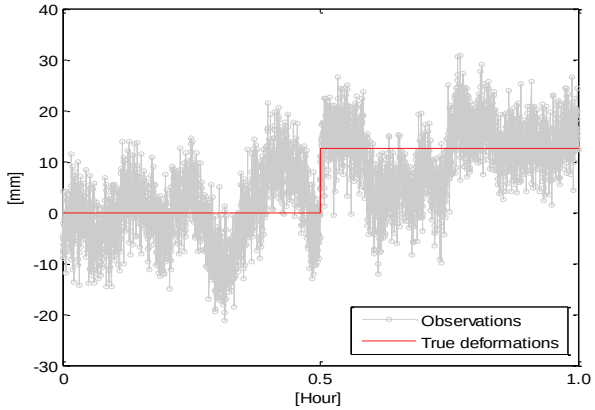

Fig. 4.21 GPS kinematic time series

The kinematic time series was processed by the different order FIR filters, the corresponding results have been shown in Table 4.13. Table 4.12 illustrates that the accuracies have been improved with increasing order of FIR filter in the static time series. But as for the kinematic time series, it is a different situation. In Fig. 4.21, there is a deformation in the GPS kinematic time series. The results in Table 4.13, demonstrate that when the order of FIR filter increases, the time delay of the detected deformation epoch will increase. If the deformation epoch is detected with time delay, the accuracies of the processed results will be affected by different time delays. It is necessary to find the suitable order of FIR filter with the highest accuracy of the processed results and acceptable time delay.

Based on the analysis of the static and kinematic GPS time series, two main factors should be considered during the order selection of FIR filter. One is the accuracy of the processed time series; the other is the time delay of the deformation detection epoch. In Fig. 4.22, the time delay will affect the accuracy of the processed kinematic time series. In Fig. 4.22 and Fig. 4.23, when

the order of FIR filter is 30, the processed time series is with the highest accuracy and the time delay of the detected epoch is 38 second. So the FIR filter with order 30 can be chosen to process the deformation time series.

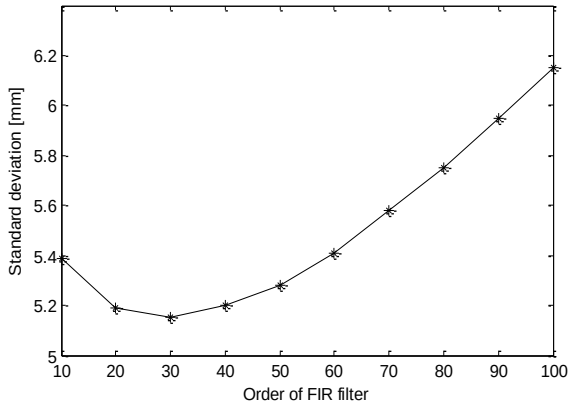

Fig. 4.22 The distribution of the standard deviations of the processed kinematic time series by different orders of FIR filters

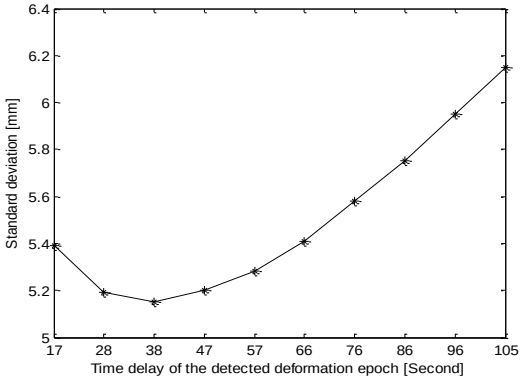

Fig. 4.23 The distribution of the standard deviations of the processed kinematic time series with different time delay of the detected deformation epoch

Summary

The principle of FIR filter has been given and the selection order and coefficients of FIR filter have been discussed in detail. The static GPS time series have been used to determine the appropriate FIR filter and the kinematic GPS series has demonstrated its efficiency.

4.4 Comparison of FIR filter, Sequential algorithm and Kalman filter

4.4.1 Relationship between FIR filter, Sequential algorithm and Kalman filter

When the Kalman filter model is compared with the sequential algorithm, it is found that if $\overline{x}_k$ equals $\hat{x}_{k-1}$ and $P_{\overline{x}_k}$ equals $P_{\hat{x}_{k-1}}$, then the Equation 4.14 are the same as Equation 4.58. That means the sequential algorithm can be considered as one special case of the Kalman filter model (Li and Kuhlmann 2008b).

The IIR filter shows that the state vector at a given epoch is obtained by a linear combination of the current observations and the state vectors at previous epochs. The Kalman filter can be considered as one sort of IIR filter, because, from the Equations 4.12-4.16, the optimal value of the current state vector can be obtained from the previous state vector and the new observations (Li and Kuhlmann 2008b).

The FIR filter demonstrates that if the filter length of FIR is *Q*, the optimal value of the state vector at a given epoch is obtained by a linear combination of the newest *Q* epochs' observations. Only parts of the observations are chosen to compute the optimal value of the newest state vector; the other previous observations have no effect on the optimal value of the state vector. An FIR filter is a special case of an IIR filter without feedback coefficients.

By contrast, the Kalman filter and the sequential algorithm obtain the optimal value of the state vector in a least mean square recursive manner based on all the observations. It is another form of a complete adjustment. The earlier observations affect the newest state vectors by the earlier state vector. To some extent, all the observations with different weights are used to compute the newest state vector in these two models (Li and Kuhlmann 2008b).

4.4.2 GPS experiment

Three different methods are employed to reduce the colored noise in the GPS real-time series.

The GPS experiment which the antennas of the reference station and the rover station are fixed is needed in order to estimate the stochastic model of GPS time series. All the variations are due to measurement deviations leading to the estimation of the stochastic model. The different stochastic models of the processed time series represent the performance of the three different methods.

Another purpose is to compare the ability of the deformation epoch detection of these three methods, so the kinematic time series which contain one deformation from GPS experiment described in Chapter 4 has been chosen (Fig. 4.26).

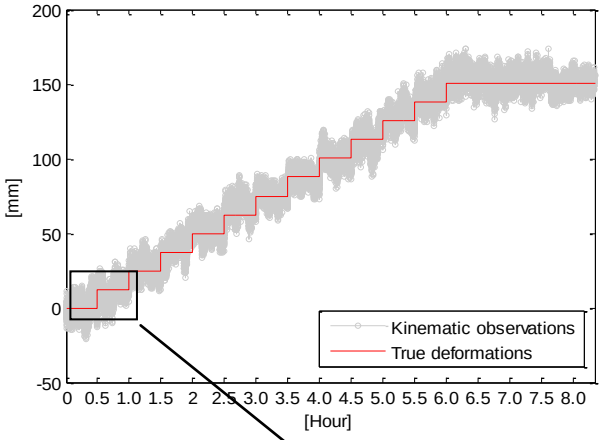

Fig. 4.24 Kinematic height observation time series

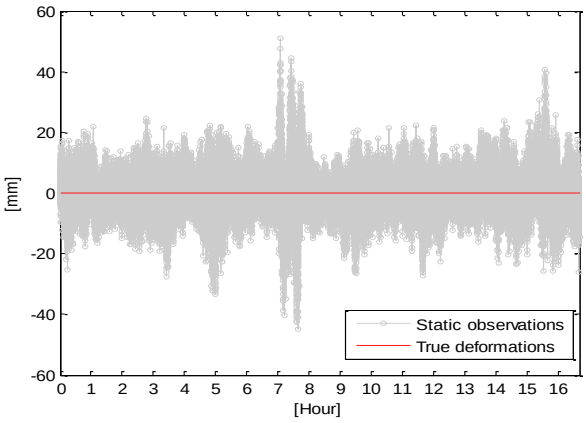

Fig. 4.25 Static height observation time series

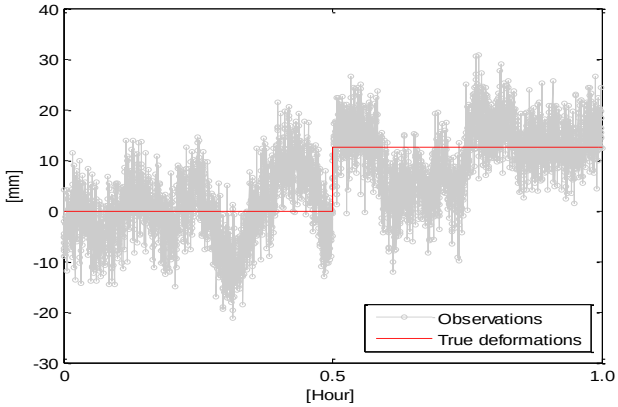

Fig. 4.26 Selected kinematic time series which includes one deformation

4.4.3 Results analysis of the processed GPS static time series

The three parameters of each stochastic model obtained from the static time series processed by different methods are shown in Table 4.14.

Table 4.14 Standard deviations of the processed time series

Static Time series / Methods	σ_δ (mm)	σ_Δ (mm)	α (1/second)	$\sigma = \sqrt{\sigma_\Delta^2 + \sigma_\delta^2}$ (mm)
Original	4.6	5.7	0.0063	7.3
FIR(order:30)	0.3	5.1	0.0076	5.1
KFs	0.5	2.6	0.0019	2.6
Sequential Algorithm	0.008	0.35	0.00005	0.35

KFs: the Kalman filter model with a shaping filter

The stochastic models of different time series processed by the three different methods (the FIR filter, the Kalman filter model with a shaping filter, and the sequential algorithm) are calculated on the basis of the results in Table 4.14. The distributions of the colored noise covariance are shown in Fig. 4.27.

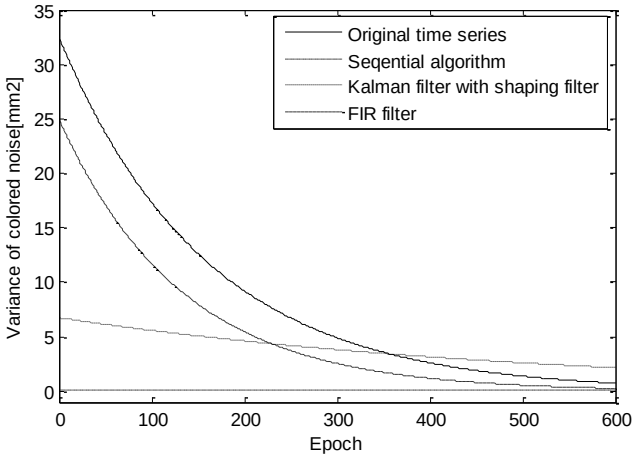

Fig. 4.27 Distribution of the variance of colored noises in different processed time series

In Fig. 4.27, it can be seen that the variances of the colored noises in the processed time series of each method decrease when compared to the variances of the colored noise in the original time series. It can be easily found that the sequential algorithm reduces the colored noise at the maximum level and the colored noise left in the processed time series can be neglected. By contrast, the colored noise is least reduced by the FIR filter.

The FIR filter model computes the new state vector only by the previous observations and removes the noise by weighting parts of previous observations. The results by the FIR filter illustrate that most of the colored noises are still kept in the processed time series. Compared with the results in Table 4.14, the denoising performance of the FIR filter is worse than that of the Kalman filter model with a shaping filter and the Sequential algorithm. If the order of the FIR

filter is large, it causes longer time delay; however, it is stable and robust against temporary uncertainties and round-off errors.

In the Kalman filter model, the new state vector is obtained not only by the newest observations but also by the previous state vector. The Kalman filter removes noises from the signal by using initialization and propagation of error covariance statistics. The shaping filter can be used to reduce the correlated noise in the GPS time series.

The sequential algorithm can be considered as a special case of the Kalman filter. Because of its special system equation $x_k = x_{k+1}$, the results of the processed time series are much smoother. Much of the white noise and colored noise have been reduced.

4.4.4 Results analysis of the processed GPS kinematic time series

For the chosen kinematic GPS time series (Fig. 4.26), the height was changed 12.5 mm after half an hour. Based on this principle of the deformation detection described in chapter 4.1.2, three different methods are used to process the GPS kinematic time series and detect the deformation epochs. The kinematic processed results are shown in the Fig. 4.28-Fig. 4.30 and the detected epochs are shown in Table 4.15.

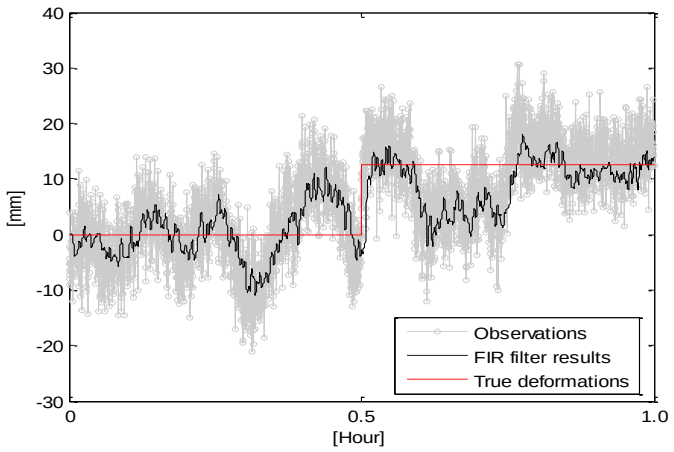

Fig. 4.28 Results of kinematic time series processed by FIR filter

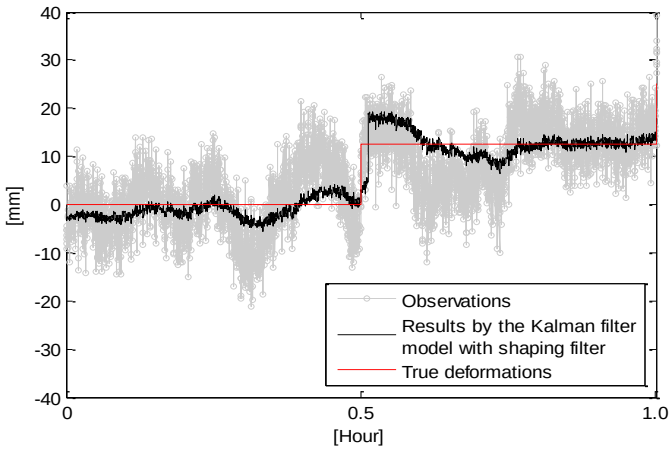

Fig. 4.29 Results of kinematic time series by Kalman filter model with a shaping filter

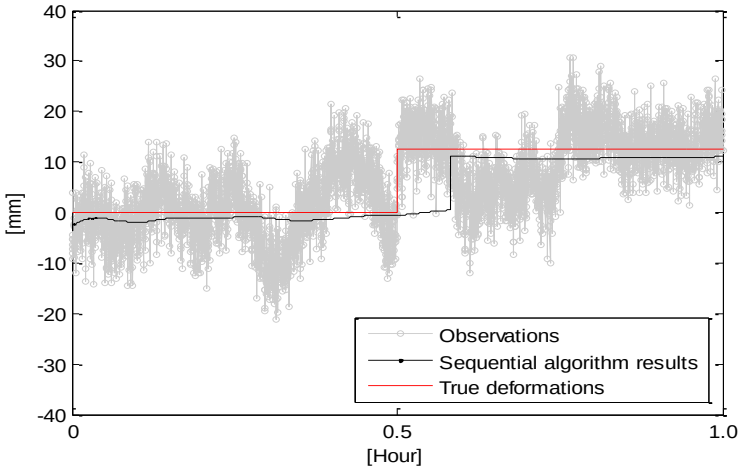

Fig. 4.30 Results of kinematic time series by sequential algorithm

From the accuracy of the processed results of the GPS static time series (Table 4.15), it can be seen that these three models can detect the 12.5 mm deformation. The results in Table 4.16 also prove this point. The sequential algorithm can detect smaller deformation when it is compared with the FIR filter, and the Kalman filter model with a shaping filter, because the processed results by the sequential algorithm have the highest precision (Table 4.15).

Table 4.15 Detected deformation epochs by FIR filter, the sequential algorithm and the Kalman filter model with a shaping filter

Methods	Detected Deformation Epochs(second)	Time Delay (second)	STD of the Processed Results(mm)	Notes
FIR	1838	38	5.1	Deformation: 12.5 mm True deformation epoch: 1800
Sequential algorithm	2096	296	2.5	
KFs	1847	47	3.0	

STD: standard deviation
KFs: Kalman filter model with a shaping filter

Table 4.15 demonstrates that the smallest time delay is 38 seconds, which was obtained by the 30-order FIR filter. By the Kalman filter model with a shaping filter, the time delay of the deformation epoch detection is 47 seconds. Compared the standard deviation, the accuracy of the results processed by the Kalman filter model with a shaping filter is higher than that of the FIR filter processing results. The largest time delay of the detected deformation epoch was 296 seconds, which was obtained by sequential algorithm. That is, because during the state vector's computation, the newest observation in the sequential algorithm has the least weight when compared with the other two methods. The previous state vectors play a more important role in the Sequential algorithm. When there is no deformation, the sequential algorithm can obtain accurate results. But when there is a deformation, the weight of the previous state vector should be reduced. According to the sequential algorithm, the weight of the previous state vector still plays

an important role in the computation of the new state vector, which causes the deformation to be detected very slowly.

4.4.5 Result analysis of different types of continuous deformation time series

As described in Chapter 4.1.3, Fig. 4.12-Fig. 4.15 demonstrate different types of movements. From the mathematical description of the sequential algorithm, it is can be used for processing the stepwise time series as mentioned above (Fig. 4.26), but is not appropriate for processing the continuous deformation time series.

The processed results will be compared between Kalman filter with a shaping filter (the identity model) and the FIR filter (order: 30).

The detection of a deformation epoch is based on the hypothesis testing with a given significance level $\alpha = 0.05$. Table 4.16 illustrates the first detected deformation epoch of the time series. The movement should be paid more attention after this epoch.

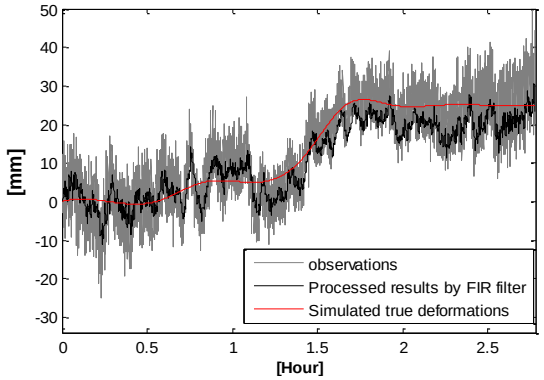

Fig. 4.31 Processed results by the FIR filter

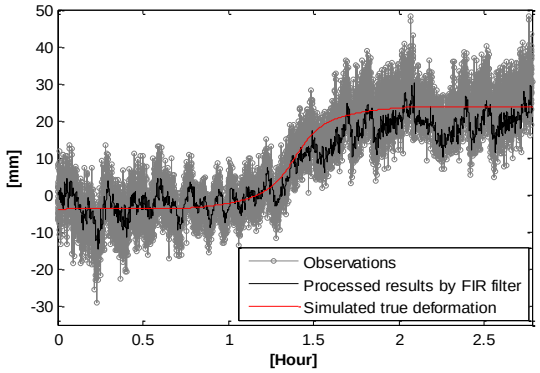

Fig. 4.32 Processed results by the FIR filter

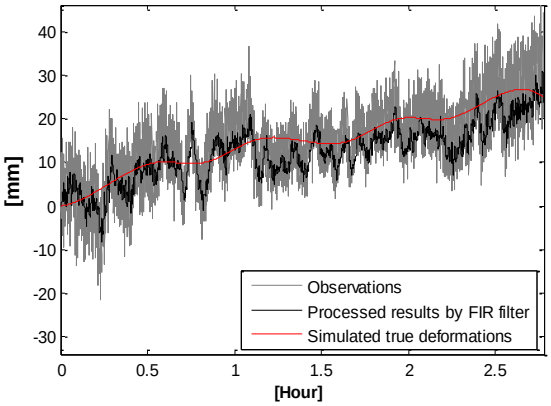

Fig. 4.33 Processed results by the FIR filter

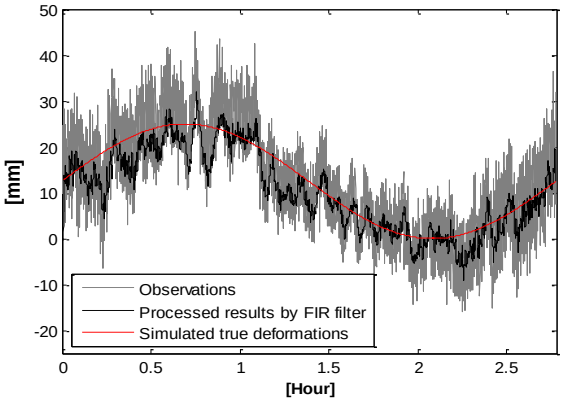

Fig. 4.34 Processed results by the FIR filter

The accuracies of the processed time series are different when different models process the same time series. For the same time series, when the accuracy of the processed time series is higher, smaller deformations can be detected and the epoch of the deformation event can be detected earlier.

Table 4.16 Deformation epoch detection of different time series processed by the FIR filter

Time series	Standard deviation of the processed time series (mm)	First detected deformation epoch (the true time series) (s)	First detected deformation epoch (the processed time series) (s)	Time delay (s)
Fig. 4.32	4.39	4932	4941	9
Fig. 4.33	4.66	4930	5151	221
Fig. 4.34	4.54	1663	1710	47
Fig. 4.35	4.18	1141	1553	412

Fig. 4.31- Fig. 4.34 and Table 4.16 are compared with Fig. 4.12a- Fig. 4.15a and Table 4.7. The processed results by the identity model with a shaping filter are with higher accuracy when compared to the FIR filter. Given a significance level $\alpha = 0.05$, by the hypothesis testing, the first detected epoch of the deformation by the identity model with shaping filter (Fig. 4.14) is epoch 1004, which is earlier than the epoch 1710 detected by the FIR filter (Fig. 4.33). The identity model with a shaping filter can detect the deformation at the magnitude of 4.7 mm, which is smaller than the deformation at magnitude of 9.1 mm by the FIR filter.

The Kalman filter with a shaping filter performs better than the FIR filter when they are used to process the real-time deformation series.

4.4.6 Summary

Three different methods for reducing the colored noise in the GPS time series have been described. Regarding the deformation detection and the reduction of the noise and outliers in the time series, a thorough comparison of these three methods has been made and the results by the three methods has been analyzed in detail.

5 Multiple Kalman Filters Model

5.1 Multiple Kalman filters model

During the deformation analysis, it is vital to detect the deformation epoch and improve the reliability of detecting deformation epoch. Numerous methods have been used to detect the deformation of the time series, for example, the multiple hypothesis filter (Willsky 1976), the generalized likelihood ratio test by using the Kalman filter innovation (Willsky 1976; Teunissen 1990; Okatan et al. 2007), the cumulative sum test (Mertikas and Rizos 1997; Mertikas 2001). Normally these statistical tests were used to detect the changes in the time series (Mikhail 1976). By contrast, the multiple Kalman filters model, based on the idea of model selection, is proposed to detect the deformation in the time series in order to improve the reliability of the detected epochs. The general idea of this algorithm is described as follows: several continuous epochs' position coordinates are saved as the state vector. It is supposed that there are different deformation trends when the new observations come. Different Kalman filters are used to describe the different possible deformation trends in the GPS real-time series. By comparing the statistical criterion value of every Kalman filter in the multiple Kalman filters model, the appropriate Kalman filter can be chosen and the deformation epoch can be detected. Because the state vector has the memory of several successive optimal position coordinates, this deformation epoch can still be detected again in the succeeding following epochs after the deformation epoch has been detected at the first epoch. Based on this character, the reliability to detect the deformation epoch can be improved (Li and Kuhlmann 2010). In order to verify the feasibilities and the improvement of the reliability of the detected epochs, one GPS experiment has been carried out.

The Kalman filter algorithm has been described in the previous section (Chapter 4); and, the multiple Kalman filters model will be introduced in the next section.

5.1.1 Principle of multiple Kalman filters model

In order to meet the requirement for the reliability and the punctuality of detecting the deformation epoch, the multiple Kalman filters model is proposed. Different Kalman filter state equations are used to describe the possible tendencies of movements. Considering the affections of the observations and the parameters in the state equations, according to the statistical criterion, the suitable Kalman filter state equation can be chosen. The detail of this model is introduced following.

5.1.1.1 Multiple Kalman filters

Each state vector in the Kalman filter takes m former continuous position coordinates into account; thus, not only the current coordinate but also m former epochs' coordinates are stored in the state vector. The choice of m depends on the sampling rate of the time series and what the

results of the time series will be used for. When *m* increases, more former epochs will be included into one state vector. In this case, more deformation trends will be needed to describe, which increase the computation complexity. When *m* is too small, it can't improve the reliability of the detected deformation epochs and give more false detected deformation epochs. Given the observations, it is better to choose the smallest *m* which can identify the deformation and improve the reliability. From statistical tests I made, *m*=3 is the smallest number which can identify the deformation epochs in the time series. We take *m*=3 in this case. Another variable the deformation d between the coordinates at two different epochs is added into the state vector. *d* should be described with two indexes *k* and *j*. The index *k* means the current epoch t_k, and *j* indicates the time shift between the current epoch t_k and the deformation epoch. $d_{k,j}$ is an important variable to detect the deformation and determine the deformation epoch.

The state vector at epoch t_k is defined as follows

$$X_k = \begin{bmatrix} x_k \\ x_{k-1} \\ x_{k-2} \\ x_{k-3} \\ d_{k,j} \end{bmatrix} \tag{5.1}$$

It is supposed that there are four different deformation possibilities among the four neighboring epochs position coordinates. Therefore, four different Kalman filters should be selected. The measurement equations in these Kalman filters are the same. The main difference is the system equations in the different Kalman filters, namely different system transformation matrixes in the Kalman filters' system equations. The measurement equations and the system equations are discussed in detail in each case.

The measurement equation in each case can be defined as

$$L_k = \begin{bmatrix} 1 & 0 & 0 & 0 & 0 \end{bmatrix} \begin{bmatrix} x_k \\ x_{k-1} \\ x_{k-2} \\ x_{k-3} \\ d_{k,j} \end{bmatrix} + \varepsilon_k \tag{5.2}$$

where L_k denotes the newest measurement, ε_k denotes the measurement noise.

The system equations of four cases are discussed as follows:

Case 1 There is no deformation among the four neighboring epochs' position coordinates, which means $x_k = x_{k-1} = x_{k-2} = x_{k-3}$ (Fig. 5.1). In this case, there is no deformation and no deformation time shift between epoch t_k and the former epochs. That is the deformation $d_{k,j} = 0$, $j = 0$.

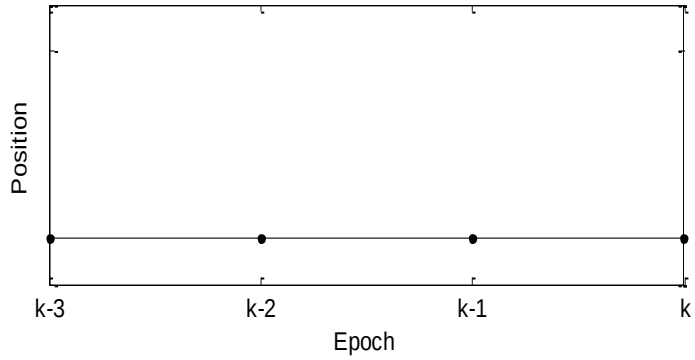

Fig. 5.1 Case 1

The system equation is described as

$$\begin{bmatrix} x_k \\ x_{k-1} \\ x_{k-2} \\ x_{k-3} \\ d_{k,0} \end{bmatrix} = \begin{bmatrix} 0 & 0 & 1 & 0 & 0 \\ 0 & 0 & 1 & 0 & 0 \\ 0 & 0 & 1 & 0 & 0 \\ 0 & 0 & 1 & 0 & 0 \\ 0 & 0 & 0 & 0 & 1 \end{bmatrix} \begin{bmatrix} x_{k-1} \\ x_{k-2} \\ x_{k-3} \\ x_{k-4} \\ d_{k,0} \end{bmatrix} + \begin{bmatrix} 1 \\ 0 \\ 0 \\ 0 \\ 0 \end{bmatrix} [\omega_k] \tag{5.3}$$

Case 2 There is a deformation between x_k and x_{k-1} among these four neighboring epochs' position coordinates. That indicates the time shift $j=1$, $x_k = x_{k-1} + d_{k,1}$, and $x_{k-1} = x_{k-2} = x_{k-3}$(Fig. 5.2).

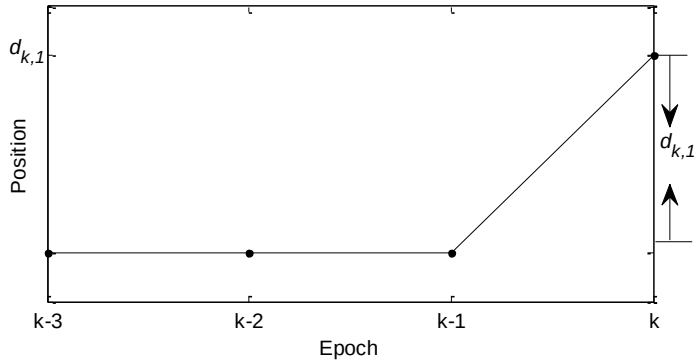

Fig. 5.2 Case 2

The system equation is defined as

$$\begin{bmatrix} x_k \\ x_{k-1} \\ x_{k-2} \\ x_{k-3} \\ d_{k,1} \end{bmatrix} = \begin{bmatrix} 0 & 0 & 1 & 0 & 1 \\ 0 & 0 & 1 & 0 & 0 \\ 0 & 0 & 1 & 0 & 0 \\ 0 & 0 & 1 & 0 & 0 \\ 0 & 0 & 0 & 0 & 1 \end{bmatrix} \begin{bmatrix} x_{k-1} \\ x_{k-2} \\ x_{k-3} \\ x_{k-4} \\ d_{k,1} \end{bmatrix} + \begin{bmatrix} 1 \\ 0 \\ 0 \\ 0 \\ 0 \end{bmatrix} [\omega_k] \tag{5.4}$$

Case 3 There is a deformation between x_{k-1} and x_{k-2} among these four neighboring epochs' position coordinates. That means compared to the present epoch t_k the deformation time shift $j=2$, $x_k = x_{k-1} = x_{k-2} + d_{k,2}$, and $x_{k-2} = x_{k-3}$ (Fig. 5.3).

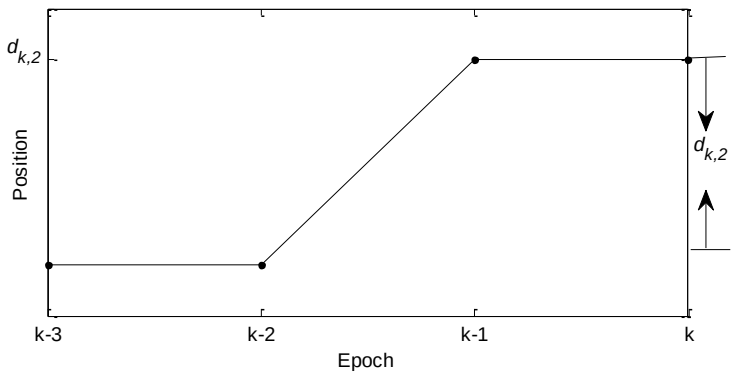

Fig. 5.3 Case 3

At epoch $t_{k\text{-}1}$ the deformations $d_{k-1,1}$ is detected at case 2, and at the next epoch t_k in case 3 the deformation $d_{k,2}$ is also detected, the relationship between the deformation vectors $d_{k,2}$ and $d_{k-1,1}$ should be found. It is known that

$$d_{k,2} = x_{k-2+1} - x_{k-2} = x_{k-1} - x_{k-2} \tag{5.5}$$

$$d_{k-1,1} = x_{k-1-1+1} - x_{k-1-1} = x_{k-1} - x_{k-2} \tag{5.6}$$

The values of $d_{k,2}$ and $d_{k-1,1}$ both equal $x_{k-1} - x_{k-2}$, thus it is obtained

$$d_{k,2} = d_{k-1,1} \tag{5.7}$$

The system equation is defined as

$$\begin{bmatrix} x_k \\ x_{k-1} \\ x_{k-2} \\ x_{k-3} \\ d_{k,2} \end{bmatrix} = \begin{bmatrix} 0 & 0 & 1 & 0 & 1 \\ 0 & 0 & 1 & 0 & 1 \\ 0 & 0 & 1 & 0 & 0 \\ 0 & 0 & 1 & 0 & 0 \\ 0 & 0 & 0 & 0 & 1 \end{bmatrix} \begin{bmatrix} x_{k-1} \\ x_{k-2} \\ x_{k-3} \\ x_{k-4} \\ d_{k-1,1} \end{bmatrix} + \begin{bmatrix} 1 \\ 0 \\ 0 \\ 0 \\ 0 \end{bmatrix} [\omega_k] \tag{5.8}$$

Case 4 There is a deformation between x_{k-2} and x_{k-3} among these four neighboring epochs' position coordinates. That indicates the time shift $j = 3$ when the deformation epoch is compared with the present epoch t_k. The relationship among these four neighboring epochs can be obtained as $x_k = x_{k-1} = x_{k-2} = x_{k-3} + d_{k,3}$ (Fig. 5.4).

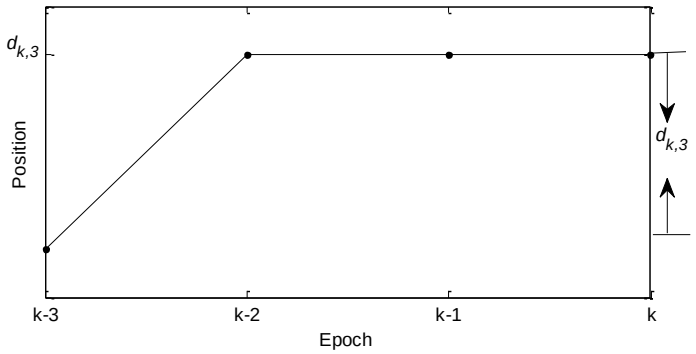

Fig. 5.4 Case 4

As analyzed above, when the time shift is 3, the formula can be obtained as

$$d_{k,3} = d_{k-1,2} = x_{k-2} - x_{k-3} \tag{5.9}$$

The system equation is described as follows,

$$\begin{bmatrix} x_k \\ x_{k-1} \\ x_{k-2} \\ x_{k-3} \\ d_{k,3} \end{bmatrix} = \begin{bmatrix} 0 & 0 & 1 & 0 & 1 \\ 0 & 0 & 1 & 0 & 1 \\ 0 & 0 & 1 & 0 & 1 \\ 0 & 0 & 1 & 0 & 0 \\ 0 & 0 & 0 & 0 & 1 \end{bmatrix} \begin{bmatrix} x_{k-1} \\ x_{k-2} \\ x_{k-3} \\ x_{k-4} \\ d_{k-1,2} \end{bmatrix} + \begin{bmatrix} 1 \\ 0 \\ 0 \\ 0 \\ 0 \end{bmatrix} [\omega_k] \tag{5.10}$$

5.1.1.2 Model selection

The multiple Kalman filters model can be considered as the combination of different Kalman filter models. In this thesis four continuous position coordinates are contained in the state vector of the multiple Kalman filters model. When the new observation comes, it is assumed that there are four different deformation possibilities. The different Kalman filters are used to represent different deformation trends. Each filter contributes to the description of the specific deformation tendency. In order to describe the deformation process correctly and identify the deformation epoch, it is necessary to select the optimal Kalman filter model at each epoch. Therefore a statistical criterion of model selection should be selected.

The objective is to select the optimal Kalman filter model of describing the deformation process correctly. In terms of probability, the model with maximum probability based on the observations should be chosen. According to Bayes theorem (Berger 1985), it is described as

$$P(A_i|L) = \frac{P(L|A_i)P(A_i)}{P(L)} \tag{5.11}$$

where A_i is the Kalman filter model with *i* parameters; $P(L)$ is the prior probability of observations *L*; $P(L|A_i)$ is the conditional probability of observations *L*, given the model A_i; $P(A_i)$ is the prior probability of the model A_i; $P(A_i|L)$ is the conditional probability of the model A_i, given observations *L*.

If the model with highest probability is chosen, then

$$\max\left[P(A_i|L)\right] = \max\left[\frac{P(L|A_i)P(A_i)}{P(L)}\right] \tag{5.12}$$

Rissanen applies minimizing the negative logarithm into Equation 5.12 instead of the maximizing the a posteriori probability, so the equation is obtained as

$$\min\left[-\log P(A_i|L)\right] = \min\left[-\log P(L|A_i) + K\right] \tag{5.13}$$

The selection of the minimum of $-\log P(L|A_i) + K$ equals the selection of the model with maximum probability. Therefore the problem turns to be the minimization of $-\log P(L|A_i) + K$ (Rissanen 1983).

Rissanen provided a simple approximation of $K = i \log \sqrt{N}$ when the model has *i* parameters and the sample size is *N*. He penalized the model complexity not only according to the number of parameters but also according to both parameters and precision. He came up with a reasonable figure for the precision any given model needed and postulated it to be $\log \sqrt{N}$ per parameter. The much more penalty is given to the higher complexity of the model. Given the observations L and the likelihood function $P(L|A_i)$, he proposed to minimize

$$-\log P(L|A_i) + i \log \sqrt{N}$$

leading to the Minimum Description Length (MDL) (Rissanen 1983).

The MDL criterion is described as follow

$$\zeta_{Ris} = -\log P(L|A_i) + i \log \sqrt{N} \tag{5.14}$$

It is composed of two parts. The first part $-\log P(L|A_i)$ is the complexity of the samples according to each model A_i; the second part $i \log \sqrt{N}$ is the penalty of the complexity of the model.

One dimensional coordinate time series can be selected as the observation *L*. The observations L_k of each case at epoch *k* follows a normal distribution with its own mean value in every different model of deformation tendency. The probability density functions of the measurement under different models are as follows

$$P(L_k|A_i) = \frac{1}{\sigma\sqrt{2\pi}} \exp\left[-\frac{(x-\mu_i)^2}{2\sigma^2}\right] \tag{5.15}$$

Based on the Equations 4.13 and 4.14, the Equation 5.15 can be written as

$$\begin{aligned} P(L_k|A_i) &= (Q_{V_k}{}^{1/2}(2\pi)^{1/2})^{-1} \exp\left[-\frac{1}{2} V_k (Q_{V_k})^{-1} V_k^T\right] \\ &= ((H_k P_{\bar{X}_k} H_k^T + R)^{1/2}(2\pi)^{1/2})^{-1} \exp\left[-\frac{1}{2}(L_k - H_k \bar{X}_k)(H_k P_{\bar{X}_k} H_k^T + R)^{-1}(L_k - H_k \bar{X}_k)^T\right] \end{aligned} \tag{5.16}$$

The term $i \log \sqrt{N}$ in the Kalman filter model selection is explained as follows: *N* is the number of the observations used in each Kalman filter model from the first epoch to the current epoch t_k, *i* is the number of the unknowns in each Kalman filter model. For example, in the first case, the newest state vector at epoch t_k is the unknown in the Kalman filters model, so *i* equals 1. According to the same principle, in the second case two unknowns which are the newest state vector at epoch t_k and the deformation between x_k and x_{k-1} exist, so *k*=2; in the third case *i*=3, and the forth case *i*=4. $i \log \sqrt{N}$ is characterized by the number of the unknowns and the observations. Different number of parameters of each model results in different affections to the precisions of different model.

The MDL criterion (5.14) in each case can be obtained as

$$\zeta_{Ris} = \frac{1}{2} V_k (Q_{V_k})^{-1} V_k^T + \frac{1}{2} \log(2\pi Q_{V_k}) + i \log \sqrt{N} \tag{5.17}$$

Based on MDL criterion, the minimization of the ζ_{RIS} will find the model with maximum probability. Given any estimated models, the model with the lower value of the MDL criterion (Equation 5.17) is to be preferred. Lower value of the criterion implies that the model better fits the time series. When the model is the correct one, the value of the statistical criterion should be the smallest when compared to the values of the other models. The deformation detection is reflected in the process of comparing the statistical criterion. When the smallest criterion is chosen, the corresponding Kalman filter and the deformation epoch can be determined. For example, if the criterion of the first case is the smallest, it indicates that no deformation is detected.

5.1.1.3 Program design

The flowchart of the multiple Kalman filters model has been shown in the Fig. 5.5.

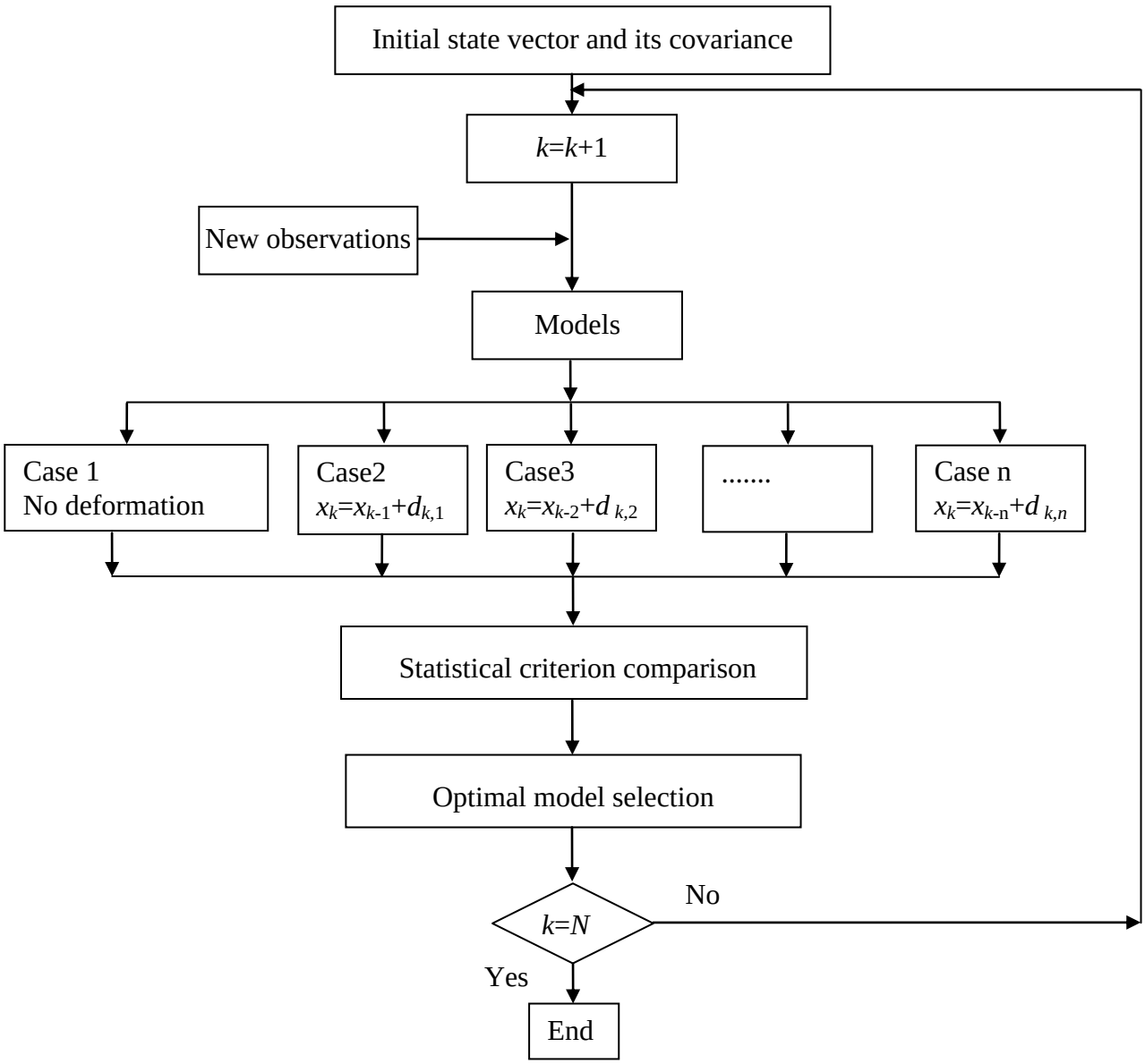

Fig. 5.5 Flowchart of the multiple Kalman filters model

Note: *N* denotes the last epoch of the observations.

5.1.2 Examples and results analysis

In this section two examples are presented to verify the effectiveness of the proposed multiple Kalman filters model.

5.1.2.1 First example: simulated time series

In order to assess the performance of the proposed model, one simulation experiment was carried out. The simulated time series was composed of the true positions and the white noise. The white noise whose standard deviation was 1 mm was generated by the Matlab function. The original coordinate was 0 mm. The deformation epochs occurred at several different epochs in the simulated time series (Fig. 5.6). From epoch 101 to epoch 200, the magnitude of the deformation 6mm was added into the time series. From epoch 201 to epoch 400, another -5mm deformation was added into the time series. From epoch 401 to epoch 500, the last additional deformation -5mm was added. The final simulated time series has been shown in Fig. 5.6. In the simulated time series, during epochs between 100 and 101, epochs between 200 and 201, epochs between 400 and 401 the deformations occurred.

Table 5.1 MDL criterion at epochs 101, 102, and 103

MDL Epoch \ Model	Case 1	Case 2	Case 3	Case 4
101	19.74	5.97	16.98	24.71
102	14.77	17.27	8.55	16.32
103	16.20	16.98	20.80	10.71

Table 5.2 MDL criterion at epochs 201, 202, and 203

MDL Epoch \ Model	Case 1	Case 2	Case 3	Case 4
201	16.33	6.35	23.86	20.03
202	19.06	18.71	9.11	29.07
203	15.38	18.95	17.95	11.69

Table 5.3 MDL criterion at epochs 401, 402, and 403

MDL Epoch \ Model	Case 1	Case 2	Case 3	Case 4
401	18.41	7.02	30.48	22.35
402	15.10	21.71	10.28	29.41
403	18.23	21.39	28.17	13.02

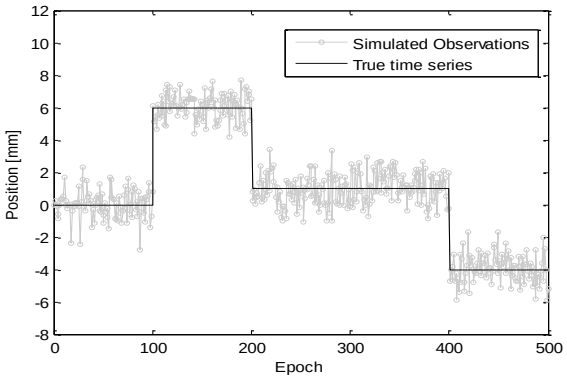

Fig. 5.6 Simulated time series

From Tables 5.1 to 5.3, the detected results by the multiple Kalman filters model are:
1st: The 2nd case at epoch 101, the 3rd case at epoch 102, and the 4th case at epoch 103;
2nd: The 2nd case at epoch 201, the 3rd case at epoch 202, and the 4th case at epoch 203;
3rd: The 2nd case at epoch 401, the 3rd case at epoch 402, and the 4th case at epoch 403.

According to the description of the deformation vector $d_{k,j}$, it can be obtained that the deformation epoch occurred between the epochs t_{k-j} and t_{k-j+1}. From Fig. 5.2, Fig. 5.3, and Fig. 5.4 it is known that the second case means the time shift $j=1$, the third case means the time shift $j=2$, and the forth case means the time shift $j=3$.

Based on the first results, the second case at epoch 201 means the deformation occurred between epochs 200 and 201; the third case at epoch 202 means the deformation occurred between epochs 200 and 201; the fourth case at epoch 203 means the deformation occurred between epochs 200 and 201. From these different cases at different epochs, the deformation epoch is determined to be between epochs 200 and 201.

In a similar analysis, the other deformation epochs are detected separately as the epoch between epochs 200 and 201, and the epoch between epochs 400 and 401. All the detected results by the multiple Kalman filters model are the same as the epochs we added in the simulated time series. The processed results are shown in Fig. 5.7. Compared to the true time series, the standard deviation of the processed time series is 0.5 mm.

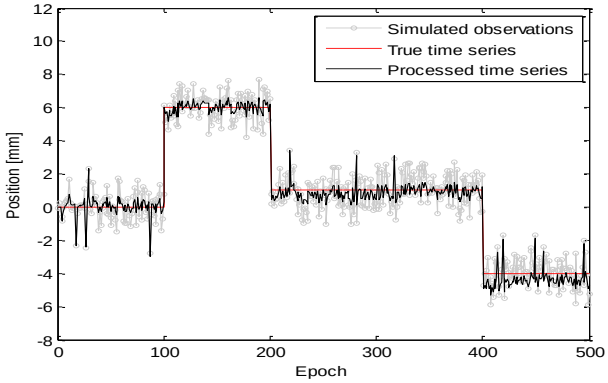

Fig. 5.7 Processed time series

5.1.2.2 Second example: GPS experiment

Three GPS time series have been chosen from the GPS experiment described in Chapter 3 and 4. The first GPS time series lasted 3.5 hours, which is 12600 seconds (Fig. 5.8). Every half hour the deformation has been changed by 25 mm. The second time series of GPS static observations lasted 17 hours (Fig. 5.9) can also be used to check the efficiency of the multiple Kalman filters model. The third time series of GPS kinematic observations include the smaller stepwise deformations of 12.5 mm which have been changed every half hour (Fig. 5.10).

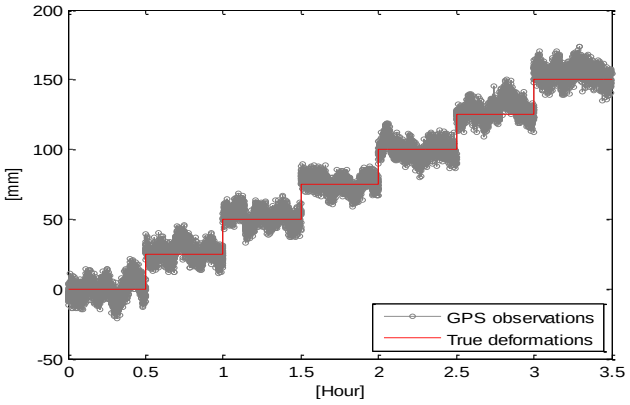

Fig. 5.8 GPS kinematic height time series (25 mm)

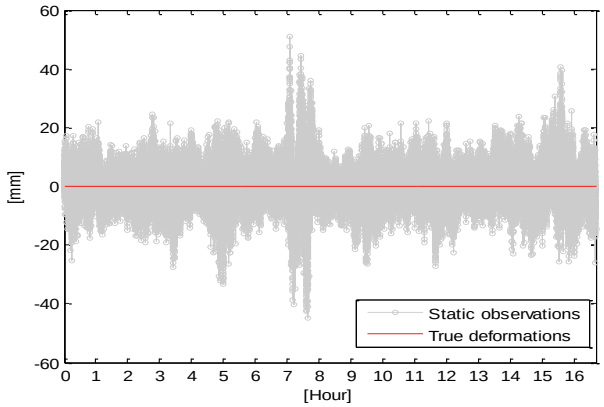

Fig. 5.9 GPS static height observation time series

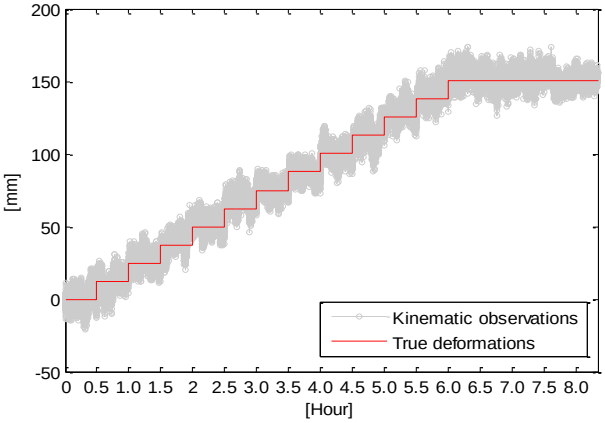

Fig. 5.10 GPS kinematic height time series (12.5 mm)

a) Application in the GPS stepwise deformation at a magnitude of 25 mm

The principle of determining the deformation epoch is that via the model selection, if at epoch t_k, case 2 is selected; at epoch t_{k+1}, case 3 is selected; at epoch t_{k+2}, case 4 is selected. During these continuous epochs, case 2 , case 3, and case 4 are correspondingly selected at epochs t_k, t_{k+1}, and t_{k+2}, then there must be a deformation and the deformation epoch occurred between epochs t_{k-j} and t_{k-j+1}. Otherwise, it can be only considered that there is an outlier.

Based on the MDL criterion shown in Tables 5.4 to 5.9, all the detected deformation epochs are shown in Table 11. For instance, at epoch 1801, case 2 is chosen, at the following epochs 1802 and 1803, case 3 and case 4 are chosen. It implies that the deformation can be found under different models. Therefore, there must be a deformation during the epochs 1800 and 1801. But if not all of the cases 2, 3 and 4 are selected during three continuous epochs, it can't be determined that a deformation exists. For instance, in Table 10 at epoch 9878, case 2 is chosen, but at the next two epochs 9879 and 9880, case 1 is chosen, which means no deformation turns out in the next epochs. In this example, the jump can't be considered as a deformation (Fig. 5.11).

Table 5.11 demonstrates that the deformation epochs are detected by the multiple Kalman filters model, such as during the epochs 1800 to 1801, epochs 3600 to 3601, epochs 5400 to 5401, epochs 7200 to 7201, epochs 9000 to 9001, and epochs 10800 to 10801. All the detected epochs are the true epochs when there is really a deformation. No other false deformation epoch are found.

In order to assess the performance of the proposed model, the precision of the time series should also be considered. Compared the true value of the time series, the standard deviation of the actual observations is 6.50 mm. After the time series was processed by the multiple Kalman filters model, the standard deviation of the processed time series is 4.87 mm. The precision has been improved 25.1%. From the deformation epoch detection and the precision of the processed time series, it is obvious that the multiple Kalman filters model works well.

Table 5.4 MDL criterion at epochs 1801, 1802, and 1803

MDL Model / Epoch	Case 1	Case 2	Case 3	Case 4
1801	23.11	12.03	27.34	27.81
1802	28.34	24.71	16.89	35.68
1803	25.38	27.68	26.16	19.94

Table 5.5 MDL criterion at epochs 3601, 3602, and 3603

MDL Model / Epoch	Case 1	Case 2	Case 3	Case 4
3601	17.60	12.34	22.64	30.54
3602	19.13	21.45	16.54	27.98
3603	23.40	22.40	29.46	21.40

Table 5.6 MDL criterion at epochs 5401, 5402, and 5403

MDL / Model / Epoch	Case 1	Case 2	Case 3	Case 4
5401	21.08	13.63	23.78	31.21
5402	28. 72	23.06	20.61	33.88
5403	23.94	27.32	24.04	23.08

Table 5.7 MDL criterion at epochs 7201, 7202, and 7203

MDL / Model / Epoch	Case 1	Case 2	Case 3	Case 4
7201	19.41	13.02	24.42	37.81
7202	20.95	23.76	17.53	30.10
7203	29. 41	24.73	36.16	23.61

Table 5.8 MDL criterion at epochs 9001, 9002, and 9003

MDL / Model / Epoch	Case 1	Case 2	Case 3	Case 4
9001	22.25	13.52	37.04	32.35
9002	24.30	28.24	17.86	44.02
9003	25.79	29.60	34.25	22.35

Table 5.9 MDL criterion at epochs 10801, 10802, and 10803

MDL / Model / Epoch	Case 1	Case 2	Case 3	Case 4
10801	30.56	13.46	36.22	44.04
10802	22.40	34.56	18.68	33.50
10803	23.58	29.21	40.66	23.11

Table 5.10 MDL criterion at epochs 9878, 9879, and 9880

MDL / Model / Epoch	Case 1	Case 2	Case 3	Case 4
9878	14.90	13.36	27.51	29.56
9879	9.10	19.75	22.01	24.01
9880	9.42	13.48	25.55	25.75

Table 5.11 Detected deformation epochs in the GPS time series

True deformation epochs	Detected epochs t_k in the second case (j=1)	Detected Epochs t_k in the third case (j=2)	Detected epochs t_k in the fourth case (j=3)	Detected deformation epochs (t_{k-j},t_{k-j+1})
During epochs 1800 and 1801	1801	1802	1803	(1800,1801)
During epochs 3600 and 3601	3601	3602	3603	(3600,3601)
During epochs 5400 and 5401	5401	5402	5403	(5400,5401)
During epochs 7200 and 7201	7201	7202	7203	(7200,7201)
During epochs 9000 and 9001	9001	9002	9003	(9000,9001)
During epochs 10800 and 10801	10801	10802	10803	(10800,10801)

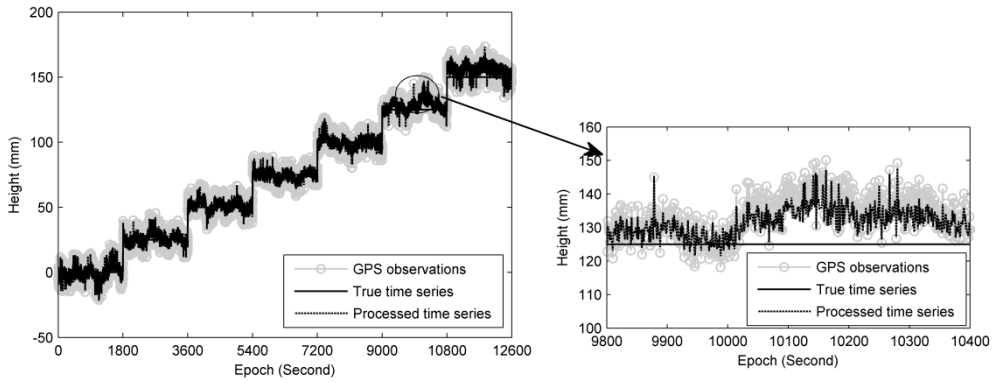

Fig. 5.11 Processed results by the multiple Kalman filters model

b) Application in the GPS static time series

Table 5.12 demonstrates that the deformation epochs are detected in the GPS static time series by the multiple Kalman filters model. In fact, there should be no detected deformation epochs in the GPS static time series. But some epochs are detected as the deformation epcohs by the multiple Kalman filters model. Table 5.12 shows that the detected epochs are in the period from epoch 25339 to 27623 (7.04 hour to 7.67 hour). It is found that the satellite geometry is very poor during this period, resulting to the higher value of the geometric dilution of precision (GDOP). That is why some epochs are detected as deformation epochs. The conclusion here is coincidence with that derived by Kalman filter with a shaping filter in section 4.1.2.3.

The processed time series has been shown in Fig. 5.12. Compared to the true time series, the standard deviation of the GPS observations is 7.3 mm. After the time series was processed by the multiple Kalman filters model, the standard deviation of the processed time series is 5.3 mm. The precision has been improved by 27.4%.

Table 5.12 Detected deformation epochs in the GPS static time series processed by the multiple Kalman filters model

True deformation epochs	Detected deformation epochs (t_{k-j},t_{k-j+1})	Note
No deformation epoch	(25338, 25339) (25401, 25402) (25412, 25413) (25658, 25659) (26586, 26587) (27145, 27146) (27348, 27349) (27622, 27623)	The detected epochs are in the period Hour (7.04 to 7.67) if in the unit of Hour.

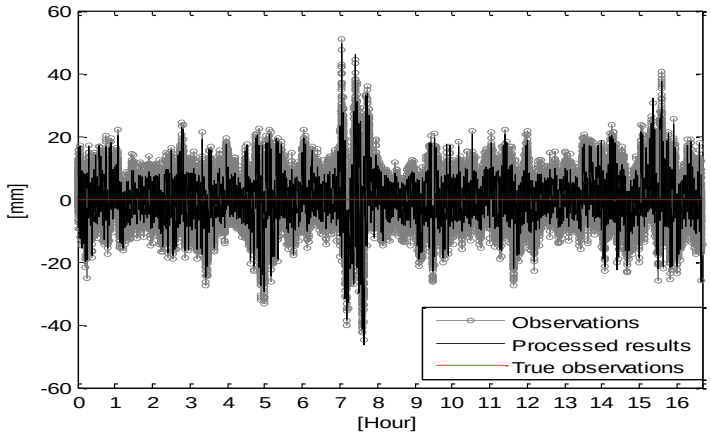

Fig. 5.12 Processed time series by multiple Kalman filters model

c) Application in the GPS stepwise deformation at a magnitude of 12.5 mm

The proposed method is used to process the smaller stepwise deformation time series (Fig. 5.10) and Table 5.13 illustrates the results of the detected deformation epochs. From Table 5.13, it can be seen that not all the deformation epochs are detected by the multiple Kalman filters model. Five true deformation epochs have not been detected by the multiple Kalman filters model. When the stepwise deformations are smaller, some stepwise changes contaminated by the co-lored noise are not so obvious. The ability of the multiple Kalman filters model to detect such contaminated stepwise changes is limited. The noise affection needs to be reduced and the multiple Kalman filters model needs modification.

Compared to the true value of the time series, the standard deviation of the true observations is 6.5 mm. After the time series was processed by the multiple Kalman filters model, the standard deviation of the processed time series is 5.3 mm.

Table 5.13 Detected deformation epochs in the GPS stepwise time series processed by the multiple Kalman filters model

True deformation epochs		Detected deformation epochs	Time delay
(Hour)	(s)	(t_{k-j},t_{k-j+1})	(s)
0.5	1800	(1809 1810)	9
1.0	3600	(3603,3604)	3
1.5	5400	Not detected	Not detected
2.0	7200	Not detected	Not detected
2.5	9000	(9052,9053)	52
3.0	10800	(10834,10835)	34
3.5	12600	Not detected	Not detected
4.0	14400	(14426,14427)	26
4.5	16200	Not detected	Not detected
5.0	18000	(10834,108315)	34
5.5	19800	Note detected	Not detected
6.0	21600	(21603,21604)	03

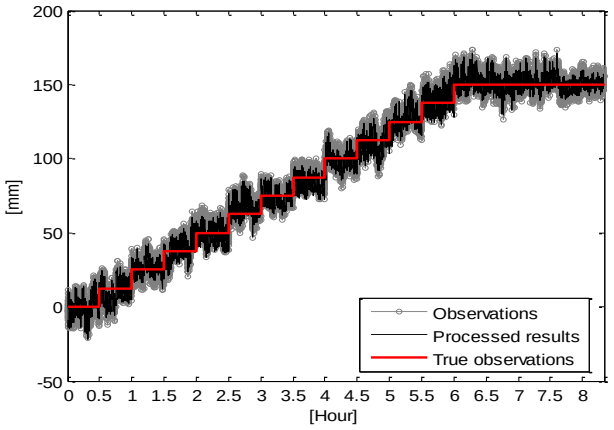

Fig. 5.13 Processed time series by multiple Kalman filters model

Summary

The principle of the multiple Kalman filters model has been described in detail and different time series are used to check its efficiency. Its advantages and limitations have been analyzed.

5.2 Modification of multiple Kalman filters model

5.2.1 Multiple Kalman filters model with shaping filters

As we know colored noises exist in the GPS time series and follow an exponential function. In order to reduce the affection of the colored noise in the GPS time series, the state vector in the multiple Kalman filters model is augmented by a shaping filter $x_{sf}(k)$ (Equation 4.25) which can describe the long movement of colored noise.

The augmented state equation can be described as

$$X_k = \begin{bmatrix} x_k \\ x_{k-1} \\ x_{k-2} \\ x_{k-3} \\ d_{k,j} \\ x_{sf}(k) \end{bmatrix}$$

The measurement equation in each case can be defined as

$$L_k = \begin{bmatrix} 1 & 0 & 0 & 0 & 0 & 1 \end{bmatrix} \begin{bmatrix} x_k \\ x_{k-1} \\ x_{k-2} \\ x_{k-3} \\ d_{k,j} \\ x_{sf}(k) \end{bmatrix} + \varepsilon_k \tag{5.18}$$

The system equation in case 1 is described as followed

$$\begin{bmatrix} x_k \\ x_{k-1} \\ x_{k-2} \\ x_{k-3} \\ d_{k,0} \\ x_{sf}(k) \end{bmatrix} = \begin{bmatrix} 0 & 0 & 1 & 0 & 0 & 0 \\ 0 & 0 & 1 & 0 & 0 & 0 \\ 0 & 0 & 1 & 0 & 0 & 0 \\ 0 & 0 & 1 & 0 & 0 & 0 \\ 0 & 0 & 0 & 0 & 1 & 0 \\ 0 & 0 & 0 & 0 & 0 & e^{-\alpha\Delta t} \end{bmatrix} \begin{bmatrix} x_{k-1} \\ x_{k-2} \\ x_{k-3} \\ x_{k-4} \\ d_{k,0} \\ x_{sf}(k-1) \end{bmatrix} + \begin{bmatrix} 1 & 0 \\ 0 & 0 \\ 0 & 0 \\ 0 & 0 \\ 0 & 0 \\ 0 & e^{-\alpha\Delta t} \end{bmatrix} \begin{bmatrix} \omega_{k-1} \\ w_{k-1} \end{bmatrix} \tag{5.19}$$

The system equation in case 2 is described as followed

$$\begin{bmatrix} x_k \\ x_{k-1} \\ x_{k-2} \\ x_{k-3} \\ d_{k,1} \\ x_{sf}(k) \end{bmatrix} = \begin{bmatrix} 0 & 0 & 1 & 0 & 1 & 0 \\ 0 & 0 & 1 & 0 & 0 & 0 \\ 0 & 0 & 1 & 0 & 0 & 0 \\ 0 & 0 & 1 & 0 & 0 & 0 \\ 0 & 0 & 0 & 0 & 1 & 0 \\ 0 & 0 & 0 & 0 & 0 & e^{-\alpha\Delta t} \end{bmatrix} \begin{bmatrix} x_{k-1} \\ x_{k-2} \\ x_{k-3} \\ x_{k-4} \\ d_{k,1} \\ x_{sf}(k-1) \end{bmatrix} + \begin{bmatrix} 1 & 0 \\ 0 & 0 \\ 0 & 0 \\ 0 & 0 \\ 0 & 0 \\ 0 & e^{-\alpha\Delta t} \end{bmatrix} \begin{bmatrix} \omega_{k-1} \\ w_{k-1} \end{bmatrix} \tag{5.20}$$

The system equation in case 3 is described as followed

$$\begin{bmatrix} x_k \\ x_{k-1} \\ x_{k-2} \\ x_{k-3} \\ d_{k,2} \\ x_{sf}(k) \end{bmatrix} = \begin{bmatrix} 0 & 0 & 1 & 0 & 1 & 0 \\ 0 & 0 & 1 & 0 & 1 & 0 \\ 0 & 0 & 1 & 0 & 0 & 0 \\ 0 & 0 & 1 & 0 & 0 & 0 \\ 0 & 0 & 0 & 0 & 1 & 0 \\ 0 & 0 & 0 & 0 & 0 & e^{-\alpha\Delta t} \end{bmatrix} \begin{bmatrix} x_{k-1} \\ x_{k-2} \\ x_{k-3} \\ x_{k-4} \\ d_{k-1,1} \\ x_{sf}(k-1) \end{bmatrix} + \begin{bmatrix} 1 & 0 \\ 0 & 0 \\ 0 & 0 \\ 0 & 0 \\ 0 & 0 \\ 0 & e^{-\alpha\Delta t} \end{bmatrix} \begin{bmatrix} \omega_{k-1} \\ w_{k-1} \end{bmatrix} \tag{5.21}$$

The system equation in case 4 is described as followed

$$\begin{bmatrix} x_k \\ x_{k-1} \\ x_{k-2} \\ x_{k-3} \\ d_{k,3} \\ x_{sf}(k) \end{bmatrix} = \begin{bmatrix} 0 & 0 & 1 & 0 & 1 & 0 \\ 0 & 0 & 1 & 0 & 1 & 0 \\ 0 & 0 & 1 & 0 & 1 & 0 \\ 0 & 0 & 1 & 0 & 0 & 0 \\ 0 & 0 & 0 & 0 & 1 & 0 \\ 0 & 0 & 0 & 0 & 0 & e^{-\alpha\Delta t} \end{bmatrix} \begin{bmatrix} x_{k-1} \\ x_{k-2} \\ x_{k-3} \\ x_{k-4} \\ d_{k-1,2} \\ x_{sf}(k-1) \end{bmatrix} + \begin{bmatrix} 1 & 0 \\ 0 & 0 \\ 0 & 0 \\ 0 & 0 \\ 0 & 0 \\ 0 & e^{-\alpha\Delta t} \end{bmatrix} \begin{bmatrix} \omega_{k-1} \\ w_{k-1} \end{bmatrix} \tag{5.22}$$

The system equation and the observation equation of each case have been given. The following procedures (model selection and its flowchart) are similar to the description of the multiple Kalman filters model in section 5.1.

5.2.2 Application in the GPS time series and result analysis

Different GPS time series (Fig.5.8, 5.9 and 5.10) are used to check the efficiency of the multiple Kalman filters model with shaping filter.

5.2.2.1 Application in the GPS time series of stepwise deformations at a magnitude of 25mm

Table 5.14 shows that during the detection of the deformation epochs, all the true deformation epochs are detected; but two false deformation epochs are detected as deformation epochs. Fig. 5.14 demonstrates that the colored noises in the GPS time series have been reduced by the shaping filter.

The standard deviation of the processed time series is 4.0 mm. Compared to standard deviation of the observations, the precision of the processed time series has been improved.

Compared with the multiple Kalman filters model, in case of the stepwise deformation of 25 mm, both can detect all the true deformation epochs. But the multiple Kalman filters model with shaping filters can reduce the affection of colored noise and the precision of the processed time series is higher than that of the processed time series by multiple Kalman filters model.

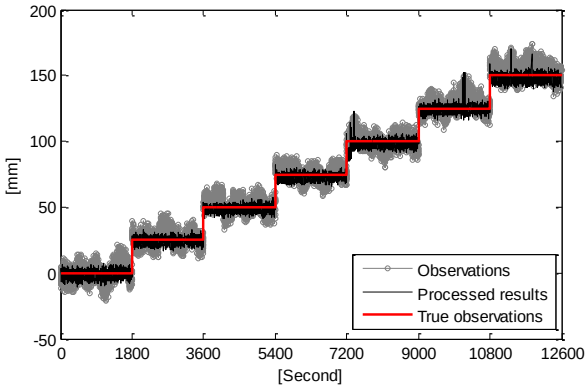

Fig. 5.14a Processed time series

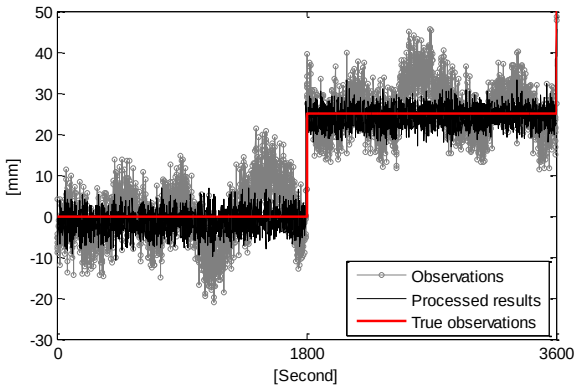

Fig. 5.14b Processed time series (first change)

Table 5.14 Detected deformation epochs in the GPS stepwise time series

True deformation epochs	Detected deformation epochs (t_{k-j},t_{k-j+1})	Time delay(s)	Note
1801	(1801 1802)	0	Two false deformation epochs (7315,7316) (10138,10139)
3601	(3601,3602)	0	
5401	(5403,5404)	2	
7201	(7207,7208)	6	
9001	(9005,9006)	4	
10801	(10802,10803)	1	

5.2.2.2 Application in the GPS static deformation time series

As we know no deformation epochs exist in the static time series (Fig. 5.9). Tables 5.15 illustrates the false detected deformation epochs obtained by multiple Kalman filters model with a

shaping filter. As analyzed above, during the epoch 25339 to 27623, the satellite geometry is very poor. The accuracy of the results is very low. Some results are not reliable so that the difference between the coordinates becomes large, in that case it can be detected as a deformation. That is the reason some epochs are detected as the deformation epochs. The standard deviation of the processed time series is 3.0 mm. The accuracy has been improved.

Compared with multiple Kalman filters model, the same conclusion is that all the detected false deformation epochs are during the period when the satellite geometry is poor. The difference is that multiple Kalman filters model with shaping filter can reduce the affection of colored noise.

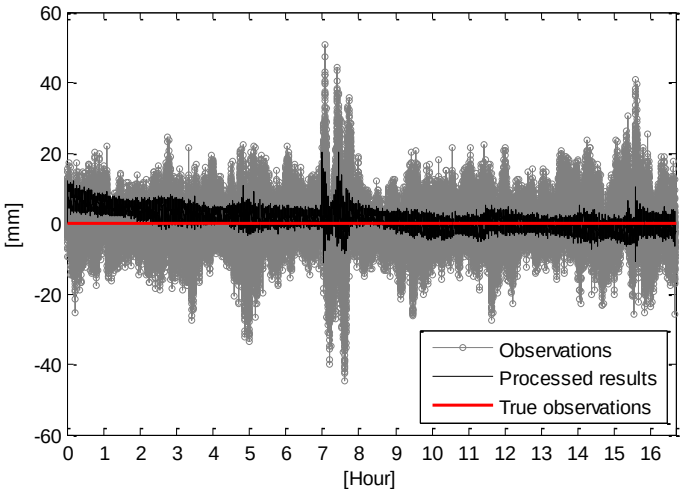

Fig. 5.15 Processed time series

Table 5.15 Detected deformation epochs in the GPS static time series

True deformation epochs	Detected deformation epochs (t_{k-j},t_{k-j+1})	Note
No deformation epoch	(25346, 25347) (25401, 25405) (26586, 26587)	The detected epochs are during the period when the satellite geometry is poor.

5.2.2.3 Application in the GPS time series of stepwise deformations at a magnitude of 12.5mm

The standard deviation of the processed time series (Fig. 5.16a) is 4.5 mm.

Table 5.16 illustrated the results of all the detected deformation epochs and Fig. 5.16 shows the processed time series by the multiple Kalman filters model with shaping filters. In case of the 12.5 mm stepwise deformation time series (Fig. 5.10), all the true deformation epochs have been detected by the multiple Kalman filters model with shaping filters. However, not all true deformation epochs have been detected by the multiple kalman filters model. In the regard of deformation epochs detection, the multiple Kalman filters model with shaping filters is better.

But at the same time, Table 5.16 shows that more false deformation epochs are detected as the deformation epochs by the multiple Kalman filters model with shaping filters when compared to Table. 5.13. The false deformation epochs will decrease the precision of the processed results. In this point this model still needs further improvement.

Table 5.16 Detected deformation epochs in the GPS kinematic time series

True deformation epochs	Detected deformation epochs (t_{k-j},t_{k-j+1})	Time delay(s)	Note
1800	(1835,1836)	35	False detected epochs
3600	(3600,3601)	0	
5400	(5410,5411)	10	1547
7200	(7205,7206)	5	3801
9000	(9000,9001)	0	9814
10800	(10823,10824)	23	18240
12600	(12620,12621)	20	12380
14400	(14510,14511)	110	21010
16200	(16386,16387)	186	
18000	(18104,18105)	104	
19800	(19931,19932)	131	
21600	(21606,21607)	6	

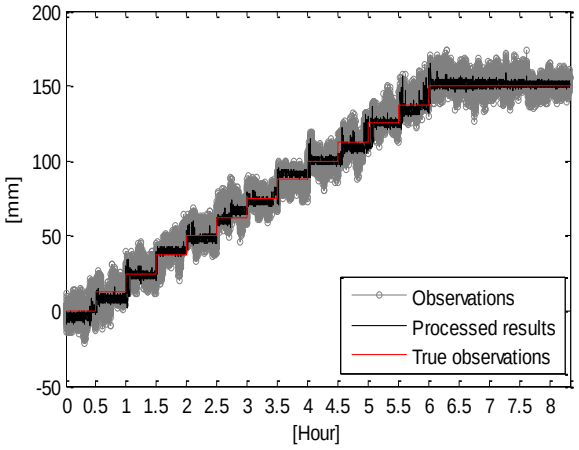

Fig. 5.16a Processed time series

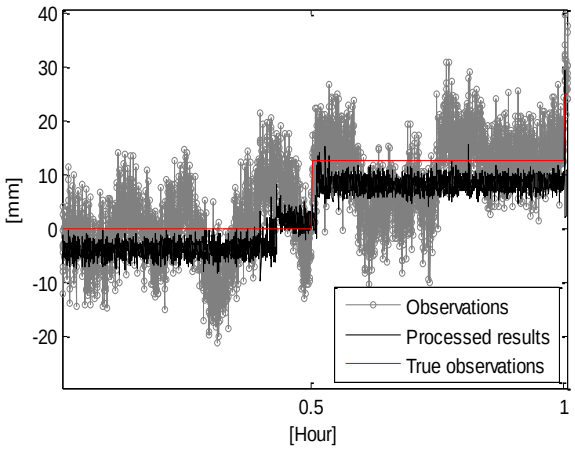

Fig. 5.16b Processed time series (first change)

5.3 Summary

Many monitoring problems can be stated as the problem of detecting a change. It is very important to detect small changes in some applications, because some economic or catastrophic consequences that result from an accumulation of small changes can be avoided. False warnings should also be given as few as possible.

The multiple Kalman filters model has been proposed to capture the deformation epochs and improve the reliability of detecting the deformation epoch. The multiple Kalman filters model is a simple and adaptable algorithm. In the multiple Kalman filters model different possible deformation trends are represented, and based on the MDL statistical criterion, the appropriate filter of modeling the deformation trend can be chosen. The time series can be processed by the multiple Kalman filters model in order to assess whether the deformation exists in the time series or not. The proposed model makes use of the statistical criterion comparison in each case instead of the hypothesis test. In order to reduce the affection of colored noise in the GPS time series, the multiple Kalman filter model is augmented with a shaping filter which can describe the long term movement of the correlated measurement deviations.

Based on comparisons of the applications in different GPS time series, the effectiveness and the limitation of the proposed model have been analyzed. The proposed model can be used to detect stepwise changes of a variety of fields and predict some natural catastrophic events in real time or near real time, for example, landslide or a cycle slip in the phase data. Yet in the future further work need to be done: besides the stepwise deformations, more complicated deformation possibilities, such as the continuous deformation, can be investigated in this model.

6 Conclusions and Recommendations

6.1 Conclusions

The focus of the thesis was mainly on how to eliminate the affection of colored noise, to improve the accuracy of the GPS real-time series and to improve the reliability of detecting deformation epochs. The theoretical analysis and field experiments were conducted in this research. The following conclusions can be drawn from the findings of the research:

1) The GPS coordinate time series are analyzed by the autocorrelation function. The property of the noise has been explored in detail, especially how to determine the correlated error property of the GPS coordinate time series. The stochastic models to determine the autocorrelation function of GPS coordinate(X, Y, H) measurement deviation are discussed in detail. The results demonstrate that the GPS real–time measurement deviation have a high autocorrelation, which should be considered in the GPS high-precision positioning. Thus, in the deformation data analysis it is not proper to simply take the measurement deviations as the white noise.

2) In this thesis, three different methods for reducing the colored noise in the GPS time series have been described: FIR filter, the Sequential algorithm and the Kalman filter.

a) The FIR filter demonstrates that if the filter length of FIR is Q , the optimal value of the state vector at a given epoch is obtained by a linear combination of the newest Q epochs' observations. Only parts of the observations are chosen to compute the optimal value of the newest state vector; the other previous observations have no effect on the optimal value of the state vector.

The Kalman filter and the Sequential algorithm obtain the optimal value of the state vector in a least mean square recursive manner based on all the observations. It is another form of a complete adjustment. The earlier observations affect the newest state vectors by the earlier state vector. To some extent, all the observations with different weights are used to compute the newest state vector in these two models.

b) For the magnitude of the detected deformation, the results show that the Sequential algorithm can detect the smallest deformation among these three methods. Considering the time delay of the detected deformation epoch, the FIR filter has better ability to detect the deformation with least time delay.

c) The deformation analysis based on the Kalman filter model with a shaping filter technique which contains the identity model and the kinematic model has been applied in the different movement tendencies of GPS time series. Not only the stepwise deformation but also the continuous deformation can be processed by the Kalman filter model with a shaping filter. From the results, it is shown that the Kalman filter model with a shaping filter can reduce the colored noise, improve the accuracy of the coordinates and describe the movement closer to the true trajectory.

The Kalman filter model with a shaping filter can be widely used to process the GPS short baseline time series in real-time so that we can obtain the precise positions and detect the deformations in time and with high reliability. The Kalman filter model with a shaping filter can be widely used in these following applications: GPS used in dam deformation monitoring, bridge deformation monitoring or landslide deformation monitoring, etc.

The Kalman filter model with a shaping filter can be used to detect and distinguish the deformation and outlier simultaneously. How to determine the state vector value when outlier and deformation occur is discussed in detail. An application to the GPS static and kinematic time series demonstrates that the method proposed can get the results with short time delay. This proposed method is useful to analyze the time series and make the right decision when deformations occur.

3) The multiple Kalman filters model is proposed to improve the reliability of detecting the deformation epochs and detect the deformation epoch with less time delay. In the multiple Kalman filters model, different possible deformation trends are represented, and based on the MDL statistical criterion, the appropriate filter of modeling the deformation trend can be chosen. The time series can be processed by the multiple Kalman filters model in order to assess whether the deformation exists in the time series or not. The proposed model makes use of the statistical criterion comparison in each case instead of the hypothesis test. In case of colored noise in GPS time series, this proposed model can be augmented by shaping filters. By the GPS experiment, the effectiveness of the proposed model has been verified. The multiple Kalman filters model can be used to detect stepwise changes of a variety of fields and predict some natural catastrophic events in real-time or near real-time, for example, landslide or a cycle slip in the phase data.

6.2 Recommendations

The following is a list of some of the areas recommended for future work:

The Kalman filter model with a shaping filter has been successfully used to isolate the colored noise from the time series. It can also be used to detect the deformation epoch with short time delay, thus, it can be applied into the landslide early warning system in the future.

The mathematical algorithm to define the boundary of distinguishing the distributions of outlier and deformation needs to be further studied. The robustness of the kalman filter with shaping filter needs to be extended in the future.

The data supporting this research were collected from the GPS experiment with limited magnitudes of movements. In the future, more GPS experiments with different sampling rates and different movements can be done. The baseline length and the height difference can also be changed.

As for the proposed multiple Kalman filter model, in the aspect of detecting smaller deformations, the proposed model needs further improvement. Besides the stepwise deformation, more complicated deformation possibilities, such as the continuous deformation, should be investigated in the future work.

List of Figures

List of Tables

References

Berger O. J. (1985) Statistical decision theory and Bayesian analysis, 2nd ed., Springer Verlag, New York.

Black H. D. and Eisner A. (1984) Correcting satellite Doppler data for tropospheric effects, J. Geophys. Res., 89(D2), 2616-2626.

Brown R. G. and Hwang P. Y. (1997) Introduction to random signals and applied Kalman filtering, 3rd ed., John Wiley & Sons, New York.

Brunner F. K., Hartinger H. and Richter B. (2000) Continuous monitoring of landslides using GPS: a progress report, In: Bauer S. J. and Weber F.K. (Eds.), Proc. Geophys. Aspects of Mass Movements, Austrian Academy of Sciences, Vienna, Austria, 75-88. *http://portal.tugraz.at/portal/page/portal/Files/i2720/publications/papers/documents/2000_idndr_BR_HH.pdf*

Cai J., Wang J., Wu J., Hu C., Grafarend E. and Chen J. (2008) Horizontal deformation rate analysis based on multiepoch GPS measurements in Shanghai, J. Surv. Eng., 134 (4), 132-137.

Cao C. (2009) Status of COMPASS/BeiDou development, Stanford's 2009 PNT Challenges and Opportunities Symposium, Stanford, California, USA, October 21-22.

http://scpnt.stanford.edu/pnt/PNT09/presentation_slides/3_Cao_Beidou_Status.pdf

Chen Y., Huang D. and Ding X. (2001) Measurement of vibrations of tall buildings with GPS: a case study, In: Chase S.B. and Aktan A.E. (Eds.), Health Monitoring & Management of Civil Infrastructure Systems, Newport Beach, USA, 4337, 477–483.

Cozzens T. (2010) The System: First IIF Satellite Speeds into Orbit, GPS World, 2010.05. *http://www.gpsworld.com/gnss-system/gps-modernization/the-system-first-iif-satellite-speeds-orbit-10013*

Dodson A. H., Meng X. and Roberts G. (2001) Adaptive method for multipath mitigation and its applications for structural deflection monitoring, International Symposium on Kinematic Systems in Geodesy, Geomatics and Navigation, Banff, Alberta, Canada, June 5-8.

Elali T. S. (2003) Discrete systems and digital signal processing with matlab, CRC press, Boca Raton.

Forward T., Stewart M., Penna N. and Tsakiri M. (2001) Steep wall monitoring using switched antenna arrays and permanent GPS network, 10th International Symposium on Deformation Measurements, Orange, California, USA, March 19-21.

Fujino Y., Murata M., Okano S. and Takeguchi M. (2000) Monitoring system of the Akashi Kaikyo bridge and displacement measurement using GPS, In: Aktan A.E. and Gosselin S.R.

(Eds.), Nondestructive Evaluation of Highways, Utilities, and Pipelines IV, Proceedings of SPIE, 3995, 229-236.

Gao.Y and Liu Z. (2002) Precise ionosphere modeling using regional GPS network data, Journal of Global Positioning Systems, 1(1), 18-24.

Gelb A. (1974) Applied optimal estimation, M.I.T. press, Cambridge, Massachusetts and London, England.

Glabsch J., Heunecke O. and Schuhbäck S. (2009) Monitoring the Hornbergl landslide using a recently developed low cost GNSS sensor network, Journal of Applied Geodesy, 3, 179-192.

Glade T., Becker R., Bell R., Burghaus S., Danscheid M., Dix A., Greiving S., Greve K., Jäger S., Kuhlmann H., Krummel H., Paulsen H., Pohl J. and Röhrs M. (2009) Geodetic Monitoring and modeling, Integrative Landslides Early Warning systems (ILEWS), Geotechnologien science Report, Karlsruhe, 89-100.

Grewal M. S. and Andrews A. P. (2001) Kalman filtering: theory and practice using matlab, 2nd ed., John Wiley and Sons, New York.

Guo J. and Ge S. (1997) Research of displacement and frequency of tall building under wind load using GPS, ION GPS'97, 10th Int. Tech. Meeting of the Sat. Div. of the U.S. Inst. of Navigation, Kansas City, USA, September16-19.

Hein G. W. and Riedl B. (2003) Real-time monitoring of highway bridges using DREAMS, Proceedings of 11th International Symposium on Deformation Measurements, Santorini Island, Greece, May 25-28.

Hofmann-Wellenhof B., Lichtenegger H. and Collins J. (2001) GPS–Theory and practice, 5th ed., Springer-Verlag, New York.

Hopfield H. S. (1969) Two–quadratic tropospheric refractivity profile for correction satellite data, J. Geophys. Res., 74(18), 4487 – 4499.

Hudnut K. W. and Behr J. A. (1998) Continuous GPS monitoring of structural deformation at pacoima dam, Seismological Research Letter, 69(4), 299-308.

IGS *http://igscb.jpl.nasa.gov/components/prods.html*

Ince C. D. and Sahin M. (2000) Real-time deformation monitoring with GPS and Kalman filter, Earth Planets Space, 52(10), 837-840.

Janssen V. (2002) GPS on the web: GPS volcano deformation monitoring, GPS Solut., 6 (1-2), 128-130.

Janssen V. (2007) Volcano deformation monitoring using GPS, Journal of Spatial Science, 52 (1), 41-54.

Jäger R., Kälber S., Oswald M. and Bertges M. (2006) GNSS/GPS/LPS based online control and alarm system (GOCA) mathematical models and technical realisation of a system for natural

and geotechnical deformation monitoring and analysis, 3rd IAG / 12th FIG Symposium, Baden, Austria, May 22-24.
http://www.fig.net/commission6/baden_2006/PDF/GPS1/Jaeger.pdf

Kalman R. E. (1960) A new approach to linear filtering and prediction problems, ASME Journal of Basic Engineering, 82(D), 35-45.

Kim D., Langley R. B., Bond J. and Chrzanowski A. (2003) Local deformation monitoring using GPS in an open pit mine: Initial Study, GPS Solut., 7(3), 176-185.

Klobuchar J. (1996) Ionospheric effects on GPS, In: Parkinson B.W. and Spilker J.J. (eds): Global Positioning System: theory and applications, American Institute of Aeronautics and astronautics, Washington DC, Vol. 1, 485-515.

Kuhlmann H. and Pelzer H. (1997) Models of Deformation Analysis, In Altan, M.O.; Gründig, L.(Eds.): Second Turkish German Joint Geodetic Days, Berlin.

Kuhlmann H. (2003) Kalman-filtering with coloured measurement noise for deformation analysis, 11th FIG International Symposium on Deformation Measurements, Santorini, Greece, May 25-28.
http://www.fig.net/figtree/commission6/santorini

Kuo S. M. and Lee B. H. (2001) Real-Time Digital Signal Processing: Implementations, Applications, and Experiments with the TMS320C55x, John Wiley and sons, New York.

Langley R. (1998) Propagation of the GPS signals, In Teunissen P. J. G. and Kleusberg A.(eds.): GPS for Geodesy, Springer Verlag, Heidelberg, 111-149.

Li L. and Kuhlmann H. (2008a) Detection of deformations and outliers in real-time GPS measurements by Kalman filter model with a shaping filter, 13th FIG International Symposium on Deformation Measurements and Analysis and 4th IAG Symposium on Geodesy for Geotechnical and Structural Engineering, Lisbon, Portugal, May 12-15.

Li L. and Kuhlmann H. (2008b) A Study on the comparison of colored noise reduction performance in the GPS time series based on three different methods: FIR filter, Kalman filter with shaping filter, and Sequential algorithm, 4th International Conference on Engineering Surveying, Bratislava, Slovak, October 23 - 24.

Li L. and Kuhlmann H. (2010) Deformation detection in the GPS real-time series by the multiple Kalman filters model, J. Surv. Eng., 136 (4), 157-164.

Lovse J. L., Teskey W. F., Lachepelle G. and Cannon M. E. (1995) Dynamic deformation monitoring of tall structure using GPS technology, J. Surv. Eng., 121(1), 35-40.

Maybeck P. S. (1994) Stochastic models, estimation and control, Vol I. Academic Press, Inc., New York.

Meier S. and Keller W. (1990) Geostatistik, Springer Verlag, Wien, New York.

Meng X. L. (2002) Real-time deformation monitoring of bridges using GPS/Accelerometers, Thesis for the degree of Doctor of Philosophy, University of Nottingham. *http://etheses.nottingham.ac.uk/archive/00000279/01/Meng's_full_thesis.pdf*

Mertikas S. P. (2001) Automatic and online detection of small but persistent shifts in GPS station coordinates by statistical process control, GPS Solut., 5(1), 39-50.

Mertikas S. P. and Rizos C. (1997) Online detection of abrupt changes in the carrier-phase measurements of GPS, J. Geod., 71(8), 469-482.

Mikhail E. M. (1976) Observations and Least Squares, IEP- A DUN-Donnelley publisher, New York.

Minkler G. and Minkler J. (1993) Theory and application of Kalman filtering, Magellan Book Company, Palm Bay.

Misra P. and Enge P. (2001) Global Positioning System: signals, measurements and performance, Ganga-Jamuna Press, Lincoln, Massachusetts.

Moghtased-Azar K. and Grafarend E. W. (2009) Surface deformation analysis of dense GPS networks based on intrinsic geometry: deterministic and stochastic aspects, J. Geod. 83(5), 431–454.

Müller T. (2010) Ermittlung geeigneter meteorologischer Korrektionsgrößen für elektrooptisch gemessene Distanzen unter Einbeziehung unterschiedlicher Modellansätze für die Ermittlung des Brechungsindexed. Bachelorarbeit. Institut für Geodäsie und Geoinformation, Universität Bonn, Bonn.

Ogaja C., Rizos C., Wang J. and Brownjohn J. (2002) GPS and building monitoring case study: Republic Plaza Building, Singapore. *http://www.ucalgary.ca/engo_webdocs/SpecialPublications/KIS%2001/PDF/0508.PDF*

Okatan A., Hajiyev Ch. and Hajiyeva U. (2007) Kalman filter innovation sequence based fault detection in leo satellite attitude determination and control system, 3rd International Conference on Recent Advances in Space Technologies, 2007, RAST '07, Istanbul, Turkey, June 14-16, 411 - 416.

Oppenheim A.V. and Schafer R.W. (1989) Discrete-time signal processing, 2nd ed. Prentice-Hall, New Jersey.

Öhler V., Krüger J. M., Beck T., Kirchner M., Trautenberg H.L., Hahn J. and Blonski D. (2009) Galileo system performance status report, ION GNSS Conference 2009, Savannah, Georgia , USA, September 22-25. *www.giove.esa.int/images/userpage/ION_2009_EADS.pdf*

Parkinson B. W. (1996) GPS error analysis, In: Parkinson B.W. and Spilker J.J. (eds): Global Positioning System: theory and applications, American Institute of Aeronautics and astronautics, Washington DC, Vol l, 469-483.

Parkinson B. W. and Enge P. K.(1996) GPS error analysis, In: Parkinson B.W. and Spilker J.J. (eds): Global Positioning System: theory and applications, American Institute of Aeronautics and astronautics, Washington DC, Vol II, 3-79.

Petovello M. G., O'Keefe K. , Lachapelle G. and Cannon M. E. (2009) Consideration of time-correlated errors in a Kalman filter applicable to GNSS, J. Geod., 83(1), 51-56.

Qiao X., Li S., You X., Du R. and Logan T. (2002) Monitoring crustal deformation by GPS and InSAR in the three gorge area, Wuhan University Journal of Natural Sciences, 7(4), 451-457.

Rabiner L. R. and Gold B. (1975) Theory and application of digital signal processing, Prentice-Hall, Englewood Cliffs, New Jersey.

Radhakrishnan N. (2006) Direct GPS measurement of Koyna Dam deformation during earth-quake, 3rd IAG / 12th FIG Symposium, Baden, Austria, May 22-24.

Rissanen J. (1983) A universal prior for integers and estimation by minimum description length, Ann. Stat., 11(2), 416–431.

Rizos C., Han, S., Roberts C., Han X., Abidin H. and Wirakusumah A.D. (2000) A continuously operating GPS-based volcano deformation monitoring in Indonesia: challenges and preliminary results. In "Geodesy Beyond 2000: The Challenges of the First Decade", Springer-Verlag, 361-366, Proc. *IAG General Assembly*, Birmingham, UK, July 19-30, 1999.
http://www.gmat.unsw.edu.au/snap/publications/rizos_etal1999b.pdf

Roberts C. and Rizos C. (2001) Mitigating differential troposphere effects for GPS-based volca-no monitoring, 5th Int. Symp. on Satellite Navigation Technology & Applications, Canberra, Australia, July 24-27.

Roberts G., Meng X. and Brown C. (2004) From St Paul's to the Tate Modern; Overcoming problems in monitoring bridge deflections using GPS, 1st FIG International Symposium on Engineering Surveys for Construction Works and Structural Engineering, Nottingham, Unit-ed Kingdom, June 28– July 1.

Roberts G.W., Dodson A. H. and Ashkenazi V. (1999) Twist and deflection: monitoring motion of humber bridge, GPS World, 10(10), 24-34.

Saastamoinen J. (1973) Contributions to the theory of atmospheric refraction, Bull. G`eod., 107(1), 13–34.

Schön S. (2007) Affine distortion of small GPS networks with large height, GPS Solut., 11(2), 107-117.

Schönwiese C.-D. (1994) Klimatologie, UTB für Wissenschaft, Eugen Ulmer, Stuttgart.

Schrick K.W. (1977) Anwendungen der Kalman-Filter-Technik: Anleitung und Beispiele, Oldenbourg Verlag, Müchen, Wien.

Schüler T. (2007) GNSS Positioning in the national report of the federal republic of Germany on the geodetic activities in the years 2003 – 2007, xxiv General Assembly of the International Union for Geodesy and Geophysics (IUGG), Perugia, Italy, July 2-13. *http://www.iugg.org/members/nationalreports/germany07.pdf*

Schwieger V. (1999) Ein Elementarfehlermodell für GPS-Überwachungsmessungen – Konstruktion und Bedeutung interepochaler Korrelationen, Wissenschaftliche Arbeiten der Fachrichtung Vermessungswesen der Universität Hannover, Nr. 231, Hannover.

Seeber G. (2003) Satellite Geodesy, 2nd Ed., Walter de Gruyter, Berlin, New York.

Singer J., Schuhbäck St., Wasmeier P., Thuro K., Heunecke O., Wunderlich T., Glabsch J. and Festl J. (2009) Monitoring the Aggenalm landslide using economic deformation measurement techniques, Austrian Journal of Earth Sciences, 102(2) ,20-34.

Strang G. and Borre K. (1997) Linear algebra, geodesy, and GPS, Wellesley-cambridge press, Massachusetts.

Spilker J. J. (1996) GPS signal structure and performance characteristics, In: Parkinson B.W. and Spilker J.J. (eds): Global Positioning System: theory and applications, American Institute of Aeronautics and astronautics, Washington DC, Vol l, 57-119.

Springer T. A. and Dach R. (2010) Innovation: GPS, GLONASS, and More, GPS World, 2010.06. *http://www.gpsworld.com/gnss-system/glonass/innovation-gps-glonass-and-more-10007*

Squarzoni C., Delacourt C. and Allemand P. (2005) Differential single-frequency GPS monitoring of the La Valette landslide (French Alps), Engineering Geology, 79 (3-4), 215-229.

Teferle F. N., Bingley R. M., Dodson A. H., Baker T. F. and Williams S. D. (2001) Evaluation of the dual-CGPS concept to monitoring vertical land movements at tide gauges, *In:* Book of Extended Abstracts of the Final Workshop of European COST Action 40, European Sea Level Observing System (EOSS), Sea Level in Europe: Observation, Interpretation and Exploitation, Dubrovnik, Croatia, 40-43.

Teunissen P. J. G. (1990) Quality control in integrated navigation systems, Proceedings of the IEEE PLANS, Las Vegas, NV, USA, March 20-23.

Thiebes B., Bell R., Glade T., Aslan A. M., Schauerte W. and Kuhlmann H. (2010) Frühwarnmodellierung, Bell,R. ; Mayer, J. ; Pohl, J. ; Greiving, S. ; Glade, T. (Ed.): Integrative Frühwarnsysteme für gravitative Massenbewegungen (ILEWS), Monitoring, Modellierung, Implementierung, Klartext Verlag, Essen, 130-154.

Volkert H. (1983) Klimatologie der Varianz meteorologischer Felder in Südbayern, Deutsche Forschungs-und Versuchsanstalt für Luft- und Raumfahrt, Dissertation, University of Munich.

Welch G. and Bishop G. (2006) An introduction to the Kalman filter, University of North Carolina at Chapel Hill, TR95-041, Chapel Hill, NC 27599-3175.

Wells D. E., Beck N., Delikaraoglou D., Kleusberg A., Krakiwsky E. J., Lachapelle G., Langley R.B., Nakiboglu M., Schwarz K. P., Tranquilla J.M. and Vanicek P. (1986) Guide to GPS positioning, Canadian GPS Associates, Fredericton N.B., Canada.

Welsch W., Heunecke O. and Kuhlmann H. (2000) Auswertung geodätischer Überwachungsmessungen, In: Möser et. al.: Handbuch Ingenieurgeodäsie. Wichmann Verlag, Heidelberg.

Willsky A. S. (1976) A survey of design methods for failure detection in dynamic systems, Automatica, 12, 601-611.

Wong K.Y., Man K. L. and Chan W.Y. (2001) Monitoring Hong Kong's bridges: real-time kinematic spans the gap, GPS World, 12(7), 10-18.

Yang Y. (2002) Robust estimator for correlated observations based on bifactor equivalent weights, J. Geod., 76(6), 353-358.

Yang Y., He H. and Xu G. (2001) Adaptively robust filtering for kinematic geodetic positioning, J. Geod., 75(2-3), 109-116.

Yang Y. and S. Zhang (2005) Adaptive fitting of systematic errors in navigation, J. Geod., 79(1-3), 43-49.

Zeimetz P. and Kuhlmann H. (2010) Validation of the laboratory calibration of geodetic antennas based on GPS measurements, FIG Congress 2010 Facing the Challenges – Building the Capacity, Sydney, Australia, April 11-16.

Acknowledgments

Over my last four years in Bonn, I have had the privilege to work with a number of people who have made my time at Bonn University enjoyable and rewarding. I would like to thank all of them.

Firstly, I would like to express my deepest gratitude to my supervisor, Professor Kuhlmann, for his patience, guidance, and support with my PhD study. He is an out-standing researcher with broad knowledge, sharp intuition and grand vision. It's no overstatement at all to say that he basically shaped my academic life. Furthermore, I would like to thank my co-referee Prof. Dr. techn. Wolf-Dieter Schuh and Prof. Förstner for discussing with me about my thesis.

I would also like to thank all the people who helped in the completion of this work. Especially with the help of my colleagues Thomas Kötter and Stephan Burghaus, the GPS campaigns have been successful.

I want to thank all the people in Institute of Geodesy and Geoinformation. They make the institute not only a wonderful place for scientific research, but also a warm and lively family that I will remember forever.

I want to thank all my friends at Bonn who helped me in various ways. Without them my life at Bonn would not be so colorful and fun. Thanks to my friends from the US for helping me correct my dissertation: Justin and Sean.

Finally, I would like to express my deep gratitude and appreciation to my parents, my brothers and my sisters-in law for their understanding, love, continuous support, encouragement and great sacrifice throughout the years of my study. Special thanks should go also to my brothers for taking care of our parents since I started my university life. This dissertation is dedicated to them.

In der Schriftenreihe des Instituts für Geodäsie und Geoinformation
der Rheinischen Friedrich-Wilhelms-Universität Bonn sind erschienen:

Heft 26 2012	Lihua Li Separability of deformations and measurement noises of GPS time series with modified Kalman filter for landslide monitoring in real-time
Heft 25 2012	Benedikt Frielinghaus Ökonomisches Entscheidungstool zur Wohnbaulandentwicklung Wirtschaftlichkeitsanalysen potenzieller Wohnbauflächen auf der Ebene des Flächennutzungsplanes
Heft 24 2011	Enrico Kurtenbach Entwicklung eines Kalman-Filters zur Bestimmung kurzzeitiger Variationen des Erdschwerefeldes aus Daten der Satellitenmission GRACE
Heft 23 2011	Sarah Böckmann Robust determination of station positions and Earth orientation parameters by VLBI intra-technique combination
Heft 22 2011	20th Meeting of the European VLBI Group for Geodesy and Astronomy Proceedings
Heft 21 2011	Philipp Zeimetz Zur Entwicklung und Bewertung der absoluten GNSS-Antennenkalibrierung im HF-Labor
Heft 20 2011	Alessandra Roy Effects on the Geodetic-VLBI Observables Due to Polarization Leakage in the Receivers
Heft 19 2011	Dietmar Weigt Auswirkungen von Flughäfen insbesondere von Fluglärm auf den Immobilienmarkt am Beispiel des Marktsegments „individuelles Wohnen“
Heft 18 2011	Anno Löcher Möglichkeiten der Nutzung kinematischer Satellitenbahnen zur Bestimmung des Gravitationsfeldes der Erde
Heft 17 2010	Basem Elsaka Simulated Satellite Formation Flights for Detecting the Temporal Variations of the Earth’s Gravity Field
Heft 16 2010	2nd International Conference on Machine Control & Guidance Proceedings
Heft 15 2009	Alexandra Weitkamp Brachflächenrevitalisierung im Rahmen der Flächenkreislaufwirtschaft
Heft 14 2008	Akbar Shabanloui A New Approach for a Kinematic-Dynamic Determination of Low Satellite Orbits Based on GNSS Observations
Heft 13 2008	Frank Friesecke Stadtumbau im Konsens!? Zur Leistungsfähigkeit und Fortentwicklung des städtebaulichen Instrumentariums unter Schrumpfungsbedingungen
Heft 12 2008	Heinz Rütz Zur Kostenanalyse der privaten Umlegung als Teil der konsensualen integrierten Baulandentwicklung
Heft 11 2008	Gaby Alexandra Boele-Keimer Kommunales Kennzahlenmanagement am Beispiel von Vermessungs- und Katasterämtern in Nordrhein-Westfalen

Heft 10 2008	Annette Eicker Gravity Field Refinement by Radial Basis Functions
Heft 9 2008	Torsten Mayer-Gürr Gravitationsfeldbestimmung aus der Analyse kurzer Bahnbögen
Heft 8 2008	Boris Kargoll On the Theory and Application of Model Misspecification Tests
Heft 7 2008	Hamza Alkhatib On Monte Carlo Methods
Heft 6 2008	Klaus Borchard Annäherungen an Städtebau und Raumentwicklung
Heft 5 2008	Jens Jähnke Zur Teilmarktbildung beim Landerwerb der öffentlichen Hand
Heft 4 2008	Atef Abd-Elhakee Makhloof The Use of Topographic Isostatic Mass Information
Heft 3 2008	Markus Vennebusch Singular Value Decomposition and Cluster Analysis
Heft 2 2007	Christian Beder Grouping Uncertain Oriented Projective Geometric Entities
Heft 1 2007	Klaus Börger Geodäsie und Quantenphysik

Vertrieb: Rheinische Friedrich-Wilhelms-Universität Bonn
Institut für Geodäsie und Geoinformation
· Bibliothek ·
Nußallee 17
53115 Bonn

Tel.: +49 (0)228 73-3566
Fax: +49 (0)228 73-2988

Internet: http://www.igg.uni-bonn.de

ISSN 1864-1113